

Unclassified

SECURITY CLASSIFICATION OF THIS PAGE

AD-A205948

ADA205948

REPORT DOCUMENTATION PAGE

Form Approved
OMB No. 0704-0188

| | | | |
|---|--|--|----------------------------|
| 1a. REPORT SECURITY CLASSIFICATION Unclassified | | 1b. RESTRICTIVE MARKINGS | |
| 2a. SECURITY CLASSIFICATION AUTHORITY | | 3. DISTRIBUTION/AVAILABILITY OF REPORT Approved for public release, distribution unlimited | |
| 2b. DECLASSIFICATION/DOWNGRADING SCHEDULE | | 5. MONITORING ORGANIZATION REPORT NUMBER(S) AFOSR-TR-89-0330 | |
| 4. PERFORMING ORGANIZATION REPORT NUMBER(S) | | 7a. NAME OF MONITORING ORGANIZATION AFOSR | |
| 5a. NAME OF PERFORMING ORGANIZATION Statcon, Inc. | | 6b. OFFICE SYMBOL (if applicable) | |
| 6c. ADDRESS (City, State, and ZIP Code) 2208 Countryside Drive Silver Spring MD 20904 | | 7b. ADDRESS (City, State, and ZIP Code) AFOSR, Bldg 410 Bolling AFB Washington D.C. 20332-6448 | |
| 8a. NAME OF FUNDING / SPONSORING ORGANIZATION AFOSR | | 8b. OFFICE SYMBOL (if applicable) NA | |
| 9. PROCUREMENT INSTRUMENT IDENTIFICATION NUMBER F49620-87-C-0035 | | 10. SOURCE OF FUNDING NUMBERS | |
| 6c. ADDRESS (City, State, and ZIP Code) AFOSR, Bldg 410 Bolling AFB Washington D.C. 20332-6448 | | PROGRAM ELEMENT NO. 61102F | PROJECT NO. K823 |
| 1. TITLE (Include Security Classification) (SDI) ACTIVE CONTROL OF FLEXIBLE SPACE STRUCTURES USING THE NITHOL SHAPE MEMORY ACTUATORS' (U) | | TASK NO. A1 | WORK UNIT ACCESSION NO. |
| 2. PERSONAL AUTHOR(S) | | | |
| 3a. TYPE OF REPORT FINAL | | 13b. TIME COVERED FROM 87/02/01 TO 87/07/31 | |
| 14. DATE OF REPORT (Year, Month, Day) | | 15. PAGE COUNT 107 | |
| 6. SUPPLEMENTARY NOTATION | | | |

| | | | |
|-----------------|-------|-----------|--|
| 7. COSATI CODES | | | 18. SUBJECT TERMS (Continue on reverse if necessary and identify by block number) Active Control, Nitinol Actuators, Space Structures |
| FIELD | GROUP | SUB-GROUP | |
| | | | |
| | | | |

9. ABSTRACT (Continue on reverse if necessary and identify by block number)

Summarizes research progress in the feasibility demonstration of active vibration control using Nitinol shape memory actuators. Tests on straight wire and helical actuators to characterize their dynamic response are described. The experimental set-up and the range of parametric variation used in a beam vibration control are also described.

| | | | |
|--|--|--|--------------------------------|
| 20. DISTRIBUTION/AVAILABILITY OF ABSTRACT <input type="checkbox"/> UNCLASSIFIED/UNLIMITED <input checked="" type="checkbox"/> SAME AS RPT. <input checked="" type="checkbox"/> DTIC USERS | | 21. ABSTRACT SECURITY CLASSIFICATION UNCLASSIFIED | |
| 22a. NAME OF RESPONSIBLE INDIVIDUAL Dr. Anthony K. Amos | | 22b. TELEPHONE (Include Area Code) (202) 767-4937 | 22c. OFFICE SYMBOL AFOSR/NA |

AFOSR-TR- 88-0336

ACTIVE CONTROL OF FLEXIBLE SPACE STRUCTURES USING NITINOL SHAPE MEMORY ACTUATORS

FINAL REPORT FOR PHASE I SDIO CONTRACT #F49620-87-C-0035

BY

DR. AMR M. BAZ
KARIM R. IMAN
AND
DR. JOHN J. MCCOY

STATCON, Inc.
8121 GEORGIA AVENUE
SUITE 507
SILVER SPRING, MARYLAND 20910

OCTOBER 1987

| | |
|--------------------|-------------------------------------|
| Accession For | |
| NTIS CRA&I | <input checked="" type="checkbox"/> |
| DTIC TAB | <input type="checkbox"/> |
| Unannounced | <input type="checkbox"/> |
| Justification | |
| By | |
| Distribution / | |
| Availability Codes | |
| Dist | Avail and/or Special |
| A-1 | |

89 000 000

TABLE OF CONTENTS

| | Page |
|---|------|
| I. Summary | 1 |
| II. Introduction | 1 |
| III. The NITINOL Shape Memory Actuator | 3 |
| IV. Dynamic Characteristics Of NITINOL Actuators | 7 |
| A. The Tested Actuators | 7 |
| B. Time Response | 7 |
| 1. Testing facility | 7 |
| 2. Results | 10 |
| 2.1 Helical Actuators | 10 |
| i. Effect of wire diameter | 10 |
| ii. Effect of wire length | 16 |
| iii. Effect of cooling strategy | 21 |
| 2.2 Straight Actuators | 21 |
| C. Frequency Response | 21 |
| 1. Testing Facility | 30 |
| 2. Results | 30 |
| i. With natural cooling strategy | 30 |
| ii. With forced cooling strategy | 34 |
| V. Mathematical Modeling Of The Dynamic Characteristics | |
| Of The Nitinol Actuator | 34 |
| A. The Model | 34 |
| 1. Energy and Phase Transformation Equations | 34 |
| 2. Equation of Motion | 42 |
| B. Dimensionless Modeling of the NITINOL Actuator | 44 |
| C. Modeling of Experimental Results | 46 |
| VI. Design And Testing Of Active Control System | |
| Using NITINOL Actuator | 47 |
| A. The Flexible Beam System | 51 |
| i. Physical system | 51 |
| ii. Mathematical model of beam-actuator element | 51 |
| 1. Stiffness Matrix | 51 |
| 2. Mass matrix | 55 |
| 3. Dynamic model | 56 |
| B. Modeling of the Control System | 56 |
| i. Layout of the control system | 58 |
| ii. Control with one NITINOL actuator | 58 |
| iii. Control with two NITINOL actuators | 68 |
| C. The Physical Control System | 68 |
| i. Electronic circuits | 68 |
| 1. Input/output circuit | 68 |
| 2. Actuator Control Circuit | 76 |
| 3. Sensor Circuit | 76 |
| ii. Performance of controller | 76 |
| 1. Performance with Single-Wire Actuator | 79 |
| 2. Performance with two-wire actuator | 79 |
| a. Original beam | 79 |
| b. Beam with added weight | 87 |
| VII. CONCLUSIONS | 87 |
| VIII. REFERENCES | 92 |

LIST OF FIGURES

| Figure | Page |
|---|------|
| 1. SHAPE MEMORY EFFECT. | 4 |
| 2. SCHEMATIC DRAWING OF A SHAPE MEMORY ACTUATOR. | 5 |
| 3. TYPICAL PLACEMENT ARRANGEMENTS OF NITINOL ACTUATORS IN GENERIC SPACE STRUCTURE. | 6 |
| 4. TIME RESPONSE TESTING FACILITY. | 9 |
| 5-a. HEATING AND COOLING TIME HISTORIES FOR A 30 mils (0.075 cm) ACTUATOR WHEN SUBJECTED TO STEP VOLTAGE CHANGES OF 5 VOLTS. | 11 |
| 5-b. HEATING AND COOLING TIME HISTORIES FOR A 35 mils (0.0875 cm) ACTUATOR WHEN SUBJECTED TO STEP VOLTAGE CHANGES OF 5 VOLTS. | 11 |
| 6-a. EFFECT OF WIRE DIAMETER OF HELICAL ACTUATOR ON ITS HEATING TIME CONSTANT WHEN SUBJECTED TO DIFFERENT STEP VOLTAGE CHANGES WITH NUMBER OF TURNS = 29. | 13 |
| 6-b. EFFECT OF WIRE DIAMETER OF HELICAL ACTUATOR ON ITS COOLING TIME CONSTANT WHEN SUBJECTED TO DIFFERENT STEP VOLTAGE CHANGES WITH NUMBER OF TURNS = 29. | 14 |
| 6-c. EFFECT OF WIRE DIAMETER OF HELICAL ACTUATOR ON ITS MAXIMUM DISPLACEMENT WHEN SUBJECTED TO DIFFERENT STEP VOLTAGE CHANGES WITH NUMBER OF TURNS = 29. | 15 |
| 7-a. HEATING AND COOLING TIME HISTORIES FOR A 16 mils (0.04 cm) ACTUATOR WHEN SUBJECTED TO STEP VOLTAGE CHANGES OF 3 VOLTS WITH NUMBER OF TURNS = 4. | 17 |
| 7-b. HEATING AND COOLING TIME HISTORIES FOR A 16 mils (0.04 cm) ACTUATOR WHEN SUBJECTED TO STEP VOLTAGE CHANGES OF 3 VOLTS WITH NUMBER OF TURNS = 11. | 17 |
| 7-c. HEATING AND COOLING TIME HISTORIES FOR A 16 mils (0.04 cm) ACTUATOR WHEN SUBJECTED TO STEP VOLTAGE CHANGES OF 3 VOLTS WITH NUMBER OF TURNS = 15. | 17 |
| 8-a. EFFECT OF WIRE LENGTH OF HELICAL ACTUATOR ON ITS HEATING TIME CONSTANT WHEN SUBJECTED TO DIFFERENT STEP VOLTAGE CHANGES FOR WIRE DIAMETER OF 16 mils (0.04 cm). | 18 |
| 8-b. EFFECT OF WIRE LENGTH OF HELICAL ACTUATOR ON ITS COOLING TIME CONSTANT WHEN SUBJECTED TO DIFFERENT STEP VOLTAGE CHANGES FOR WIRE DIAMETER OF 16 mils (0.04 cm). | 19 |

LIST OF FIGURES
(CONTINUED)

| | |
|---|----|
| 8-c. EFFECT OF WIRE LENGTH OF HELICAL ACTUATOR ON ITS MAXIMUM DISPLACEMENT WHEN SUBJECTED TO DIFFERENT STEP VOLTAGE CHANGES FOR WIRE DIAMETER OF 16 mils (0.04 cm). | 20 |
| 9-a. EFFECT OF WIRE LENGTH OF HELICAL ACTUATOR ON ITS HEATING TIME CONSTANT WHEN SUBJECTED TO DIFFERENT STEP VOLTAGE CHANGES FOR WIRE DIAMETER OF 25 mils (0.0625 cm). | 22 |
| 9-b. EFFECT OF WIRE LENGTH OF HELICAL ACTUATOR ON ITS COOLING TIME CONSTANT WHEN SUBJECTED TO DIFFERENT STEP VOLTAGE CHANGES FOR WIRE DIAMETER OF 25 mils(0.0625 cm). | 23 |
| 9-c. EFFECT OF WIRE LENGTH OF HELICAL ACTUATOR ON ITS MAXIMUM DISPLACEMENT WHEN SUBJECTED TO DIFFERENT STEP VOLTAGE CHANGES FOR WIRE DIAMETER OF 25 mils (0.0625 cm). | 24 |
| 10-a. TIME HISTORIES FOR HEATING AND COOLING OF 16 mils (0.04 cm) ACTUATOR WITH 29 TURNS WHEN SUBJECTED TO 10 VOLT STEP CHANGES AT COOLING AIR VELOCITY = 0 m/s. | 25 |
| 10-b. TIME HISTORIES FOR HEATING AND COOLING OF 16 mils (0.04 cm) ACTUATOR WITH 29 TURNS WHEN SUBJECTED TO 10 VOLT STEP CHANGES AT COOLING AIR VELOCITY = 0.8 m/s. | 25 |
| 10-c. TIME HISTORIES FOR HEATING AND COOLING OF 16 mils (0.04 cm) ACTUATOR WITH 29 TURNS WHEN SUBJECTED TO 10 VOLT STEP CHANGES AT COOLING AIR VELOCITY = 2.8 m/s. | 25 |
| 10-d. TIME HISTORIES FOR HEATING AND COOLING OF 16 mils (0.04 cm) ACTUATOR WITH 29 TURNS WHEN SUBJECTED TO 10 VOLT STEP CHANGES AT COOLING AIR VELOCITY = 5.6 m/s. | 25 |
| 10-e. TIME HISTORIES FOR HEATING AND COOLING OF 16 mils (0.04 cm) ACTUATOR WITH 29 TURNS WHEN SUBJECTED TO 10 VOLT STEP CHANGES AT COOLING AIR VELOCITY = 7.2 m/s. | 25 |
| 11. EFFECT OF COOLING AIR VELOCITY ON HEATING AND COOLING TIME CONSTANTS AS WELL AS MAXIMUM DISPLACEMENT OF 16 mils ACTUATOR WITH 29 TURNS WHEN SUBJECTED TO 10 VOLTS STEP CHANGES. | 26 |
| 12-a. EFFECT OF APPLIED VOLTAGE ON THE HEATING TIME CONSTANT OF STRAIGHT WIRE ACTUATORS OF DIFFERENT LENGTH AND 16 mils IN DIAMETER. | 27 |

LIST OF FIGURES
(CONTINUED)

| | |
|--|----|
| 12-b. EFFECT OF APPLIED VOLTAGE ON THE COOLING TIME CONSTANT OF STRAIGHT WIRE ACTUATORS OF DIFFERENT LENGTH AND 16 mils IN DIAMETER. | 28 |
| 12-c. EFFECT OF APPLIED VOLTAGE ON THE MAXIMUM DISPLACEMENT OF STRAIGHT WIRE ACTUATORS OF DIFFERENT LENGTH AND 16 mils IN DIAMETER. | 29 |
| 13. SCHEMATIC DRAWING OF THE FREQUENCY RESPONSE TEST FACILITY. | 31 |
| 14-a. HEATING AND COOLING TIME HISTORIES FOR 16 mils ACTUATOR WITH 29 TURNS WHEN SUBJECTED TO SUDDEN VOLTAGE CHANGES OF 10 VOLTS AT A FREQUENCY OF 1/36 Hz UNDER NATURAL COOLING CONDITIONS. | 32 |
| 14-b. HEATING AND COOLING TIME HISTORIES FOR 16 mils ACTUATOR WITH 29 TURNS WHEN SUBJECTED TO SUDDEN VOLTAGE CHANGES OF 10 VOLTS AT A FREQUENCY OF 1/20 Hz UNDER NATURAL COOLING CONDITIONS. | 32 |
| 14-c. HEATING AND COOLING TIME HISTORIES FOR 16 mils ACTUATOR WITH 29 TURNS WHEN SUBJECTED TO SUDDEN VOLTAGE CHANGES OF 10 VOLTS AT A FREQUENCY OF 1/7 Hz UNDER NATURAL COOLING CONDITIONS. | 33 |
| 15-a. HEATING AND COOLING TIME HISTORIES FOR 16 mils ACTUATOR WITH 29 TURNS WHEN SUBJECTED TO SUDDEN VOLTAGE CHANGES OF 10 VOLTS AT A FREQUENCY OF 1/36 Hz UNDER FORCED COOLING CONDITIONS (AIR COOLING VELOCITY = 7.2 m/s). | 35 |
| 15-b. HEATING AND COOLING TIME HISTORIES FOR 16 mils ACTUATOR WITH 29 TURNS WHEN SUBJECTED TO SUDDEN VOLTAGE CHANGES OF 10 VOLTS AT A FREQUENCY OF 1/20 Hz UNDER FORCED COOLING CONDITIONS (AIR COOLING VELOCITY = 7.2 m/s). | 36 |
| 15-c. HEATING AND COOLING TIME HISTORIES FOR 16 mils ACTUATOR WITH 29 TURNS WHEN SUBJECTED TO SUDDEN VOLTAGE CHANGES OF 10 VOLTS AT A FREQUENCY OF 1/7 Hz UNDER FORCED COOLING CONDITIONS (AIR COOLING VELOCITY = 7.2 m/s). | 36 |
| 16. A COMPARISON BETWEEN THE FREQUENCY RESPONSE CHARACTERISTICS OF 16 mils ACTUATOR UNDER NATURAL AND FORCED COOLING STRATEGIES. | 37 |
| 17. SIMPLIFIED DRAWING OF A TYPICAL NITINOL ACTUATOR SYSTEM. | 38 |
| 18. VOLTAGE, TEMPERATURE, FORCE, AND DISPLACEMENT PROFILES OF A TYPICAL NITINOL ACTUATOR. | 40 |

LIST OF FIGURES
(CONTINUED)

| | |
|---|----|
| 19-a. A COMPARISON BETWEEN EXPERIMENTAL AND MODELED DIMENSIONLESS HEATING TIME CONSTANTS FOR NITINOL ACTUATORS OF DIFFERENT GEOMETRIES SUBJECTED TO DIVERSE VOLTAGE CHANGES. | 48 |
| 19-b. A COMPARISON BETWEEN EXPERIMENTAL AND MODELED DIMENSIONLESS COOLING TIME CONSTANTS FOR NITINOL ACTUATORS OF DIFFERENT GEOMETRIES SUBJECTED TO DIVERSE VOLTAGE CHANGES. | 49 |
| 19-c. A COMPARISON BETWEEN EXPERIMENTAL AND MODELED DIMENSIONLESS MAXIMUM DISPLACEMENTS FOR NITINOL ACTUATORS OF DIFFERENT GEOMETRIES SUBJECTED TO DIVERSE VOLTAGE CHANGES. | 50 |
| 20. SCHEMATIC DRAWING OF THE FLEXIBLE CANTILEVER BEAM. | 52 |
| 21. SCHEMATIC DRAWING OF BEAM-NITINOL ACTUATOR ELEMENT. | 53 |
| 22-a. LAYOUT OF AN ACTIVE VIBRATION CONTROL SYSTEM USING NITINOL ACTUATOR. | 59 |
| 22-b. SCHEMATIC DRAWING OF A COMPUTER-CONTROLLED ACTIVE CONTROL SYSTEM. | 60 |
| 23-a. TIME HISTORY OF THE EXPERIMENTAL AMPLITUDE OF TRANSVERSE VIBRATION OF THE CANTILEVER BEAM UNDER FREE VIBRATION CONDITIONS (DAMPING RATIO = 0.02). | 61 |
| 23-b. TIME HISTORY OF THE THEORETICAL AMPLITUDE OF TRANSVERSE VIBRATION OF THE CANTILEVER BEAM UNDER FREE VIBRATION CONDITIONS (DAMPING RATIO = 0.02). | 62 |
| 24. FLOW CHART OF THE CONTROL SYSTEM ANALYSIS ALGORITHM. | 63 |
| 25. ENERGIZATION STRATEGIES OF NITINOL ACTUATOR. | 64 |
| 26-a. TIME HISTORY OF THEORETICAL AMPLITUDE OF VIBRATION OF THE BEAM WHEN CONTROLLED WITH ONE NITINOL ACTUATOR WITH A DEAD BAND OF 0.0025 in. | 65 |
| 26-b. TIME HISTORY OF THEORETICAL AMPLITUDE OF VIBRATION OF THE BEAM WHEN CONTROLLED WITH ONE NITINOL ACTUATOR WITH A DEAD BAND OF 0.005 in. | 66 |
| 26-c. TIME HISTORY OF THEORETICAL AMPLITUDE OF VIBRATION OF THE BEAM WHEN CONTROLLED WITH ONE NITINOL ACTUATOR WITH A DEAD BAND OF 0.0075 in. | 67 |
| 27-a. TIME HISTORY OF THEORETICAL AMPLITUDE OF VIBRATION OF THE BEAM WHEN CONTROLLED WITH ONE NITINOL ACTUATOR WITH A DEAD BAND OF 0.005 in AND A VELOCITY FEEDBACK LOGIC. | 69 |
| 27-b. TIME HISTORY OF THEORETICAL AMPLITUDE OF VIBRATION OF THE BEAM WHEN CONTROLLED WITH ONE NITINOL ACTUATOR WITH A DEAD BAND OF 0 in AND A VELOCITY FEEDBACK LOGIC. | 70 |
| 28. ACTIVE CONTROLLER WITH TWO NITINOL ACTUATORS. | 71 |

LIST OF FIGURES
(CONTINUED)

| | |
|--|----|
| 29-a. TIME HISTORY OF THEORETICAL AMPLITUDE OF TRANSVERSE VIBRATION OF THE BEAM WHEN CONTROLLED WITH TWO NITINOL ACTUATORS WITH DEAD BAND OF 0.005 in AND VELOCITY FEEDBACK LOGIC. | 72 |
| 29-b. TIME HISTORY OF THEORETICAL AMPLITUDE OF TRANSVERSE VIBRATION OF THE BEAM WHEN CONTROLLED WITH TWO NITINOL ACTUATORS WITH DEAD BAND OF 0.001 in AND VELOCITY FEEDBACK LOGIC. | 73 |
| 29-c. TIME HISTORY OF THEORETICAL AMPLITUDE OF TRANSVERSE VIBRATION OF THE BEAM WHEN CONTROLLED WITH TWO NITINOL ACTUATORS WITH DEAD BAND OF 0.0005 in AND VELOCITY FEEDBACK LOGIC. | 74 |
| 30. SCHEMATIC DRAWING OF THE INPUT/OUTPUT CIRCUIT. | 75 |
| 31. ACTUATOR CONTROL CIRCUIT. | 77 |
| 32. SCHEMATIC DRAWING OF SENSOR CIRCUIT. | 78 |
| 33-a. TIME HISTORY OF THE EXPERIMENTAL AMPLITUDE OF VIBRATION OF THE BEAM, WITH ONE ACTUATOR, UNDER FREE VIBRATION CONDITIONS. | 80 |
| 33-b. TIME HISTORY OF THE EXPERIMENTAL AMPLITUDE OF VIBRATION OF THE BEAM WHEN CONTROLLED WITH ONE ACTUATOR (ACTUATOR VOLTAGE = 0.4 V AND DEAD BAND = 0.0025 in). | 80 |
| 34-a. TIME HISTORY OF THE EXPERIMENTAL AMPLITUDE OF VIBRATION OF THE BEAM WHEN CONTROLLED WITH ONE ACTUATOR (ACTUATOR VOLTAGE = 0.6 V AND DEAD BAND = 0.0025 in). | 81 |
| 34-b. TIME HISTORY OF THE EXPERIMENTAL AMPLITUDE OF VIBRATION OF THE BEAM WHEN CONTROLLED WITH ONE ACTUATOR (ACTUATOR VOLTAGE = 0.8 V AND DEAD BAND = 0.0025 in). | 81 |
| 35-a. TIME HISTORY OF THE EXPERIMENTAL AMPLITUDE OF VIBRATION OF THE BEAM, WITH TWO ACTUATORS, UNDER FREE VIBRATION CONDITIONS. | 82 |
| 35-b. TIME HISTORY OF THE EXPERIMENTAL AMPLITUDE OF VIBRATION OF THE BEAM WHEN CONTROLLED WITH TWO ACTUATORS (ACTUATOR CURRENT = 0.6 A AND DEAD BAND = 0 in). | 83 |
| 35-c. TIME HISTORY OF THE EXPERIMENTAL AMPLITUDE OF VIBRATION OF THE BEAM WHEN CONTROLLED WITH TWO ACTUATORS (ACTUATOR CURRENT = 1 A AND DEAD BAND = 0 in). | 84 |
| 36-a. TIME HISTORY OF THE EXPERIMENTAL AMPLITUDE OF VIBRATION OF THE BEAM WHEN CONTROLLED WITH TWO ACTUATORS (ACTUATOR CURRENT = 1 A AND DEAD BAND = 0.0008 in). | 85 |

LIST OF FIGURES
(CONTINUED)

| | |
|--|----|
| 36-b. TIME HISTORY OF THE EXPERIMENTAL AMPLITUDE OF VIBRATION OF THE BEAM WHEN CONTROLLED WITH TWO ACTUATORS (ACTUATOR CURRENT = 1 A AND DEAD BAND = 0.0016 in). | 86 |
| 37-a. TIME HISTORY OF THE EXPERIMENTAL AMPLITUDE OF VIBRATION OF THE BEAM WITH 12.45 gm PLACED AT 12.5 cm FROM FIXED END, USING TWO ACTUATORS, UNDER FREE VIBRATION CONDITIONS. | 88 |
| 37-b. TIME HISTORY OF THE EXPERIMENTAL AMPLITUDE OF VIBRATION OF THE BEAM WITH 12.45 gm PLACED AT 12.5 cm FROM FIXED END WHEN CONTROLLED WITH TWO ACTUATORS (ACTUATOR CURRENT = 1 A AND DEAD BAND = 0.0016 in). | 89 |
| 38-a. TIME HISTORY OF THE EXPERIMENTAL AMPLITUDE OF VIBRATION OF THE BEAM WITH 12.45 gm PLACED AT 20 cm FROM FIXED END, USING TWO ACTUATORS UNDER FREE VIBRATION CONDITIONS. | 90 |
| 38-b. TIME HISTORY OF THE EXPERIMENTAL AMPLITUDE OF VIBRATION OF THE BEAM WITH 12.45 gm PLACED AT 20 cm FROM FIXED END WHEN CONTROLLED WITH TWO ACTUATORS (ACTUATOR CURRENT = 1 A AND DEAD BAND = 0.0016 in). | 91 |

LIST OF TABLES

| Table | Page |
|---|------|
| 1. Main Properties of NITINOL Actuators | 8 |
| 2. Parameters of the Actuators Tested | 8 |
| 3. Modeling Coefficients for τ_h , τ_c and X_{\max} | 47 |
| 4. The Dynamic Characteristics of the Tested Flexible Beam System | 57 |

NOMENCLATURE

| | | |
|--------------------|---|-----------------|
| A | surface of actuator, | m^2 |
| c_a | specific heat of cooling medium, | $J/kg^\circ C$ |
| c_p | specific heat of actuator material, | $J/kg^\circ C$ |
| D | coil diameter of actuator, | m |
| d | diameter of actuator wire, | m |
| d_b | dead band of controller | |
| d_i | distance between actuator and beam axes | m |
| E | Young's modulus, | N/m^2 |
| E_a | Young's modulus of actuator, | N/m^2 |
| E_b | Young's modulus of beam, | N/m^2 |
| E_i | Young's modulus of element i , | N/m^2 |
| f | modal force vector, | N |
| F | actuator force, | N |
| F_{max} | maximum actuator force, | N |
| Gr | Frashoff number | |
| G | modulus of rigidity, | N/m^2 |
| g | gravitational acceleration, | m/s^2 |
| h | convective heat transfer coefficient between actuator and ambient, | $W/m^2^\circ C$ |
| I | current passing through the actuator, | Amp |
| I_a | area moment of inertia of actuator, | m^4 |
| I_b | area moment of inertia of beam, | m^4 |
| I_i | area moment of inertia of element i , | m^4 |
| J_i | polar moment of inertial of element i , | $kg\ m^2$ |
| K | stiffness matrix of flexible system | |
| k_a | thermal conductivity of cooling medium, | $W/m^\circ C$ |
| K_i | stiffness matrix of flexible system | |
| K_s | stiffness of flexible system, | N/m |
| K_w | stiffness of actuator wire, | N/m |
| L | length of actuator wire, | m |
| L_i | length of element i , | m |
| m | mass of actuator, | kg |
| m_i | mass of element i , | kg |
| M | mass matrix of flexible system | |
| M_i | external moment acting at node i , | $N\ m$ |
| M_N | moment developed by NITINOL actuator, | $N\ m$ |
| M_e | equivalent moving mass of actuator at its appendages, | kg |
| N | number of turns of helical actuator | |
| Nu | Nusselt number | |
| Pr | Prandtl number | |
| Q_L | latent heat of transformation of NITINOL, | J/kg |
| S_y | yield strength of NITINOL, | N/m^2 |
| t | time, | s |
| $t_{\frac{1}{2}c}$ | time to drop to half the maximum deflection during cooling, | s |
| $t_{\frac{1}{2}h}$ | time to rise to half the maximum deflection during heating, | s |

NOMENCLATURE (CONTINUED)

| | | |
|------------|--|-------------|
| T_a | temperature of ambient, | $^{\circ}C$ |
| T_{\max} | maximum temperature of actuator, | $^{\circ}C$ |
| T_T | phase transformation temperature of NITINOL, | $^{\circ}C$ |
| U | modal displacement of flexible system, | m |
| \ddot{U} | modal acceleration of flexible system, | m/s^2 |
| V_i | shear forces acting on element i , | N |
| $W_{a,b}$ | actuator and beam mass per unit length respectively, | kg/m |
| X | position along beam longitudinal axis, | m |
| X_{\max} | maximum deflection of NITINOL actuator, | m |
| Y | transverse deflection of beam, | m |
| Y_R | reference position of beam in transverse direction, | m |

Greek Letters

| | | |
|-------------------------|---|------------------|
| β | coefficient of thermal expansion of cooling medium, | $^{\circ}C^{-1}$ |
| γ_i | actuator placement strategy number (1 or 0) | |
| $\delta, \ddot{\delta}$ | deflection and acceleration vectors of flexible system, | $m, m/s^2$ |
| θ_i | angular deflection of element i , | rad |
| σ | diagonal matrix of normal modes of vibration | |
| μ_a | viscosity of cooling medium, | kg/ms |
| ρ | density of actuator material, | kg/m^3 |
| ρ_a | density of cooling medium, | kg/m^3 |
| τ_c | cooling time constant of actuator, | s |
| τ_h | heating time constant of actuator, | s |
| τ_{th} | thermal time constant of actuator, | s |
| ϕ | modal shape matrix of flexible system | |

I. SUMMARY

This report deals with the utilization of a new class of shape memory actuators in controlling and suppressing the vibrations of flexible structures in general and beams in particular. The need for such active control systems is becoming inevitable because the new trends in the design of large structures have rendered these structures to be mechanically flexible and inherently low in natural damping.

The report demonstrates experimentally the feasibility of using the shape memory actuators in actively controlling the vibration of a simple cantilever beam. Emphasis is placed on the measurement of the dynamic characteristics of the shape memory actuator in the time and frequency domains under various design and operating conditions.

The obtained dynamic characteristics of the actuators are utilized as a basis for designing an active computer-controlled system to suppress the vibration of the flexible cantilever beam. The performance of the control system is evaluated for the beam subjected to step displacements.

The obtained results demonstrate the potential of the NITINOL shape memory actuators as a viable means for damping the vibration of flexible systems.

II. INTRODUCTION

Space structures are typically very flexible and possess a low degree of internal damping. This makes them poor natural platforms for weapons systems and antennae, which must be able to accommodate retargeting maneuvers without detrimental jitter from vibrations and thermomechanical flutter. Vibration control systems, both active and passive, provide an obvious answer to the need to minimize the deformations of space structures subject to low frequency dynamic loading⁽¹⁾.

In passive systems, the vibratory energy is dissipated through, for example, controlled interfacial slip in structural joints^(2,3), or wave propagation at interfacial joints between wave materials⁽⁵⁾. Passive systems have the advantage of being relatively simple, simple to design and simple to construct. Their disadvantages include too severe a limitation in the band of frequencies in which they control efficiently for some applications, and that they generally act at the expense of the rigidity of the structure.

Active control systems suffer neither of these disadvantages. However, these systems are inherently more complicated and we have far less experience with them. Moreover, most of the experience we do have is via theoretical modelling⁽⁶⁻¹⁵⁾. Of the limited number of attempts at the experimental validation and implementation of active control systems⁽¹⁶⁻²⁰⁾, proof mass^(16,17), brushless motors^(18,19) and viscous dampers⁽²⁰⁾ have been among the most commonly used type actuators. Recently, piezo-electric actuators have also gained acceptance, because they have no moving parts and also because of their light weight, high force and low power consumption. Design and testing of active controllers utilizing piezo-actuators have demonstrated their effectiveness in damping out the vibration of flexible beams⁽²⁰⁻²⁴⁾ and hollow cylindrical masts⁽²⁵⁾. In spite of their advantages, piezo-actuators require very high excitation voltages — between 300 to 1400 V — to control vibrations in the micro inch range. Due to such limitations this study has been initiated to utilize the rapidly advancing technology of the NITINOL SHAPE MEMORY ACTUATORS to control the vibrations of flexible systems. This class of actuators represents an attractive alternative as it requires relatively low voltages (about 5 volts) to generate displacements in the neighborhood of an inch. Such distinct physical properties of the NITINOL actuators make them simple to use and to control as well.

NITINOL SHAPE MEMORY ACTUATORS have also proven to be successful in many other applications. Examples include the HITACHI robot hand⁽²⁵⁾ and robotic device⁽²⁶⁾, radiator valves⁽²⁷⁾, green house vents⁽²⁷⁾, and liquid/gas switches⁽²⁷⁾. In all these applications the NITINOL actuators have demonstrated their light weight, large force and displacement capability, and low power consumption. Accordingly, such actuators provide exciting possibilities for miniaturization, simplicity and reliability.

In this study emphasis is placed on measuring the time and frequency response characteristics of differently configured actuators (different wire diameters, different lengths), at different voltage levels (the heating mechanism), different cooling strategies, and different loading levels. This data is used to provide the basis for a mathematical model of the dynamic characteristics of the actuator, which is key input in the design of any vibration control system.

Furthermore, the study demonstrates theoretically and experimentally the feasibility

of using the NITINOL SHAPE MEMORY ACTUATOR to suppress the vibration of a specific structure — a cantilevered beam.

III. THE NITINOL SHAPE MEMORY ACTUATOR

The shape memory actuator relies in its operation on the unique behavior of the alloy NITINOL which is an acronym for Nickel Titanium Naval Ordinance Laboratory, when it undergoes a martensitic transformation. When the actuator, shown as a helical spring in Figure 1, is cooled below its martensitic transformation temperature and deformed, it will remember its original shape and return to it if heated back past the transformation temperature. The phase transformation to austenite produces significant forces as the alloy recovers its original shape. Therefore, the alloy can act as an actuator converting thermal energy to mechanical energy.

With the recent advances in NITINOL technology, phase transformation temperatures of about 40 to 50°C are common. Therefore natural cooling of the actuator, *A*, to ambient room temperature will make it assume its martensite phase. A passive restoring spring, *B*, as shown in Figure 2, can be used to stretch the cold martensite actuator to assume position P_1 . When heat is applied to the actuator, by passing an electric current through it, it undergoes the phase transformation, shrinks to assume a new position, P_2 , and provides in the process a significant force F . This force can pull the piston, *C*, inside the cylinder, *D*, in effect moving the end *E* relative to the end *O*. Accordingly, if the two ends, *E* and *O*, are connected to two points on the flexible structure, the spacing between these points can be controlled within acceptable limits in the presence of external disturbances. Figure 3 shows typical placement arrangements of the NITINOL actuator in a generic space structure. In this figure three basic configurations of the actuator are used. In the first two configurations, the actuator is shaped as a helical spring to perform either linear or angular actuations. In the third configuration, the actuator is a straight wire. The helical configurations are suitable for producing large deformations whereas the simple straight configuration lends itself to generate smaller deflections.

The performance of any of these configurations will depend on the dynamic behavior of the actuator alloy, as influenced by its geometrical and physical properties, as well as

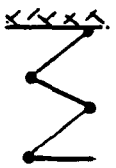
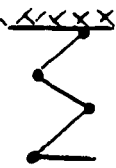
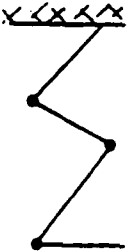
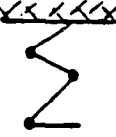
| ACTUATOR SHAPE | TEMPERATURE | STRESS | PHASE |
|--|-------------|-------------------|------------|
| 1.  | HIGH | UNDEFORMED | AUSTENITE |
| 2.  | LOW | UNDEFORMED | MARTENSITE |
| 3.  | LOW | DEFORMED | MARTENSITE |
| 4.  | HIGH | ORIGINAL SHAPE | AUSTENITE |

FIGURE 1. SHAPE MEMORY EFFECT.

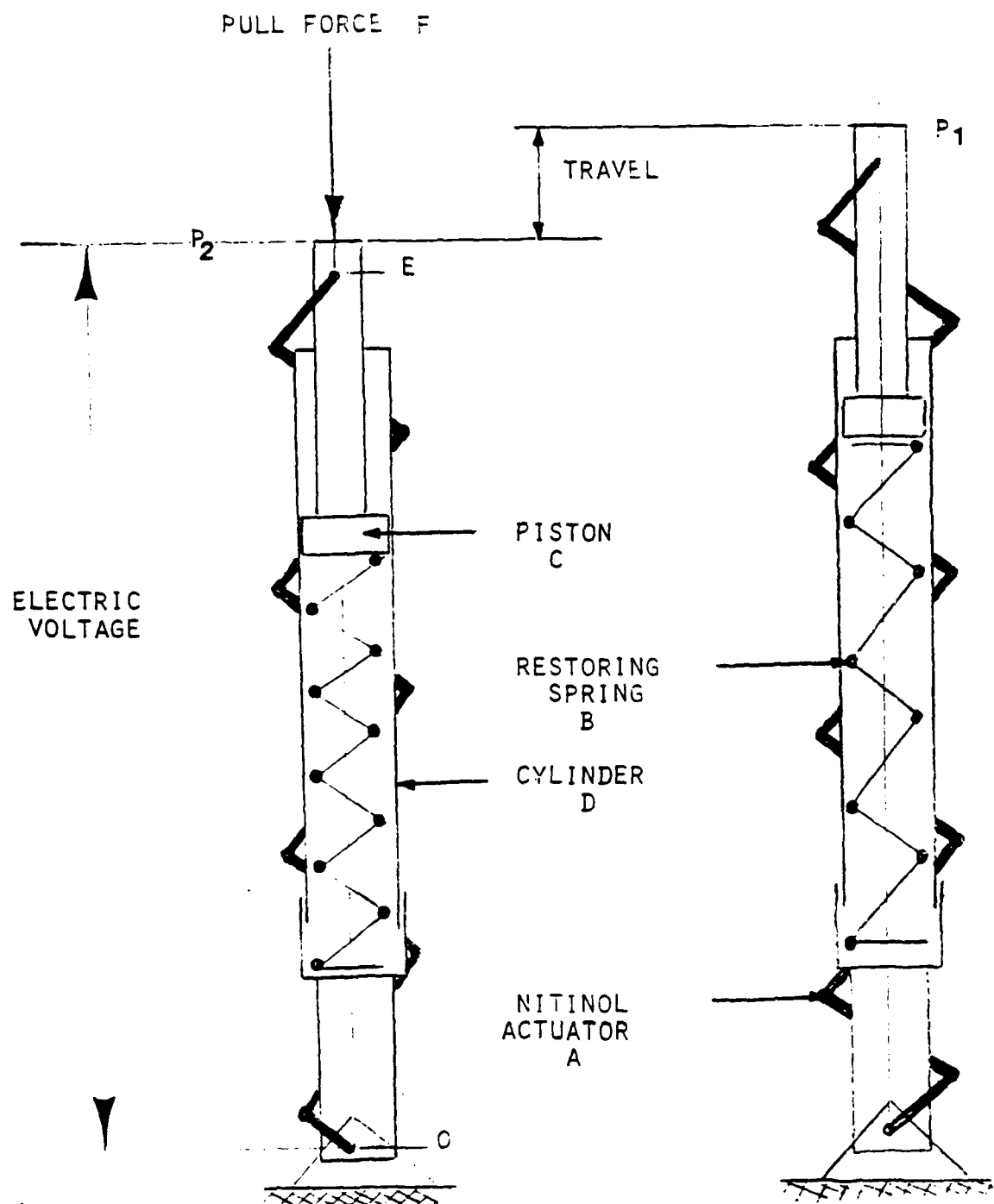


FIGURE 2. SCHEMATIC DRAWING OF A SHAPE MEMORY ACTUATOR.

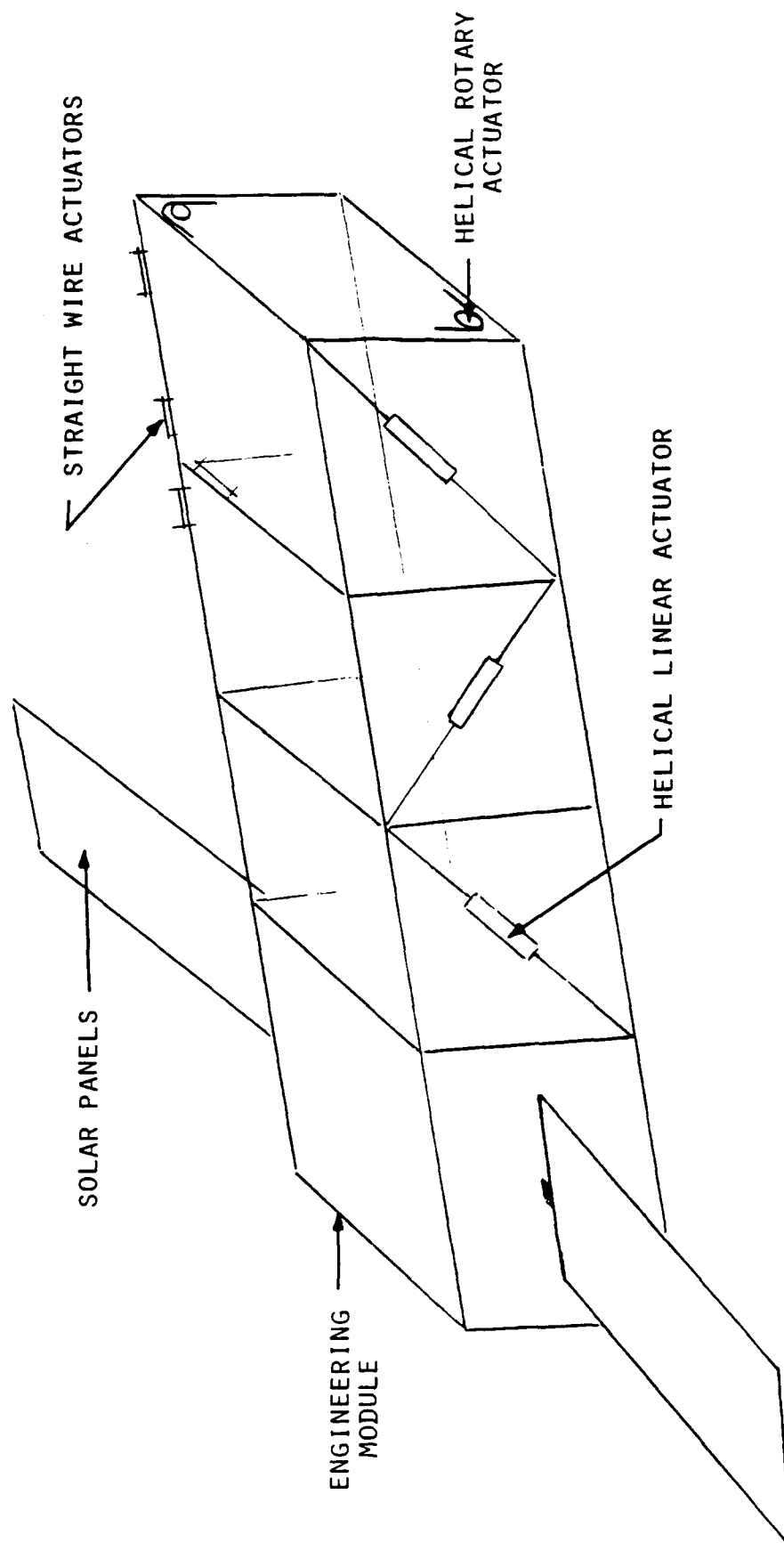


FIGURE 3. TYPICAL PLACEMENT ARRANGEMENTS
OF NITINOL ACTUATORS IN GENERIC SPACE STRUCTURE.

the design and operating parameters of the actuator itself.

IV. DYNAMIC CHARACTERISTICS OF NITINOL ACTUATORS

The dynamic characteristics of NITINOL actuators are determined from measuring the time and frequency response characteristics of helical and straight wire actuators of different geometrics under different operating conditions.

A. The Tested Actuators

Table 1 lists the main properties of the NITINOL alloy used in manufacturing the various actuators by Innovative Technology International, Inc. Table 2 lists the main geometrical parameters of the actuators considered in this study.

B. Time Response

1. Testing facility.

Figure 4 shows a schematic drawing of the test set-up used in monitoring the time response of the NITINOL actuators. The NITINOL actuator, *A* is placed in the set-up such that one end of it is clamped to a tube, *B*, while its other end is attached to another tube, *C*. The two tubes are free to move relative to each other in a telescopic fashion. Phenolic plastic is used to manufacture these two tubes in order to make them electrically non-conducting. In this way, all the inputted electric power will be used to heat the NITINOL actuator.

The relative motion of the two tubes is monitored continuously by the non-contacting Linear Variable Differential Transformer (LVDT), *G*. This transducer provides a linear voltage over a large travel range (0.025 m) and offers no frictional resistance which would affect the obtained results.

Heating the NITINOL actuator, by applying an electric voltage, causes it to shrink thereby forcing the telescopic tube, *C*, inside tube, *B*. This motion is resisted by a return spring, *D*, and weight, *E*. When the electric voltage is switched off the actuator will cool, past its transformation temperature. The potential energy stored in the return spring and the weight will return the actuator to its original length. The upward and the downward motions of the actuator are monitored on a chart recorder, along with the time history of

TABLE 1. MAIN PROPERTIES OF NITINOL ACTUATORS

| PROPERTIES | VALUES |
|--|------------------------|
| <u>I. Phase Properties</u> | |
| 1. Transformation Temperature (T_T) | 50° C |
| 2. Latent Heat of Transformation (Q_L) | 12,620 J/kg |
| 3. Percentage Shape Memory | 4-8% |
| <u>II. Physical Properties</u> | |
| 4. Density (ρ) | 6.5 gm/cm ³ |
| 5. Thermal Conductivity (k) | 0.18 w/cm°C |
| 6. Thermal Capacitance (c_p) | 883 J/kg°C |
| 7. Coefficient of Thermal Expansion | |
| Martensite | 11E-6 /°C |
| Austenite | 6.6E-6 /°C |
| <u>III. Mechanical</u> | |
| 8. Young's Modulus (E) | 70 GPa |
| 9. Poisson's ratio (ν) | 0.33 |
| 10. Yield Strength (S_y) | ≈ 420 MPa |

TABLE 2. PARAMETERS OF THE ACTUATORS TESTED

| ACTUATOR NO. | TYPE | WIRE DIAMETER (in/cm) | NO. OF TURNS or LENGTH (m) | WEIGHT (gm) | TESTS |
|--------------|----------------|-----------------------|----------------------------|-------------|------------------------------------|
| 1 | H ¹ | .016/0.04 | 4 turns | 0.137 | T ² |
| 2 | H | | 11 turns | 0.326 | T |
| 3 | H | | 15 turns | 0.472 | T |
| 4 | H | | 29 turns | 0.784 | T, F ³ , C ⁴ |
| 5 | H | 0.022/0.055 | 29 turns | 1.657 | T |
| 6 | H | 0.025/0.0625 | 7 turns | 0.643 | T |
| 7 | H | | 12 turns | 0.955 | T |
| 8 | H | | 17 turns | 1.354 | T |
| 9 | H | 0.030/0.075 | 29 turns | 2.998 | T |
| 10 | H | 0.035/0.0875 | 29 turns | 4.225 | T |
| 11 | S ⁵ | 0.016/0.04 | 0.05 m | 0.0428 | T |
| 12 | S | | 0.125 m | 0.107 | T |

H = Helical actuator T = Time response F = Frequency response
C = Cooling strategy S = Straight actuator

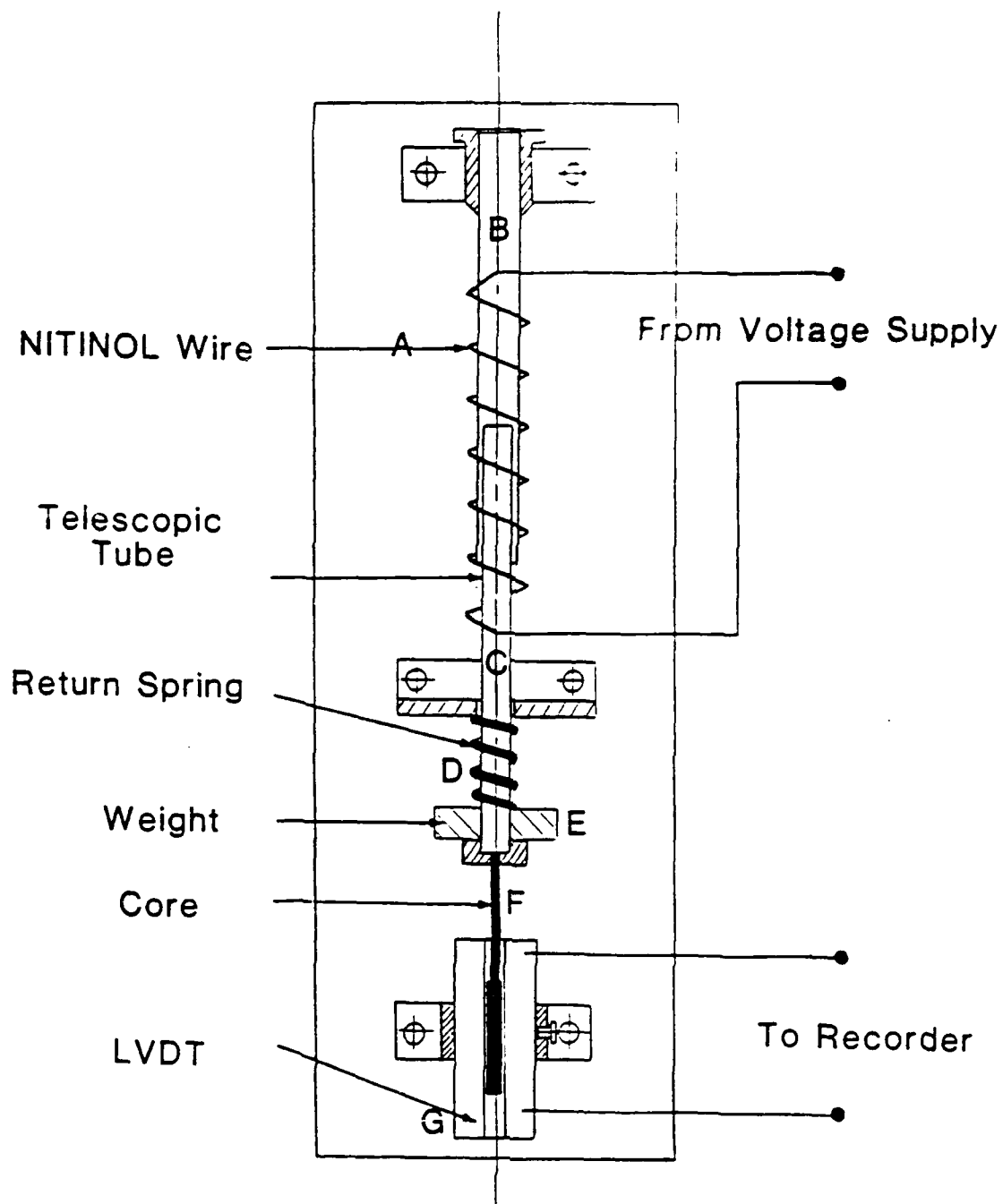


FIGURE 4. TIME RESPONSE TESTING FACILITY.

the applied electric voltage. These recordings are used to determine the effect of applied voltage on the heating and cooling time constants of actuators made of different wire diameters and lengths.

2. Results

2.1 Helical Actuators

(i) **Effect of wire diameter.** The effect of varying the wire diameter on the time response characteristics of the actuators can best be understood by considering a sample of the heating and cooling histories recorded for actuators that have wire diameters of 30 and 35 mils (or 0.075 and 0.0875 cms). Figures 5-a and 5-b provide such a sample for actuators subjected to step voltage changes of 5 volts. The displayed histories are for helical actuators that have a coil diameter of 3/8 in (0.938 cm) and 29 turns.

Figure 5-a shows the response to a step input voltage to be an exponential approach to a steady state plateau. At this point, the actuation force resulting from the phase change is counterbalanced by the compressive force generated in the return spring and a state of equilibrium is attained. When the voltage is switched off, the actuator cools, by natural convection, and softens as it passes through its transformation temperature. In its martensitic phase the actuator can be easily stretched to its original unheated position by the recovery of the potential energy stored in the return spring. The figure shows that the expansion process of the actuator during the cooling phase is also exponential.

Two time constants, τ_h and τ_c , are therefore necessary to quantify the speed of response of the actuator during the heating and the cooling processes respectively. These two time constants are defined as:

$$\tau_h = 1.443 t_{\frac{1}{2}h} \quad (1)$$

and

$$\tau_c = 1.443 t_{\frac{1}{2}c} \quad (2)$$

where $t_{\frac{1}{2}h,c}$ are the times needed to rise or drop to half the maximum amplitude of deflection during heating and cooling respectively.

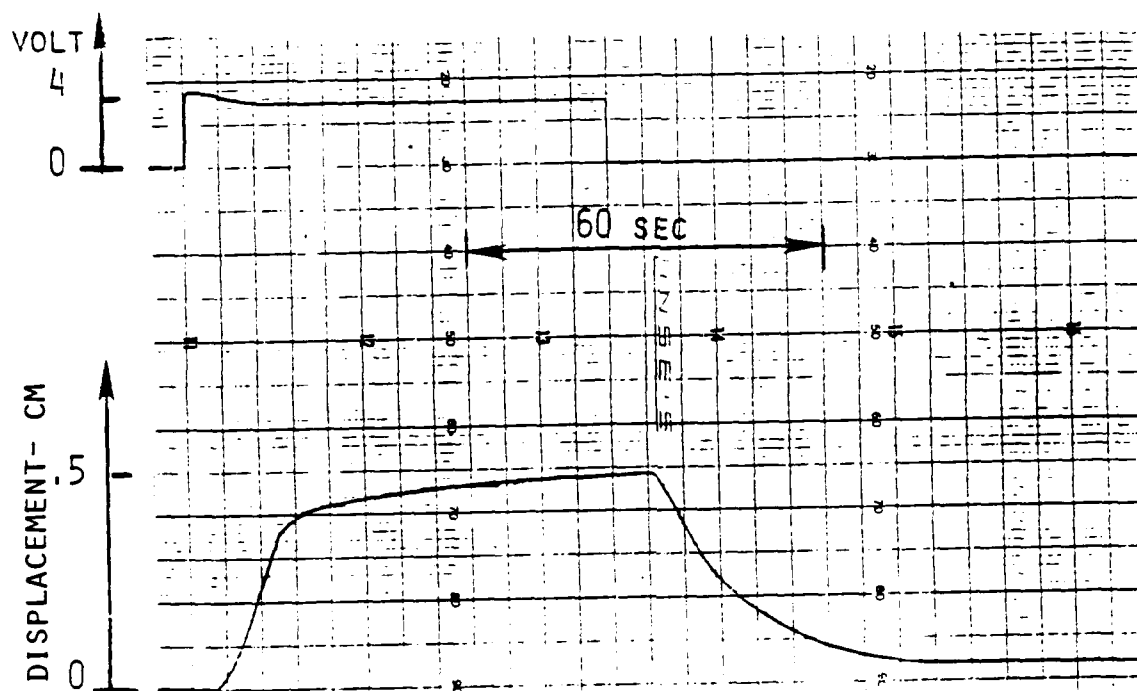


**FIGURE 5-a. HEATING AND COOLING TIME HISTORIES
FOR A 30 mils (0.075 cm) ACTUATOR
WHEN SUBJECTED TO STEP VOLTAGE CHANGES OF 5 VOLTS.**

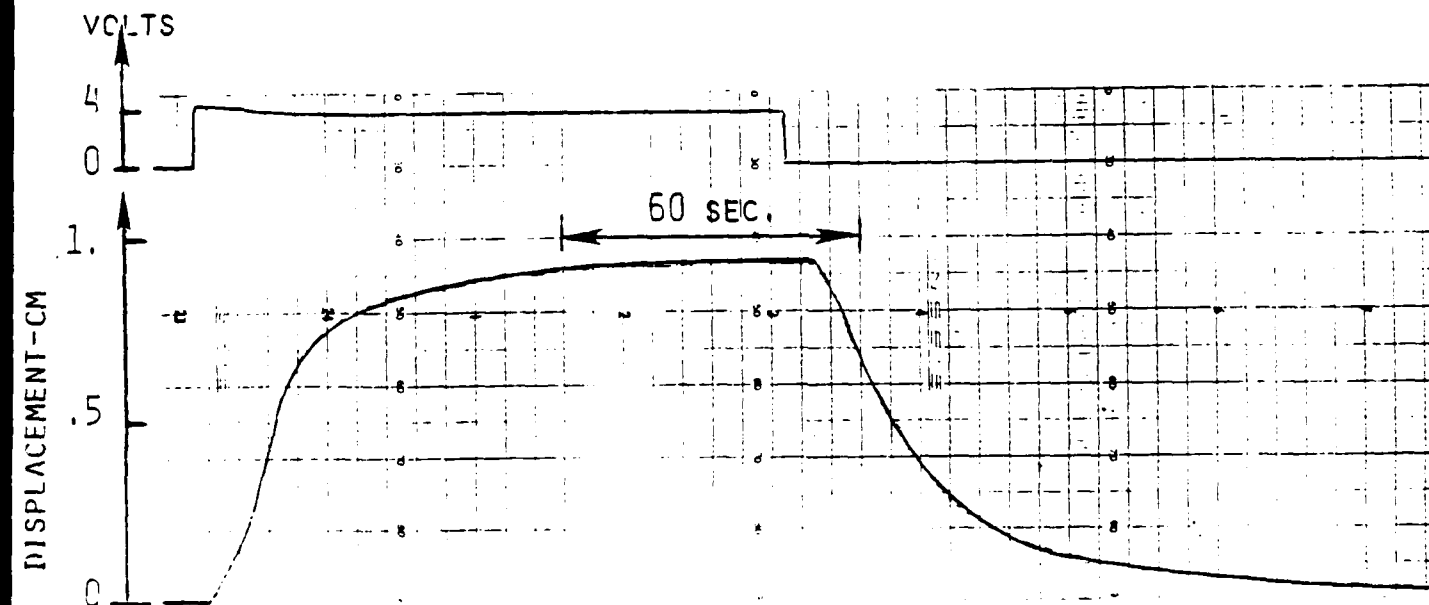


**FIGURE 5-b. HEATING AND COOLING TIME HISTORIES
FOR A 35 mils (0.0875 cm) ACTUATOR
WHEN SUBJECTED TO STEP VOLTAGE CHANGES OF 5 VOLTS.**

For the history illustrated in Figure 5-a we have $\tau_h = 12.1$ s and $\tau_c = 17.3$ s. Also obtained from the figure is the amplitude of maximum travel of the actuator, 0.48 cm, for a return spring with a stiffness, K_s , of 580 N/m.

It is interesting here to note that the time history of the input voltage signal exhibits a degree of overshoot during its application to the actuator. This can be attributed to a change in the electrical resistance of the actuator alloy as it undergoes the phase change from martensite to austenite, an observation reported by Benson et. al.⁽³¹⁾ For a constant current power supply the increase in resistance results in the slight decrease in the voltage that one can observe in the figure.

Figure 5-b indicates similar trends for an actuator made of a 35 mils (0.0875 cm) wire. One should, however, note that increasing the diameter of the actuator wire results in a significant increase in the maximum amplitude of deflection. But, this is at the expense of delaying considerably the speed of response during the heating and the cooling processes. Under the same conditions as those used in testing the 30 mils actuator, the 35 mils actuator produces a maximum travel of 0.95 cm with $\tau_h = 19$ s and $\tau_c = 26$ s.

A compilation of results obtained by analyzing histories of actuators made of wire diameters of 16, 22, 30, and 35 mils (0.04, 0.055, 0.075, and 0.0875 cm), subjected to various levels of step voltage changes, up to 10 volts, is given in Figures 6-a, 6-b, and 6-c.

Figure 6-a shows the effect of changing the level of the input step voltage on the heating time constant, τ_h , for actuators of different wire diameters. Figures 6-b and 6-c show the combined effect of changing the input voltage and wire diameter on the cooling time constant, τ_c , and on the maximum displacement, respectively.

From Figure 6-a, it is clear that increasing the wire diameter results in slowing the response speed, during heating. This is mainly due to the increased mass and thermal capacitance of the actuator. That such a reduction in the response speed can be offset by increasing the level of the input voltage can also be seen from Figure 6-a. The higher the input voltage the faster the actuator will go into its phase transformation and the faster it will be able to provide its force recovery capability.

Increasing the actuator diameter also results in slowing the response during cooling, as manifested in Figure 6-b. Improvement in the speed of cooling can be achieved by

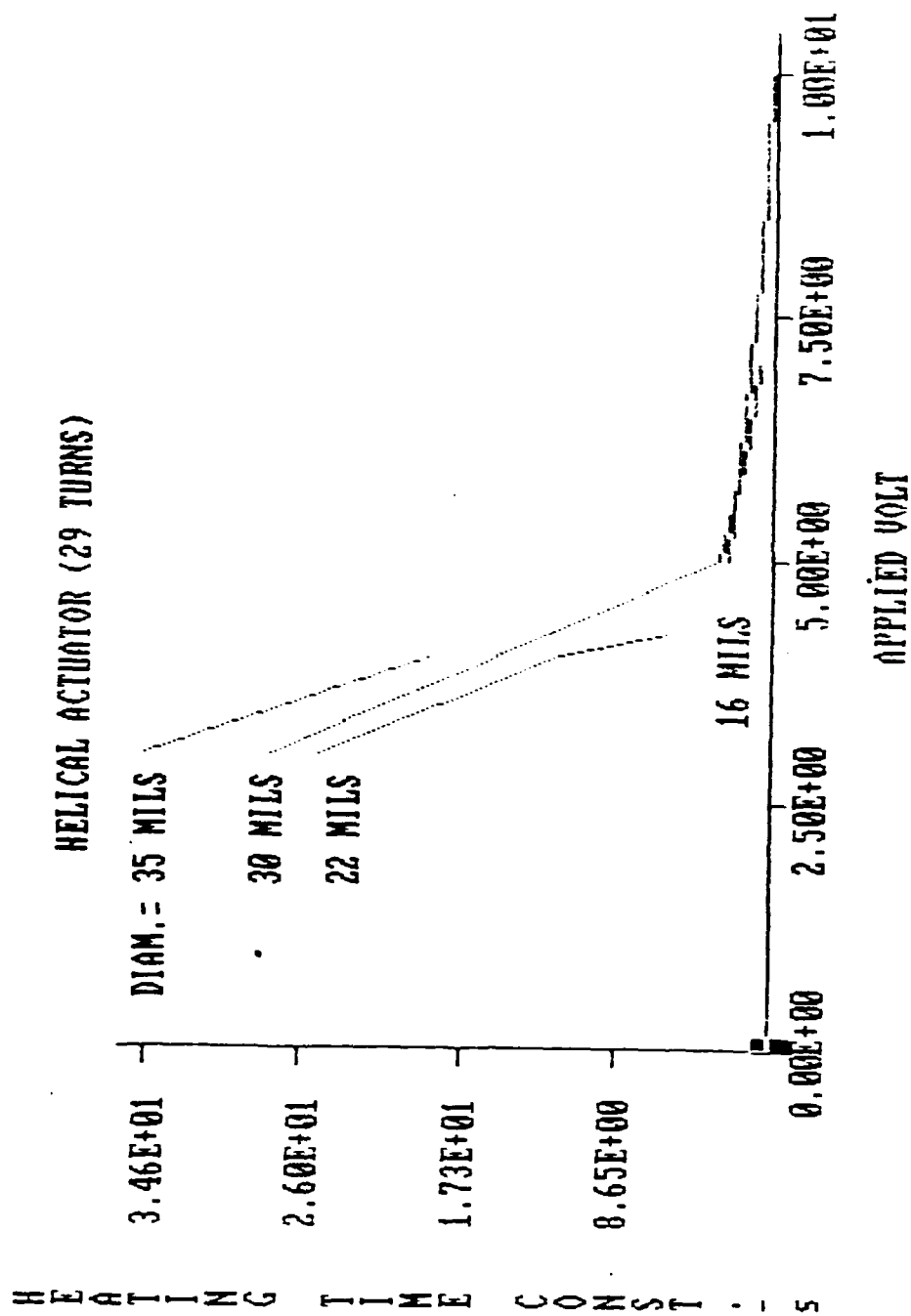


FIGURE 6-a. EFFECT OF WIRE DIAMETER OF HELICAL ACTUATOR
ON ITS HEATING TIME CONSTANT
WHEN SUBJECTED TO DIFFERENT STEP VOLTAGE CHANGES
WITH NUMBER OF TURNS = 29.

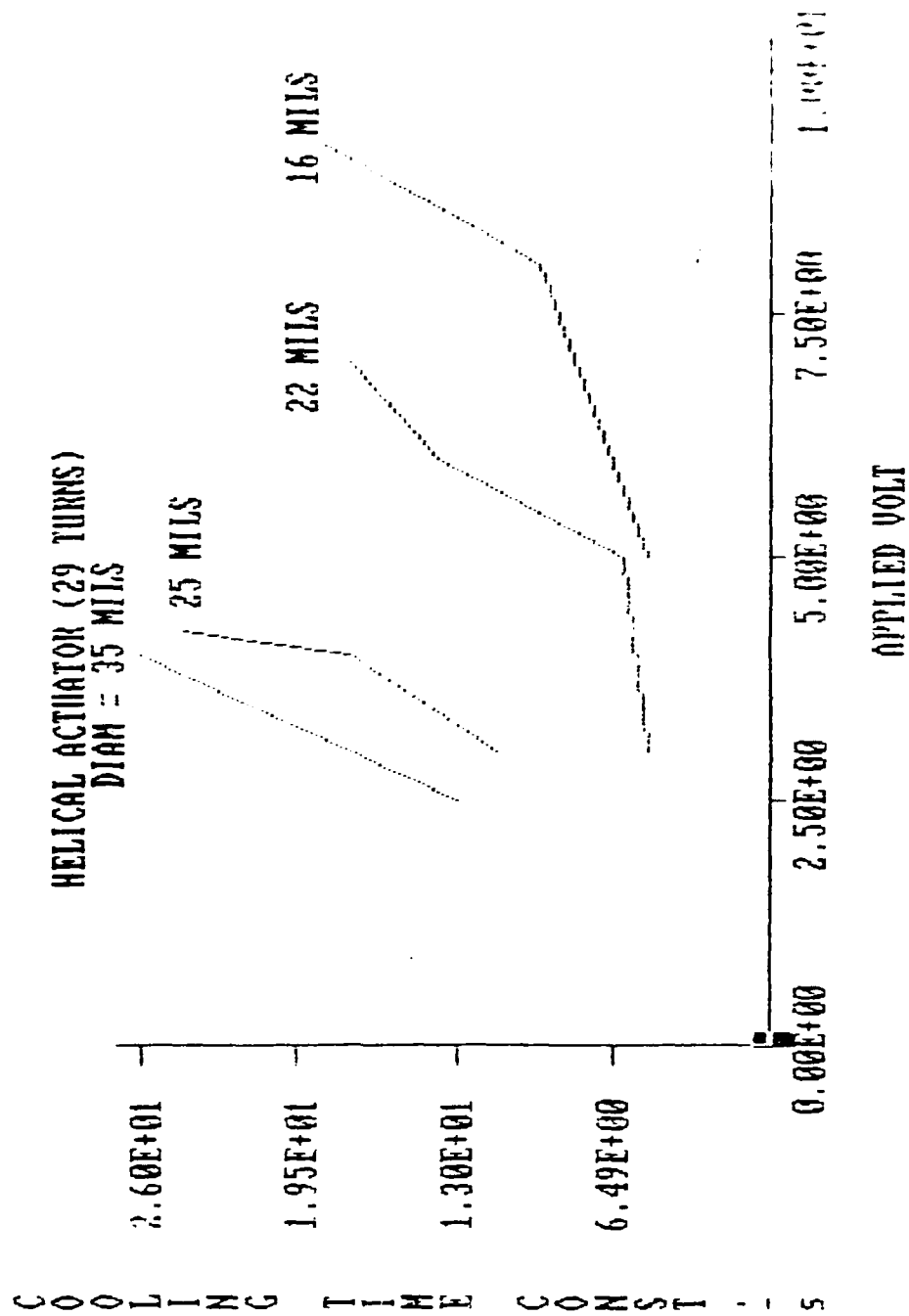


FIGURE 6-b. EFFECT OF WIRE DIAMETER OF HELICAL ACTUATOR
ON ITS COOLING TIME CONSTANT
WHEN SUBJECTED TO DIFFERENT STEP VOLTAGE CHANGES
WITH NUMBER OF TURNS = 29.

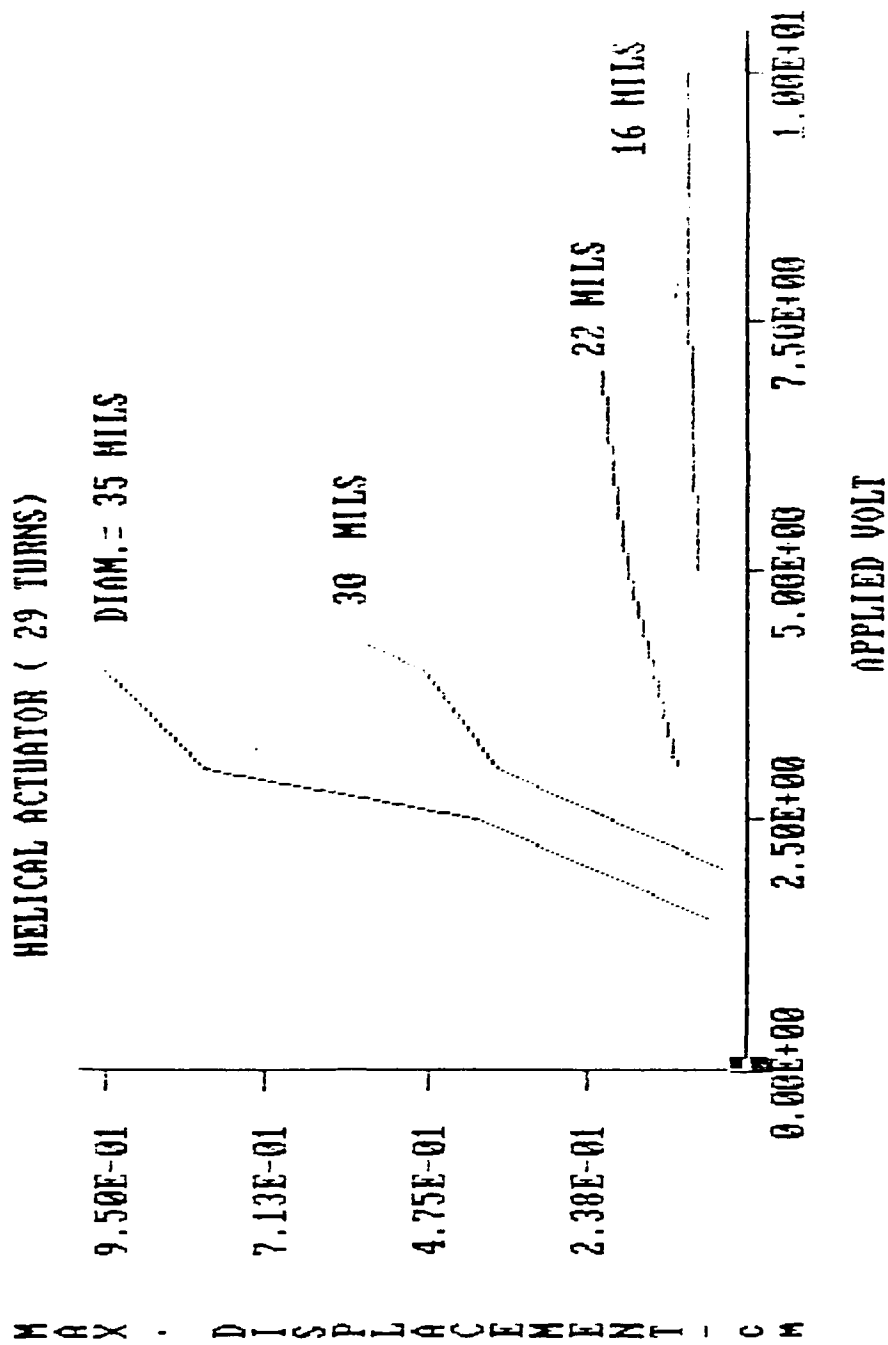


FIGURE 6-c. EFFECT OF WIRE DIAMETER OF HELICAL ACTUATOR
ON ITS MAXIMUM DISPLACEMENT
WHEN SUBJECTED TO DIFFERENT STEP VOLTAGE CHANGES
WITH NUMBER OF TURNS = 29.

reducing the level of input voltage, the opposite of that required for improving the heating speed.

Figure 6-c shows the maximum deflection of the actuators to increase considerably by increasing either the wire diameter or the level of the input voltage.

In general one might conclude, therefore, that for control purposes, where the speed of response is of prime importance, actuators with smaller wire diameters are essential.

(ii) **Effect of wire length.** The effect of the actuator wire length on its time response characteristics can be demonstrated by a sample of the heating and cooling histories for a 16 mils actuator manufactured with 4, 11, and 15 turns. This is shown in Figures 7-a, 7-b, and 7-c respectively. These time responses were obtained for the three actuators subjected to step voltage changes of 3 volts.

The computed heating time constant, τ_h , obtained from these figures are 0.6, 2.2, and 2.6 s for the actuator lengths of 4, 11, and 15 turns, respectively.

Increasing the actuator length results, therefore, in slowing the response during heating. This is to be expected because of the increase in the thermal capacitance of long actuators. Further, increasing the actuator length also increases its electric resistance, R , thereby reducing its electric power consumption, V^2/R , for a given input voltage, V . These two factors account for the observed slow response during heating.

The computed cooling time constants, τ_c , for these same actuators are 11.5, 5.6, and 2.6 s, respectively. Increasing the actuator length produces a significant improvement in the response speed during cooling. Such an observation is attributed first to the increase in the dissipation surface area of the wire and second to the decrease in the input electric power, V^2/R described above.

Finally, a comparison between Figures 7-a through 7-c indicates that the actuator maximum displacement increases as the actuator length decreases.

A compilation of results obtained from the analysis of the histories of other actuators, subjected to step voltage changes up to 10 volts, is summarized in Figures 8-a, 8-b, and 8-c. The figures show the effect that the level of applied step voltage has on the heating time constant, cooling time constant and maximum deflection respectively for actuators of different lengths and 16 mils in diameter.

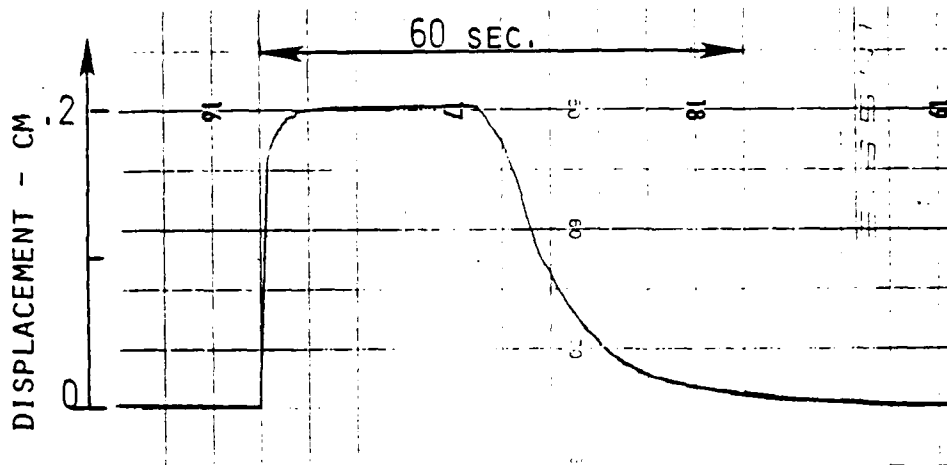


FIGURE 7-a. HEATING AND COOLING TIME HISTORIES
FOR A 16 mils (0.04 cm) ACTUATOR
WHEN SUBJECTED TO STEP VOLTAGE CHANGES OF 3 VOLTS
WITH NUMBER OF TURNS = 4.

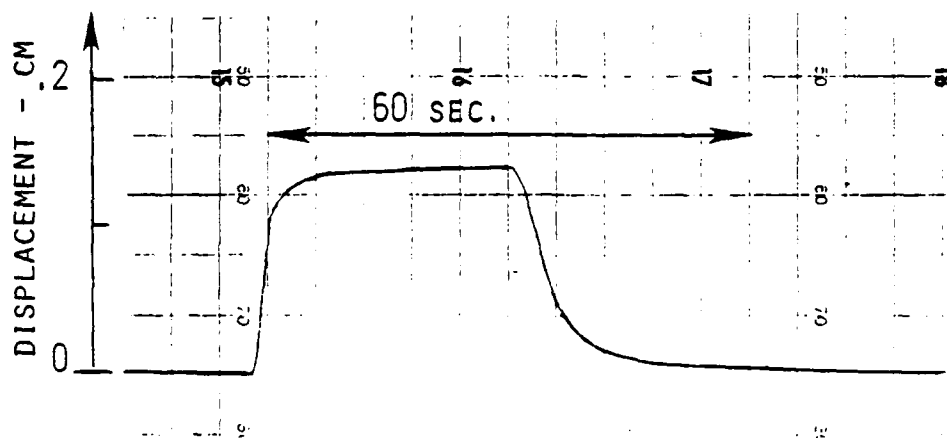


FIGURE 7-b. HEATING AND COOLING TIME HISTORIES
FOR A 16 mils (0.04 cm) ACTUATOR
WHEN SUBJECTED TO STEP VOLTAGE CHANGES OF 3 VOLTS
WITH NUMBER OF TURNS = 11.

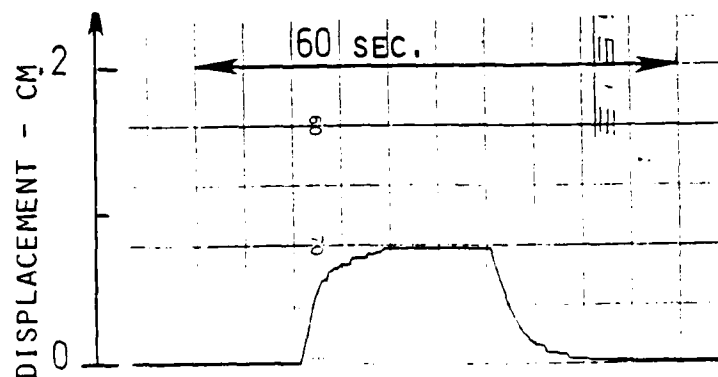


FIGURE 7-c. HEATING AND COOLING TIME HISTORIES
FOR A 16 mils (0.04 cm) ACTUATOR
WHEN SUBJECTED TO STEP VOLTAGE CHANGES OF 3 VOLTS
WITH NUMBER OF TURNS = 15.

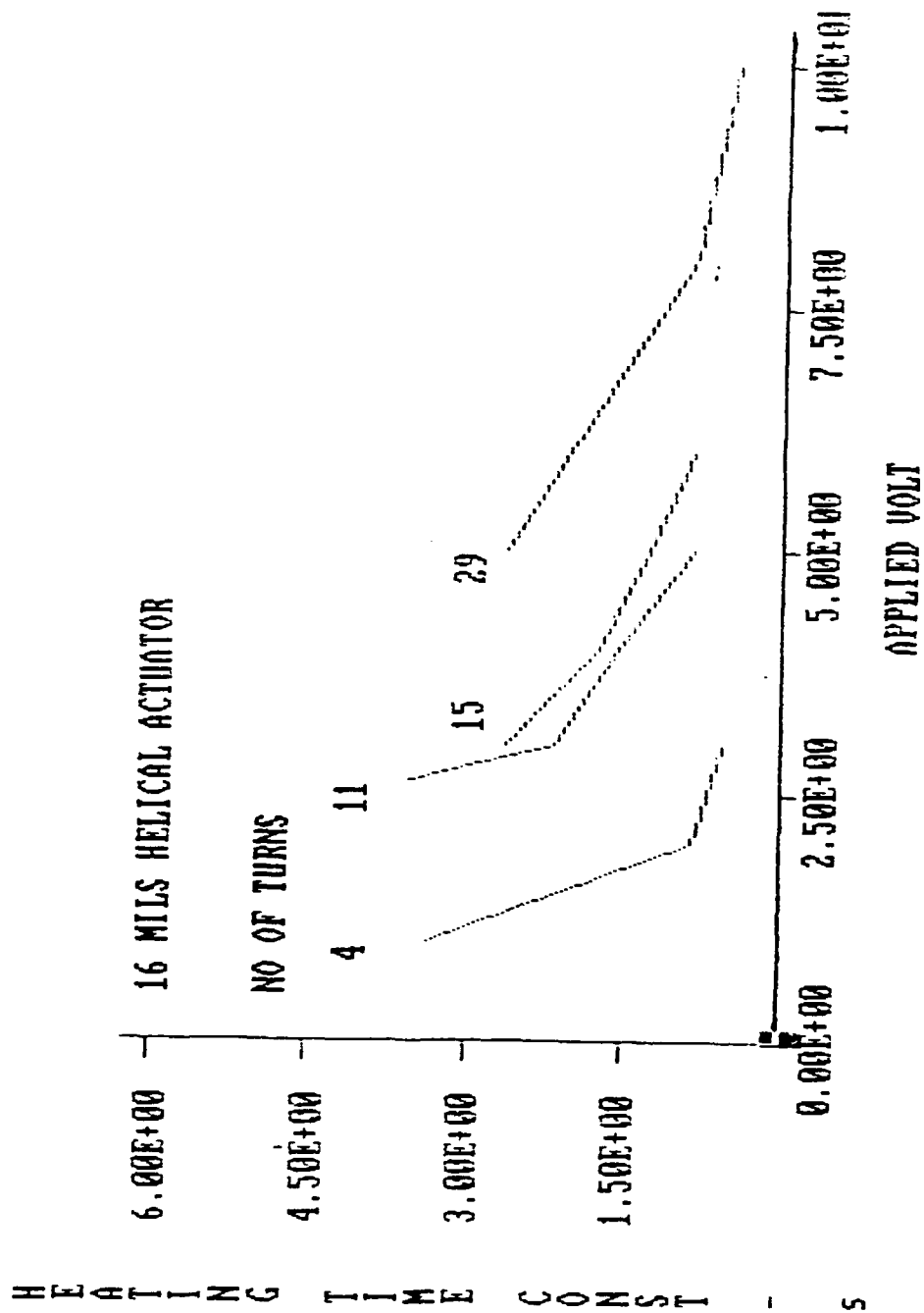
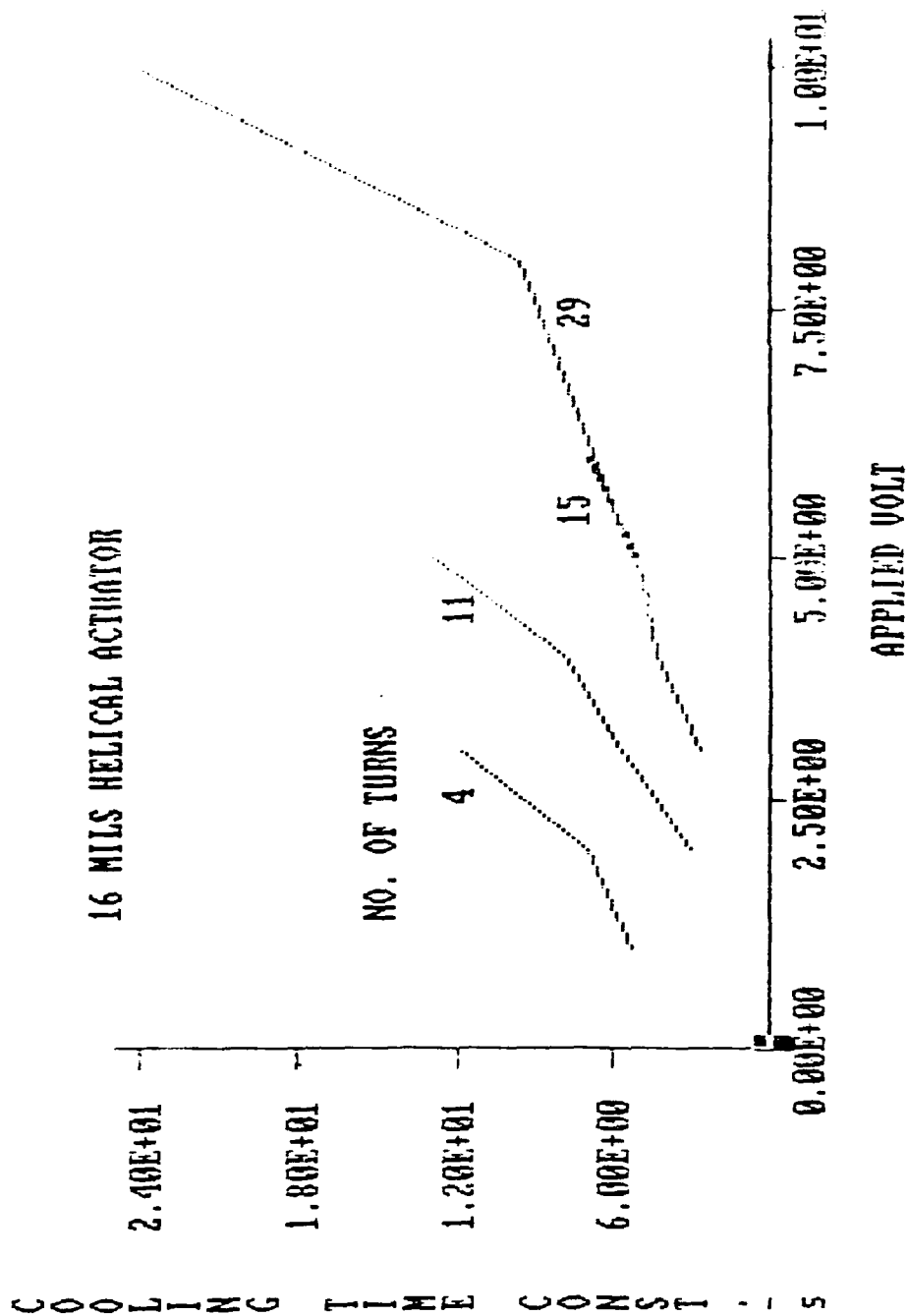


FIGURE 8-a. EFFECT OF WIRE LENGTH OF HELICAL ACTUATOR
ON ITS HEATING TIME CONSTANT
WHEN SUBJECTED TO DIFFERENT STEP VOLTAGE CHANGES
FOR WIRE DIAMETER OF 16 mils (0.04 cm).



**FIGURE 8-b. EFFECT OF WIRE LENGTH OF HELICAL ACTUATOR
ON ITS COOLING TIME CONSTANT
WHEN SUBJECTED TO DIFFERENT STEP VOLTAGE CHANGES
FOR WIRE DIAMETER OF 16 mils (0.04 cm).**

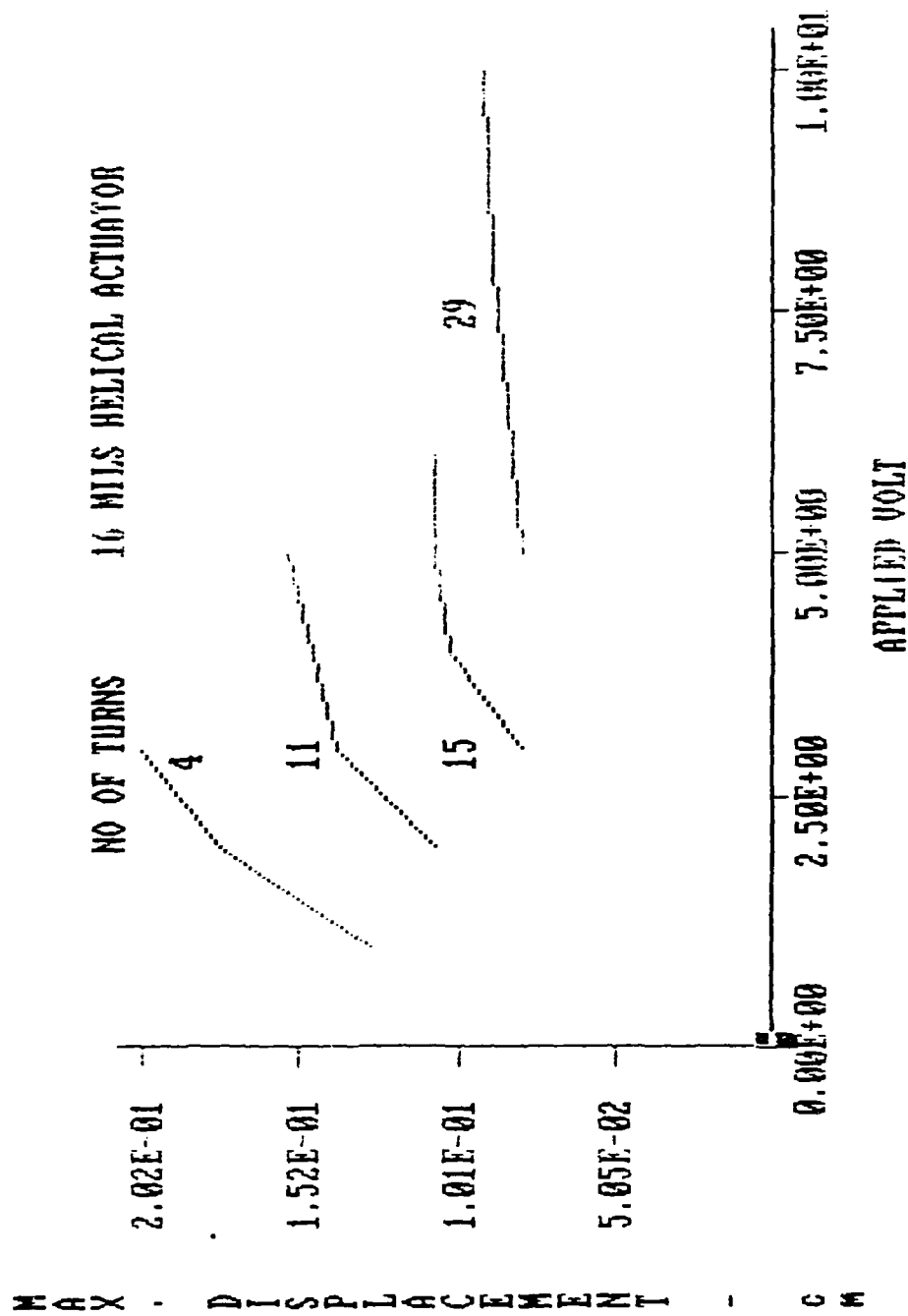


FIGURE 8-c. EFFECT OF WIRE LENGTH OF HELICAL ACTUATOR
ON ITS MAXIMUM DISPLACEMENT
WHEN SUBJECTED TO DIFFERENT STEP VOLTAGE CHANGES
FOR WIRE DIAMETER OF 16 mils (0.04 cm).

Figures 9-a, 9-b, and 9-c show the corresponding characteristics when the wire diameter of the actuator is increased to 25 mils (0.0625 cm).

(iii) **Effect of cooling strategy.** The effect of changing the cooling strategy of the actuator from natural to forced convection, is studied for actuators that are made of 16 mils wires with 29 turns. Figures 10-a through 10-e show the histories during cooling obtained by blowing air on the actuator, at velocities ranging between 0 and 7.2 m/s. In these figures, the actuator is subjected to step voltage changes of 10 volts. It is evident that the speed of response of cooling is improved significantly with increased convection currents. For example, for a convection velocity of 7.2 m/s, the cooling time constant drops to 2.6 s. The figures further indicate that forced air convection has not affected the response history during heating, nor has it affected the maximum amplitude of deflection to any significant extent.

A summary of the results obtained from the analysis of Figures 10-a through 10-e is given in Figure 11.

2.2 Straight Actuators.

The effect of using plain straight wires, on the dynamic characteristics of the actuators is studied for actuators made of 16 mils (0.04 cm) wires.

Figures 12-a, 12-b, and 12-c summarize the effect of the applied voltage on the heating and cooling time constants and on the maximum deflection for straight actuators of different lengths. These figures exhibit the same trends observed in the case of helical actuators but most importantly one could see that the heating and cooling time constants are much smaller. Furthermore, the voltages required to energize the actuator are also much smaller. But these advantages are at the expense of smaller deflections.

C. Frequency Response.

The response characteristics of the NITINOL actuator subjected to pulsating voltage changes of different frequencies is studied for a helical actuator made of 16 mils (0.04 cm) wire with 29 turns.

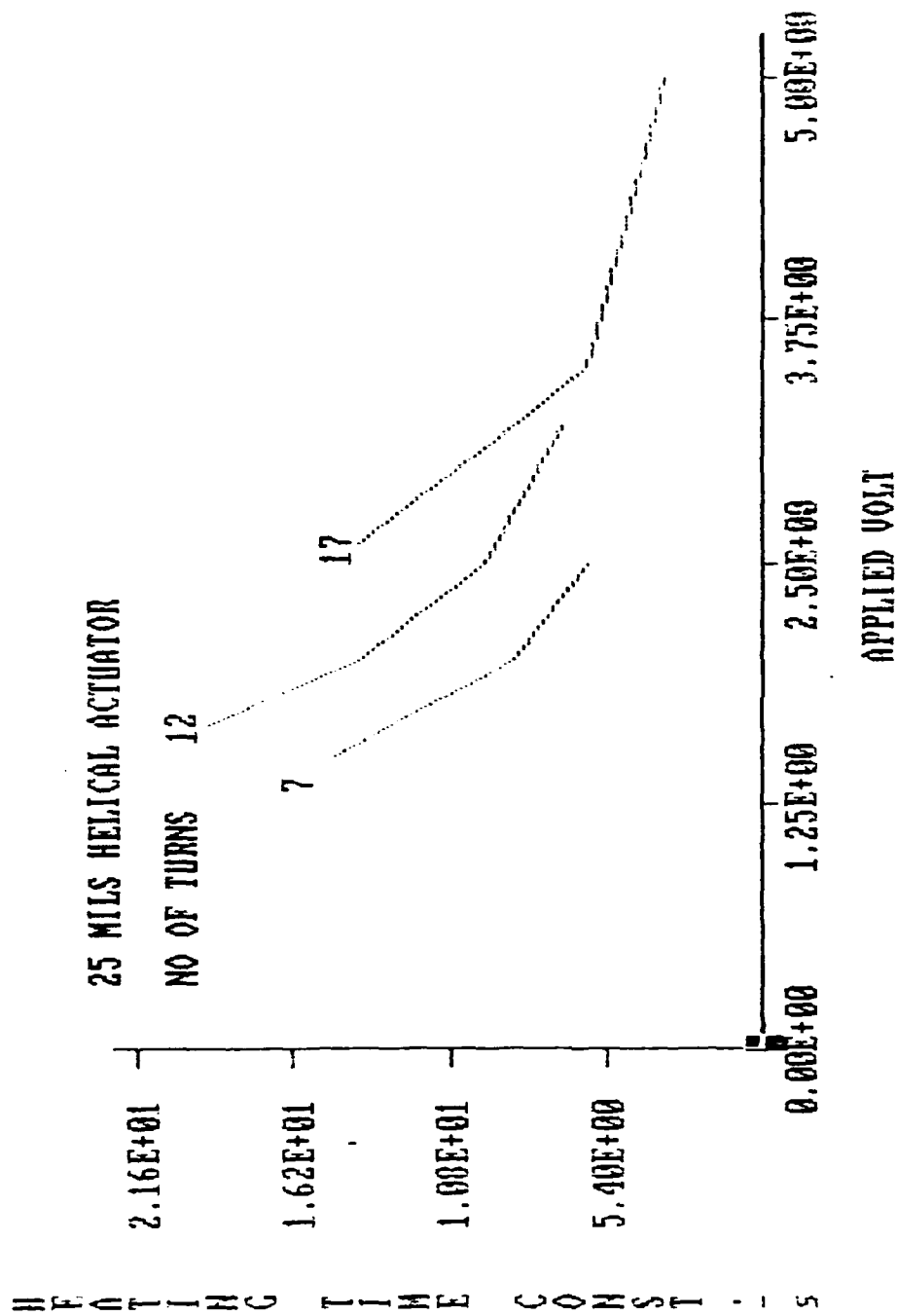


FIGURE 9-a. EFFECT OF WIRE LENGTH OF HELICAL ACTUATOR
ON ITS HEATING TIME CONSTANT
WHEN SUBJECTED TO DIFFERENT STEP VOLTAGE CHANGES
FOR WIRE DIAMETER OF 25 mils (0.0625 cm).

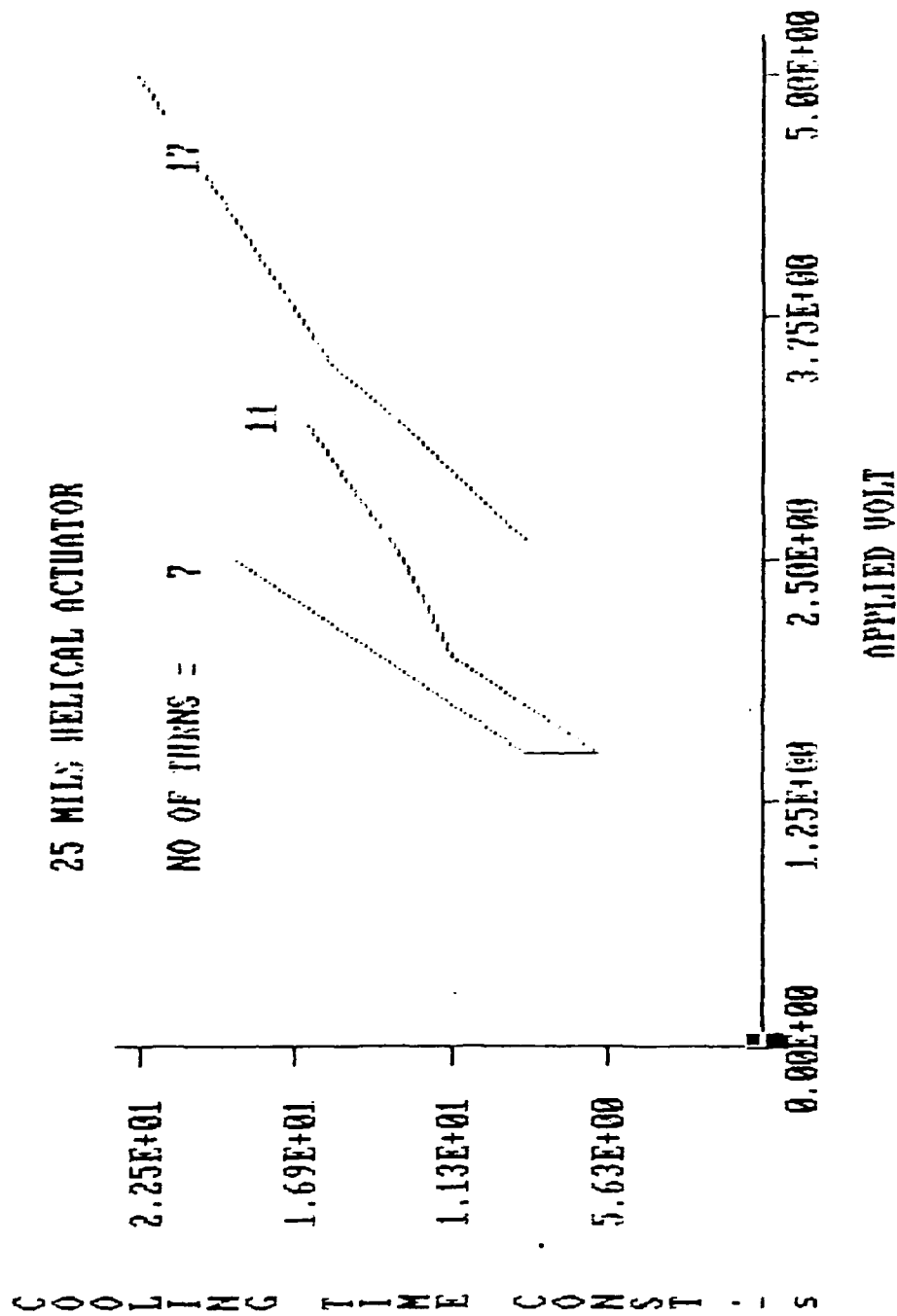
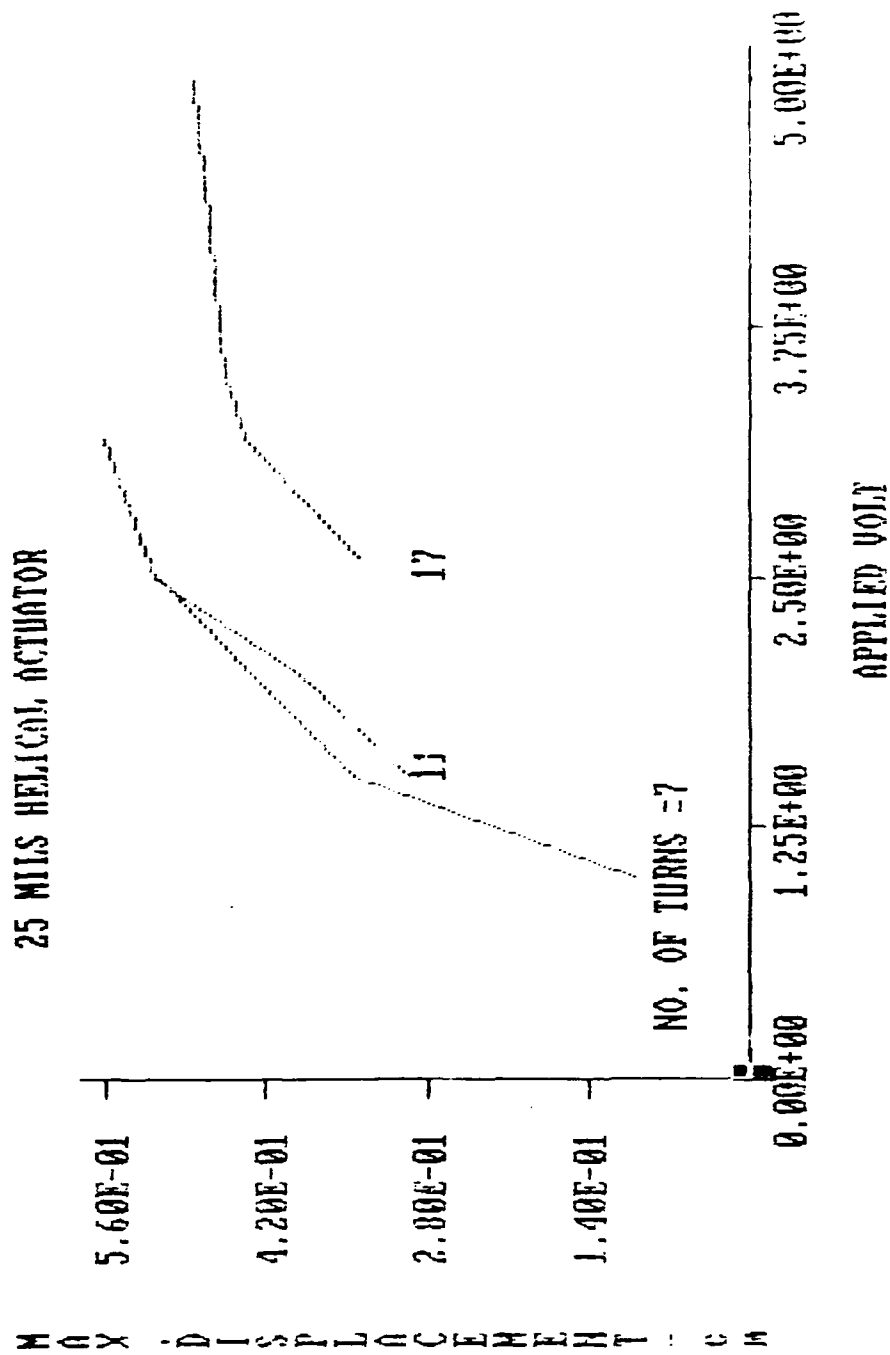


FIGURE 9-b. EFFECT OF WIRE LENGTH OF HELICAL ACTUATOR
ON ITS COOLING TIME CONSTANT
WHEN SUBJECTED TO DIFFERENT STEP VOLTAGE CHANGES
FOR WIRE DIAMETER OF 25 mils(0.0625 cm).



**FIGURE 9-c. EFFECT OF WIRE LENGTH OF HELICAL ACTUATOR
ON ITS MAXIMUM DISPLACEMENT
WHEN SUBJECTED TO DIFFERENT STEP VOLTAGE CHANGES
FOR WIRE DIAMETER OF 25 mils (0.0625 cm).**

TIME HISTORIES FOR HEATING AND COOLING
OF 16 mm (0.04 cm) ACTUATOR
WITH 29 TURNS WHEN SUBJECTED TO 10 VOLT STEP CHANGES

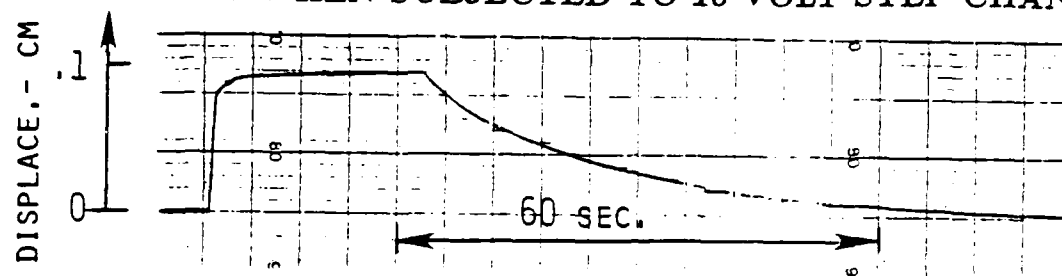


FIGURE 10-a. COOLING AIR VELOCITY = 0 m/s.

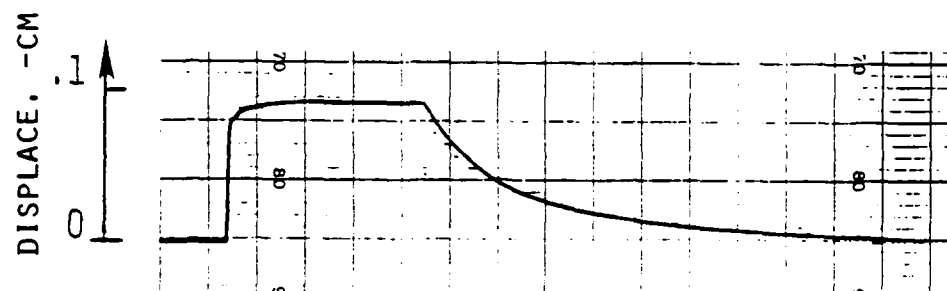


FIGURE 10-b. COOLING AIR VELOCITY = 0.8 m/s

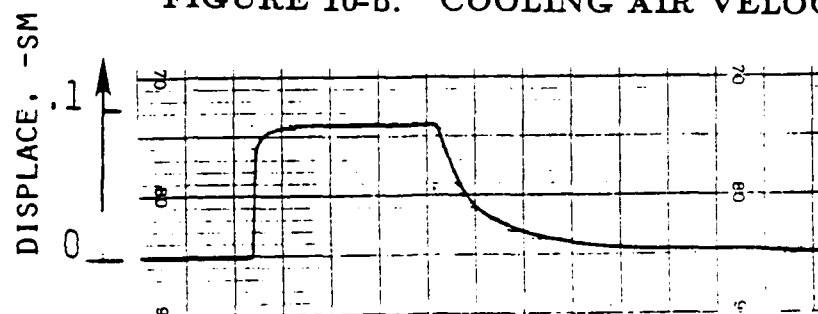


FIGURE 10-c. COOLING AIR VELOCITY = 2.8 m/s

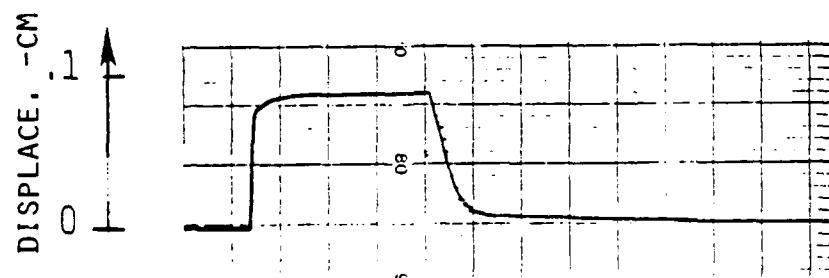


FIGURE 10-d. COOLING AIR VELOCITY = 5.6 m/s



FIGURE 10-e. COOLING AIR VELOCITY = 7.2 m/s

16 MILS HELICAL ACTUATOR (29 TURNS)

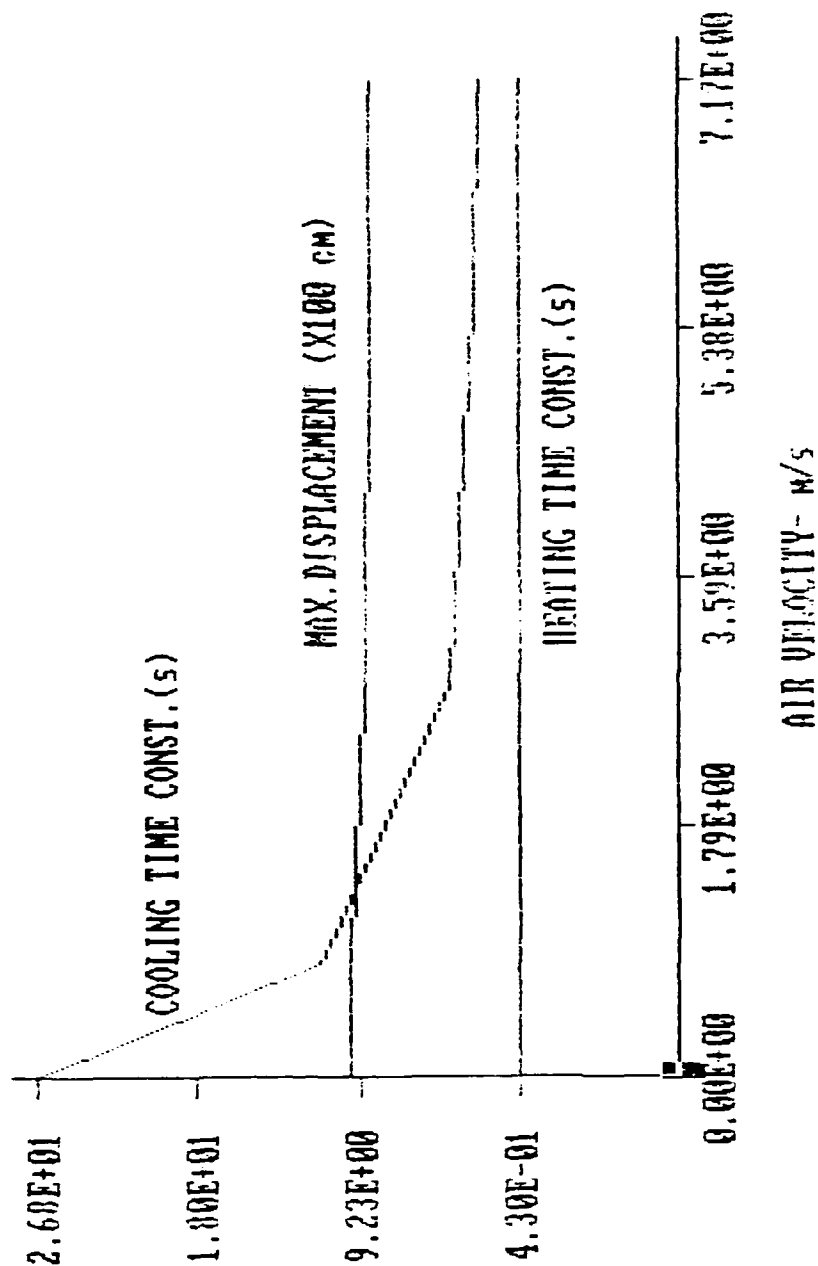


FIGURE 11. EFFECT OF COOLING AIR VELOCITY ON HEATING AND COOLING TIME CONSTANTS AS WELL AS MAXIMUM DISPLACEMENT OF 16 mils ACTUATOR WITH 29 TURNS WHEN SUBJECTED TO 10 VOLTS STEP CHANGES.

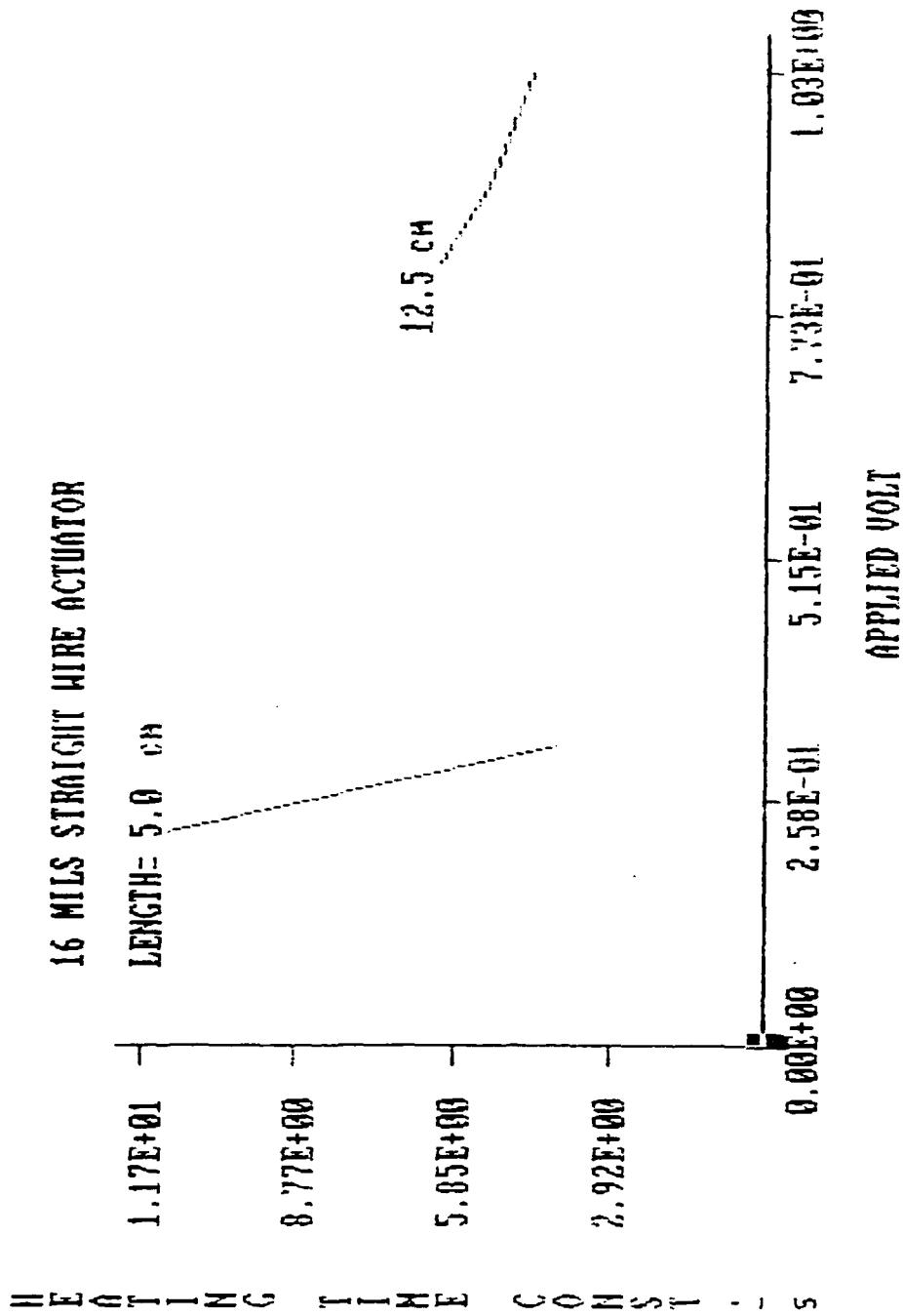


FIGURE 12-a. EFFECT OF APPLIED VOLTAGE
ON THE HEATING TIME CONSTANT OF
STRAIGHT WIRE ACTUATORS OF DIFFERENT LENGTH
AND 16 mils IN DIAMETER.

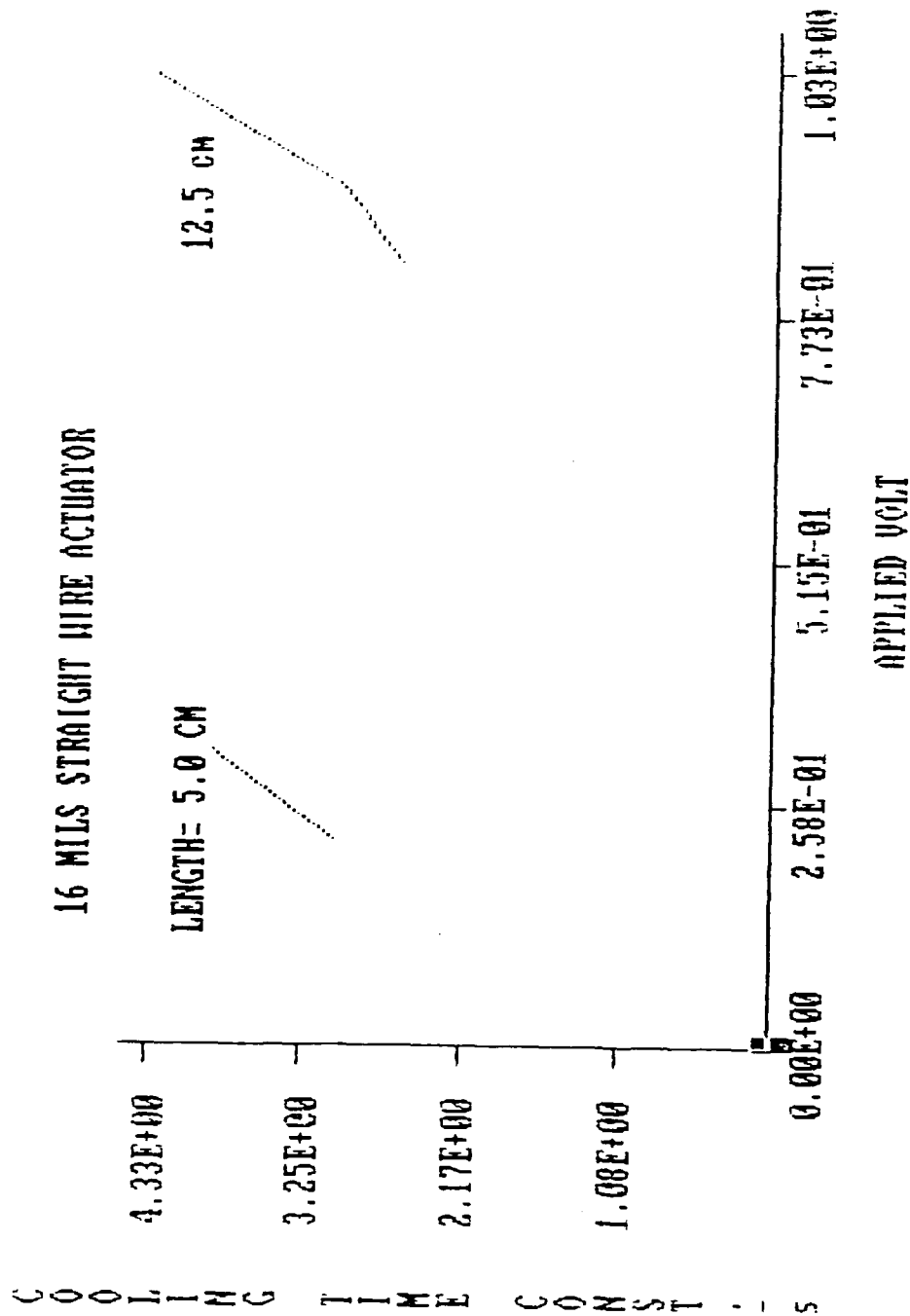


FIGURE 12-b. EFFECT OF APPLIED VOLTAGE
ON THE COOLING TIME CONSTANT OF
STRAIGHT WIRE ACTUATORS OF DIFFERENT LENGTH
AND 16 mils IN DIAMETER.

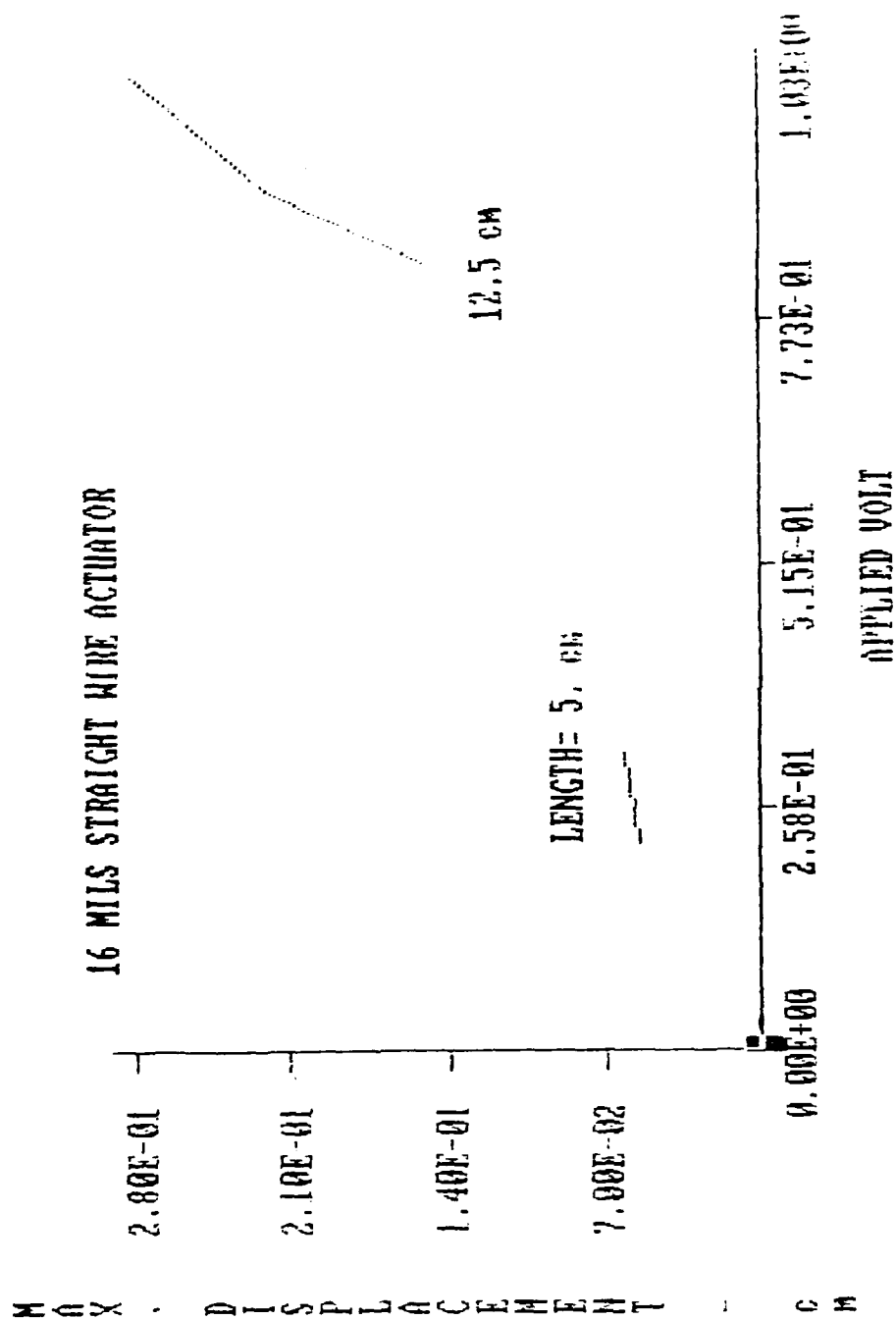


FIGURE 12-c. EFFECT OF APPLIED VOLTAGE
ON THE MAXIMUM DISPLACEMENT OF
STRAIGHT WIRE ACTUATORS OF DIFFERENT LENGTH
AND 16 MILS IN DIAMETER.

1. Testing Facility.

Figure 13 shows a schematic drawing of the testing facility used for studying the frequency response of the NITINOL actuators. The core of the facility is a microprocessor (6510), *A*, to which a peripheral adapter (PIA-MC6821), *B*, is interfaced. The adapter is used to drive a high voltage/high current Darlington Transistor (MC 1416) driver, *C*, which is used to energize a relay coil, *D*. When energized the coil allows for a constant voltage from the power supply, *E*, to be applied across the actuator, *F*. The level of the input voltage step can be controlled by a potentiometer. The resulting displacement of the actuator is monitored by the LVDT displacement sensor. The displacement and input pulsating voltage signals are recorded and plotted on a chart recorder.

2. Results

(i) **With natural cooling.** Figures 14-a, 14-b, and 14-c show the histories of the displacement of the NITINOL actuator when subjected to pulsating voltage inputs of 10 volts, at frequencies of $1/36$, $1/20$, and $1/7$, respectively.

Figure 14-a shows an oscillatory response with the maximum deflection point, *A*, obtained during heating and another maximum, *B*, other than its original position, *C*, obtained during cooling. This type response is attributed to a very slow cooling process which does not allow the actuator to attain its original temperature before the second pulse is applied.

Increasing the frequency of application of the pulsating voltage to $1/10$ Hz results in the response shown in Figure 14-b. The figure indicates that the actuators response is still oscillatory but with reduced amplitude of oscillation. Also, the maximum deflection of the actuator is observed to be reduced slightly with the increased excitation frequency.

Further increase in the excitation frequency to $1/7$ Hz has the actuator reach a static position, as shown in Figure 14-c, which is slightly lower than those attained at the two lower frequencies. Under such conditions the actuator is not responding to the input excitations as it becomes incapable of cooling down because of the frequent heating effect. An equilibrium state is attained in which the heat losses from the actuator are counterbalanced by the electric heat which is supplied over very short periods of time.

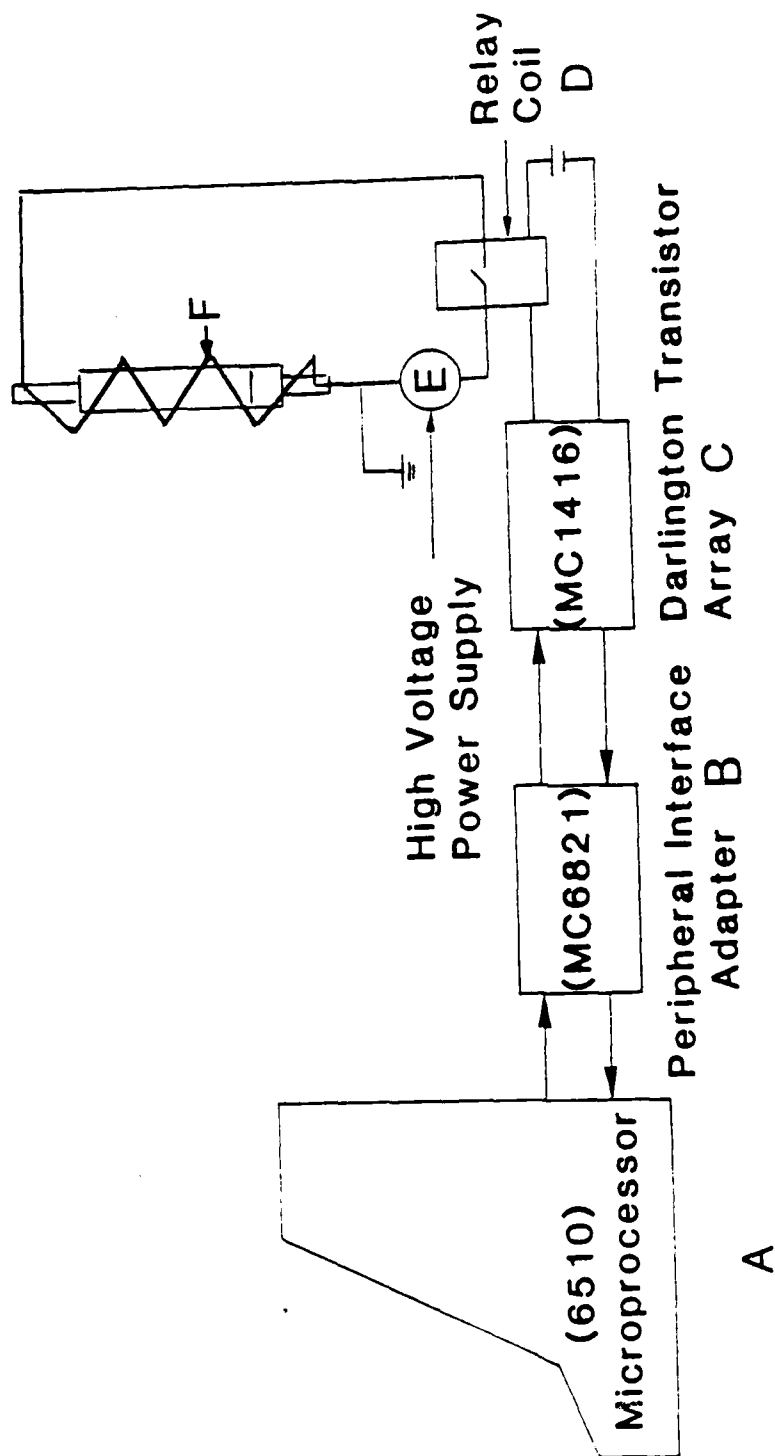


FIGURE 13. SCHEMATIC DRAWING OF THE
FREQUENCY RESPONSE TEST FACILITY.

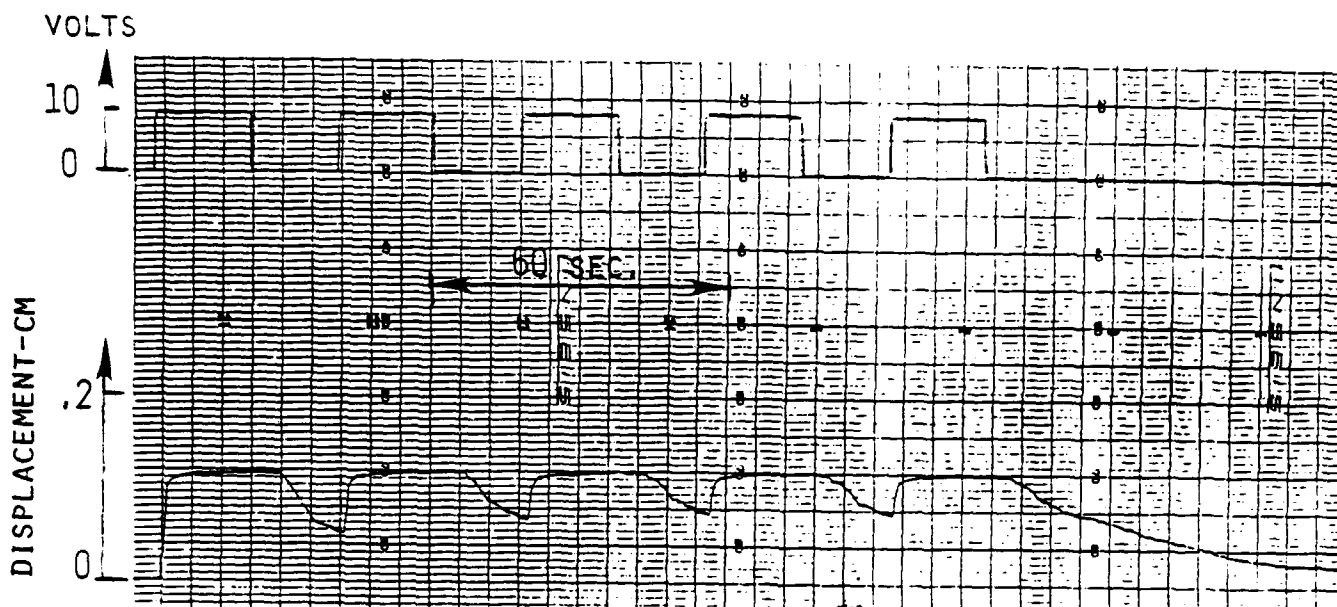


FIGURE 14-a. HEATING AND COOLING TIME HISTORIES
FOR 16 mils ACTUATOR WITH 29 TURNS
WHEN SUBJECTED TO SUDDEN VOLTAGE CHANGES OF 10 VOLTS
AT A FREQUENCY OF $1/36$ Hz UNDER NATURAL COOLING CONDITIONS.

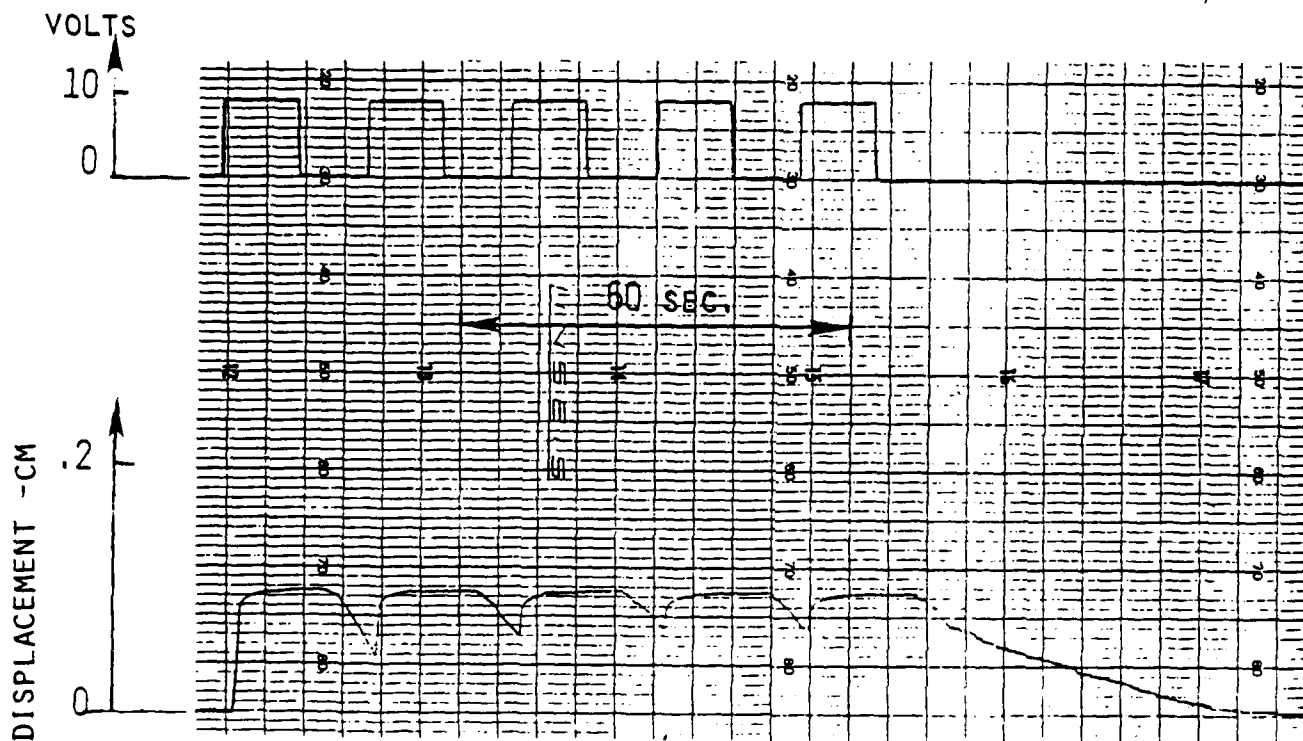


FIGURE 14-b. HEATING AND COOLING TIME HISTORIES
FOR 16 mils ACTUATOR WITH 29 TURNS
WHEN SUBJECTED TO SUDDEN VOLTAGE CHANGES OF 10 VOLTS
AT A FREQUENCY OF $1/20$ Hz UNDER NATURAL COOLING CONDITIONS.

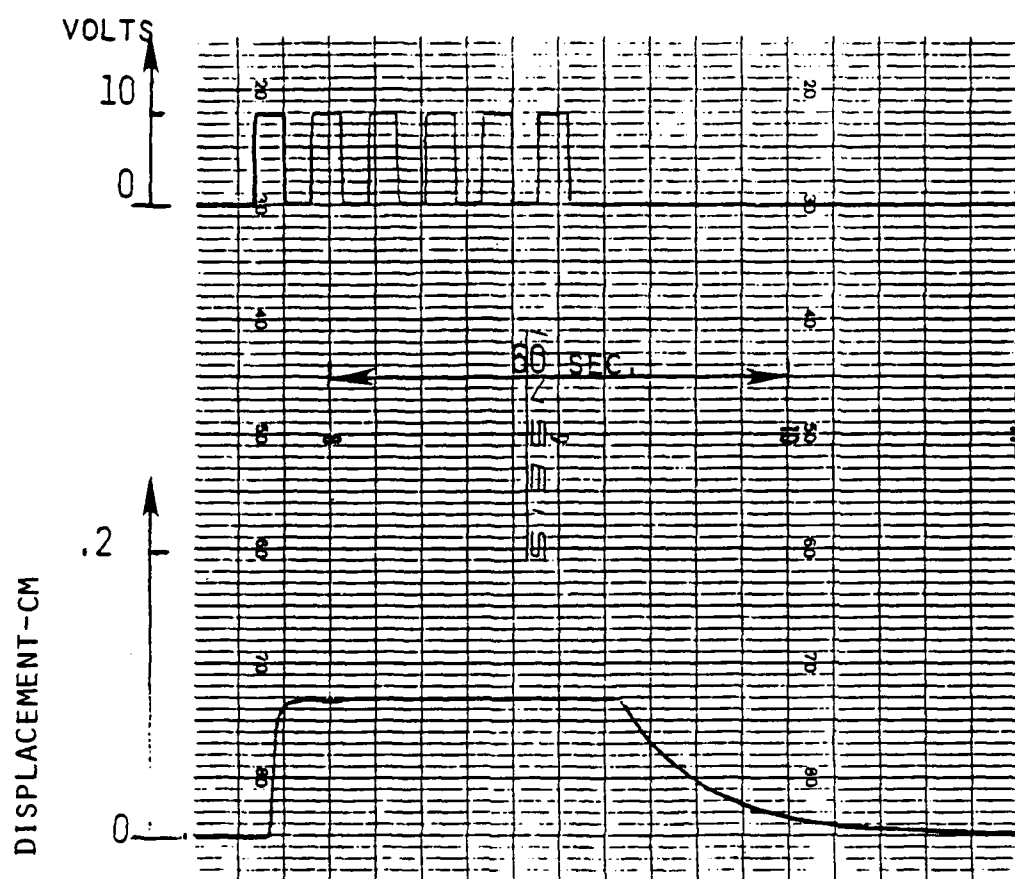


FIGURE 14-c. HEATING AND COOLING TIME HISTORIES
 FOR 16 mils ACTUATOR WITH 29 TURNS
 WHEN SUBJECTED TO SUDDEN VOLTAGE CHANGES OF 10 VOLTS
 AT A FREQUENCY OF $1/7$ Hz UNDER NATURAL COOLING CONDITIONS.

(ii) **With forced cooling strategy.** When air flows past the actuator at a velocity of 7.2 m/s, a considerable improvement in the actuator frequency response characteristics results. Figures 15-a, 15-b, and 15-c show such improvement for excitation frequencies of 1/36, 1/20, and 1/7 Hz respectively. For the two lower frequencies the actuator responds completely to the input excitations, oscillating between its original position and the maximum deflection limit. At the higher frequency limit the performance deteriorates but it is still far superior to that recorded with the natural cooling.

Figure 16 provides a comparison between the frequency response characteristics of the NITINOL actuator as influenced by the cooling strategy. In this figure, the amplitude ratio is defined as the ratio of the actual travel of the actuator to its maximum travel. The considerable improvement obtained for a forced cooling strategy in the actuator frequency response characteristics, is clearly seen.

V. MATHEMATICAL MODELING OF THE DYNAMIC CHARACTERISTICS OF THE NITINOL ACTUATOR

A simplified mathematical model is developed in this section to enable prediction of the dynamical characteristics of the NITINOL actuator. The model will incorporate the requirements of energy and momentum balance as well as a model for the phase transformation. The development of the model is guided by the experimental results obtained in the previous section.

A. The Model.

Figure 17 shows a schematic drawing of a typical NITINOL actuator system similar to the test set-up used in this study.

1. Energy and Phase Transformation Equations.

A voltage, V , and current, I , are applied to a NITINOL actuator, originally at ambient temperature, T_a , results in a temperature, T , which changes with time, t , as governed by an equation of energy balance,

$$\text{energy input} = \text{energy lost} + \text{energy stored},$$

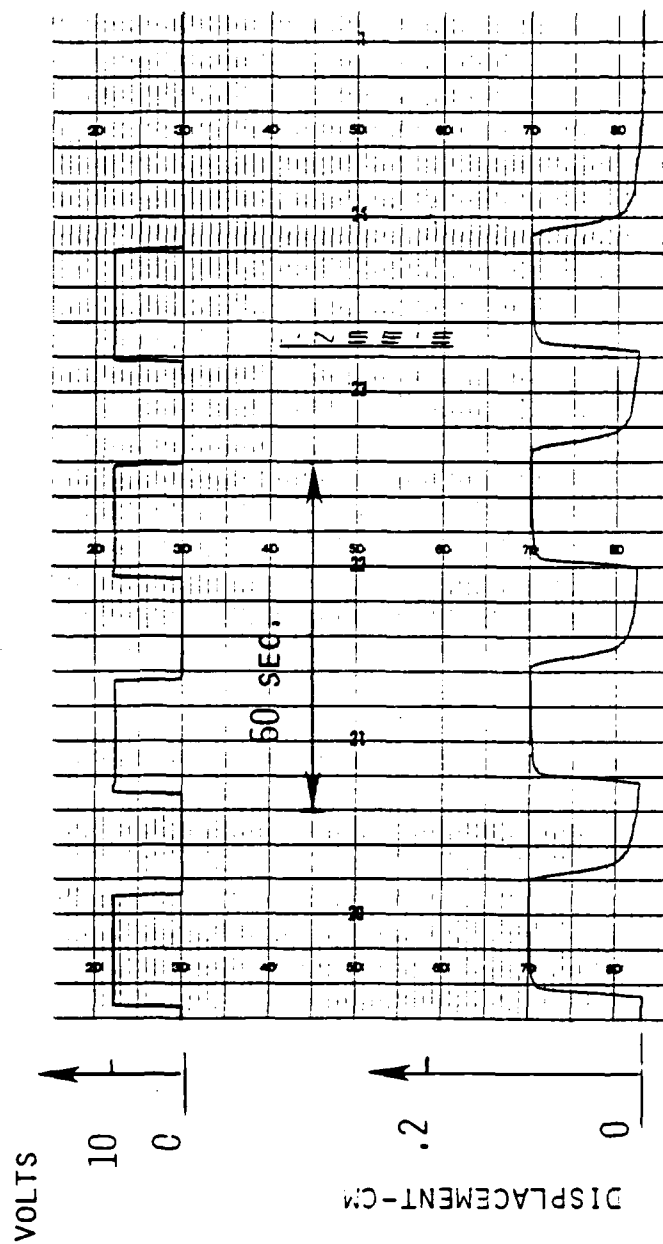
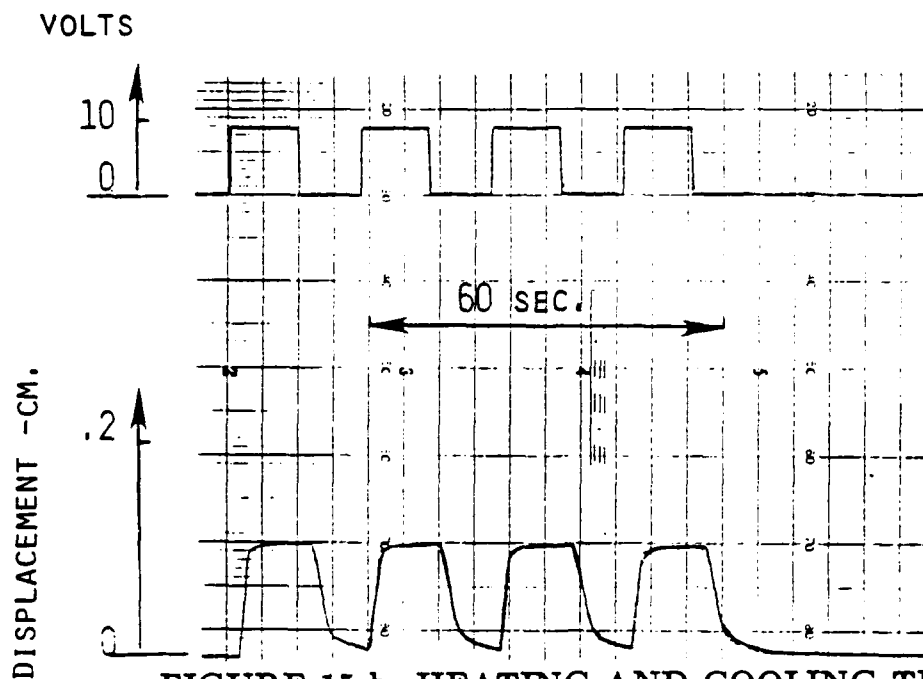
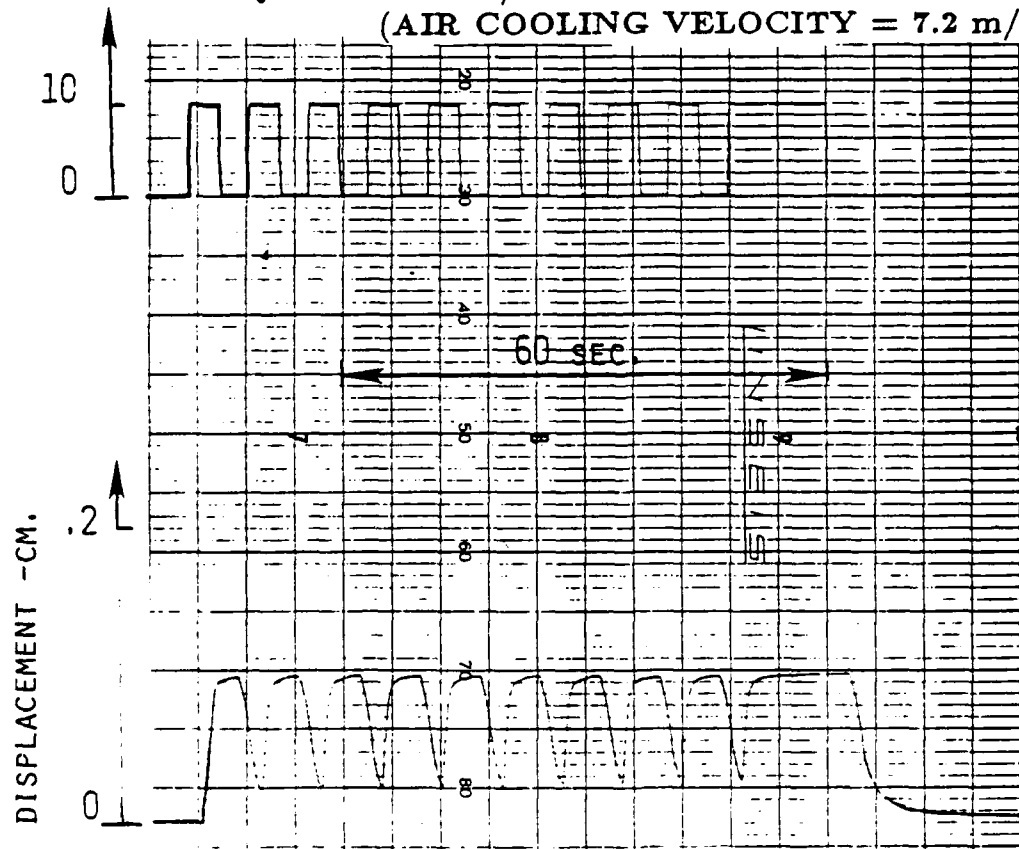


FIGURE 15-a. HEATING AND COOLING TIME HISTORIES
 FOR 16 mils ACTUATOR WITH 29 TURNS
 WHEN SUBJECTED TO SUDDEN VOLTAGE CHANGES OF 10 VOLTS
 AT A FREQUENCY OF 1/36 Hz UNDER FORCED COOLING CONDITIONS
 (AIR COOLING VELOCITY = 7.2 m/s).



**FIGURE 15-b. HEATING AND COOLING TIME HISTORIES
FOR 16 mils ACTUATOR WITH 29 TURNS
WHEN SUBJECTED TO SUDDEN VOLTAGE CHANGES OF 10 VOLTS
VOLTS AT A FREQUENCY OF 1/20 Hz UNDER FORCED COOLING CONDITIONS
(AIR COOLING VELOCITY = 7.2 m/s).**



**FIGURE 15-c. HEATING AND COOLING TIME HISTORIES
FOR 16 mils ACTUATOR WITH 29 TURNS
WHEN SUBJECTED TO SUDDEN VOLTAGE CHANGES OF 10 VOLTS
AT A FREQUENCY OF 1/7 Hz UNDER FORCED COOLING CONDITIONS
(AIR COOLING VELOCITY = 7.2 m/s).**

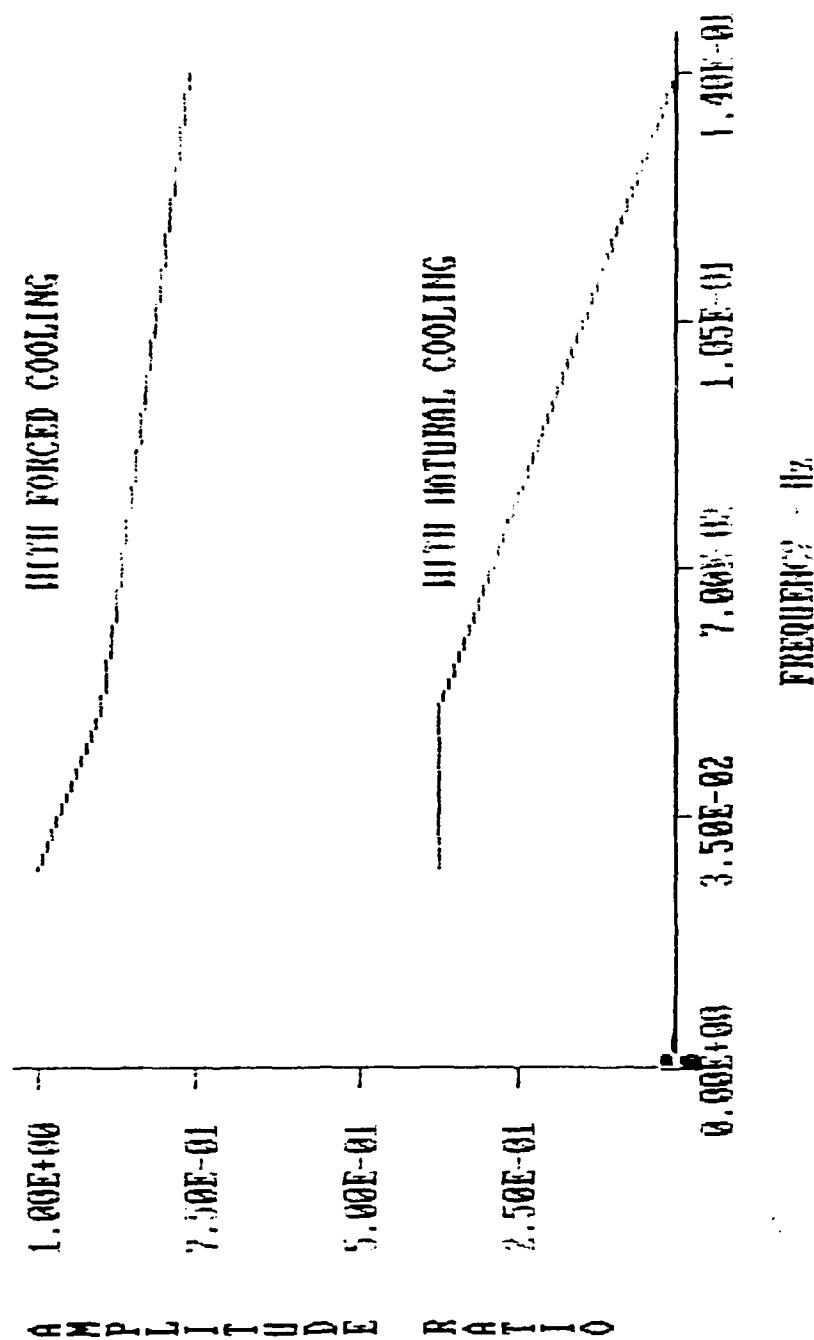


FIGURE 16. A COMPARISON BETWEEN THE
FREQUENCY RESPONSE CHARACTERISTICS OF 16 mils ACTUATOR
UNDER NATURAL AND FORCED COOLING STRATEGIES.

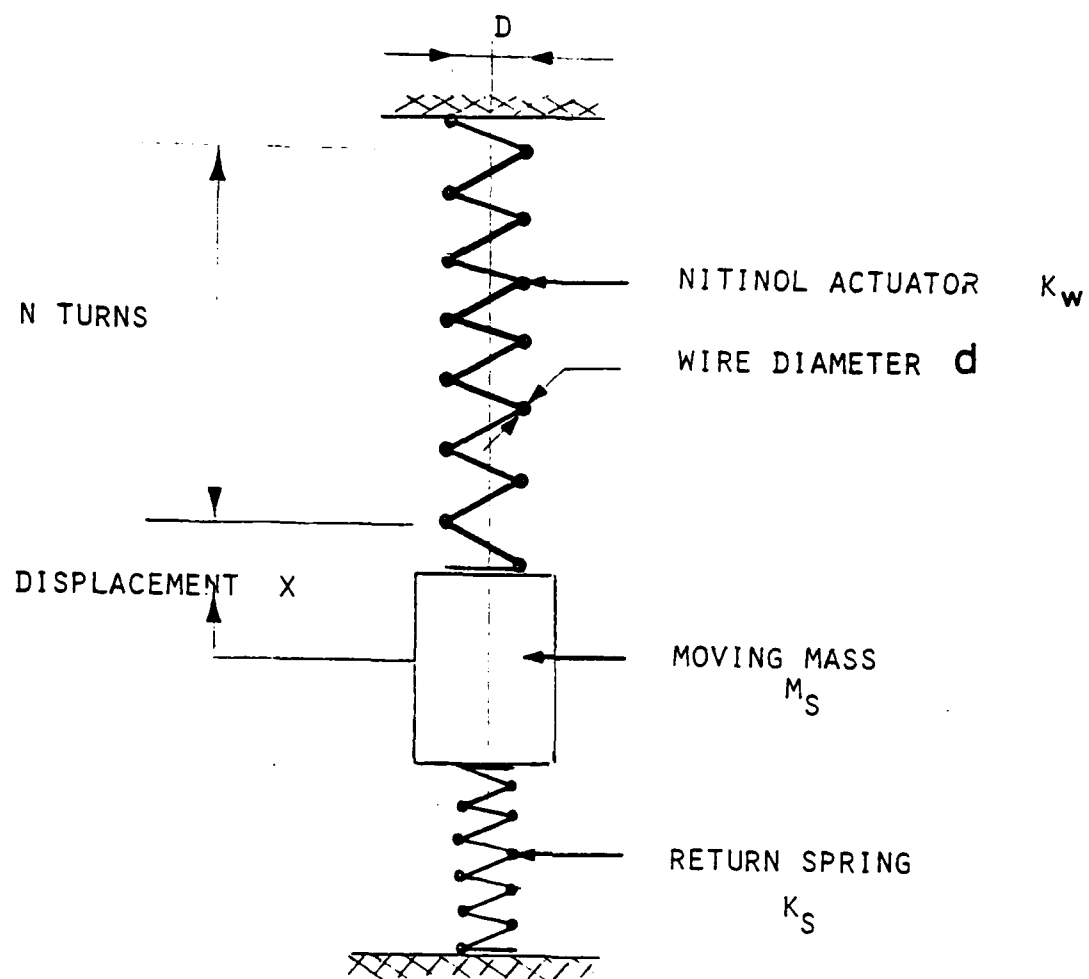


FIGURE 17. SIMPLIFIED DRAWING OF A TYPICAL NITINOL ACTUATOR SYSTEM.

or

$$V \cdot I = hA(T - T_a) + m c_p \frac{dT}{dt}, \quad (3)$$

where

h is the convective heat transfer coefficient between actuator and ambient

A is actuator surface area, given by

$$A = \pi d L, \quad (4)$$

d is diameter of actuator wire

L is length of actuator wire

m is actuator mass, given by

$$m = \rho \frac{\pi}{4} d^2 L \quad (5)$$

and

ρ is density of actuator material.

c_p is specific heat of actuator material.

Figure 18-b shows a typical temperature history of the actuator, subjected to the sudden voltage change, displayed in Figure 18-a. The wire temperature rise is exponential, a form dictated by Equation (3). When the wire temperature reaches its phase transformation temperature, T_T , its temperature will remain constant at T_T until the process of phase transformation is completed.

The time, t_1 , needed to reach T_T can be determined from Equation (3),

$$t_1 = \tau_{th} \ln \left[\frac{1}{\left\{ 1 - \frac{(T_T - T_a)}{(VI/hA)} \right\}} \right], \quad (6)$$

where τ_{th} is the thermal time constant of the NITINOL actuator, given by

$$\tau_{th} = \frac{m c_p}{h A}. \quad (7)$$

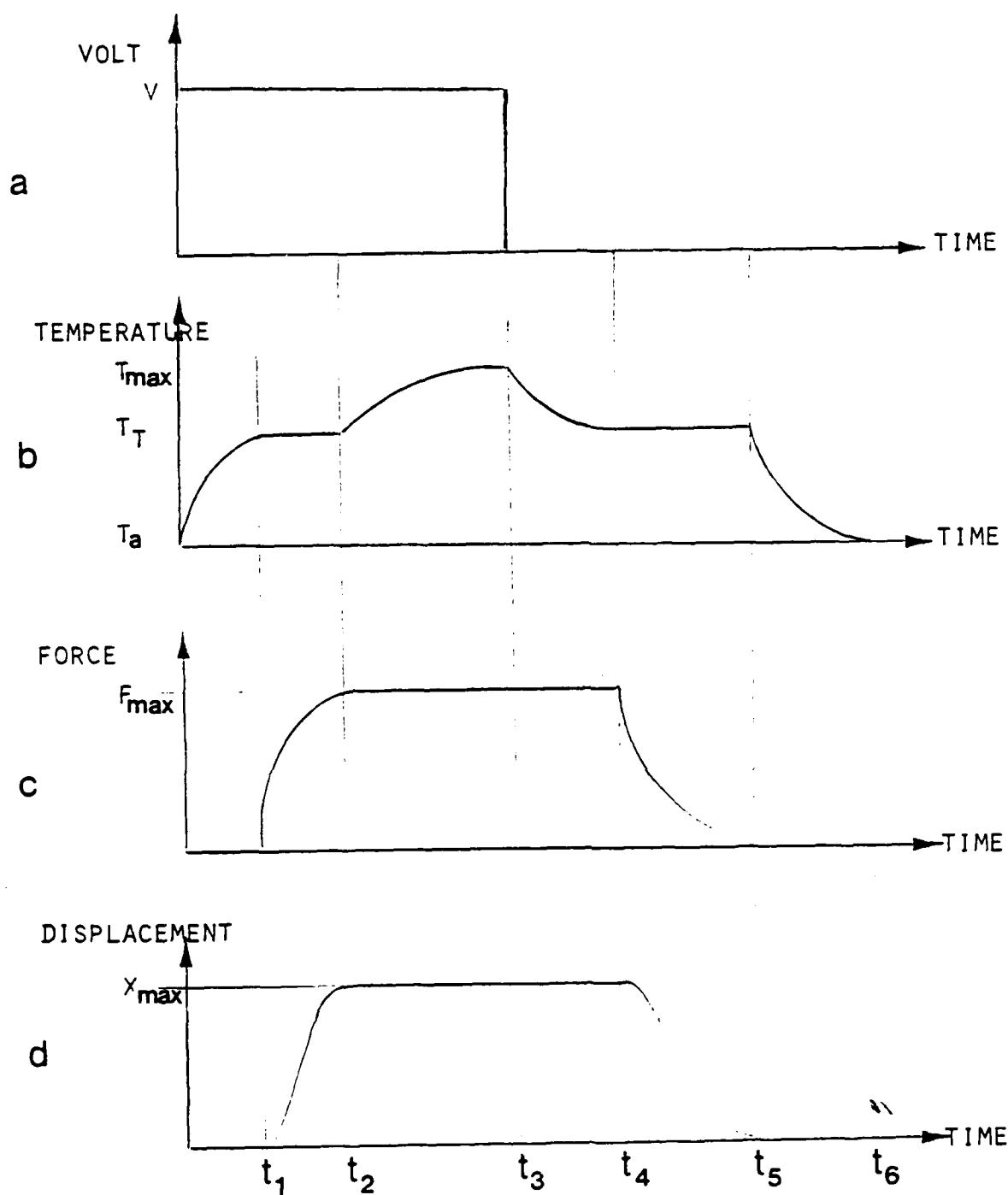


FIGURE 18. VOLTAGE, TEMPERATURE, FORCE, AND DISPLACEMENT PROFILE OF A TYPICAL NITINOL ACTUATOR.

Also, the time, $(t_2 - t_1)$, needed to complete the phase transformation can be determined from:

$$(t_2 - t_1) = 4\tau_h \quad (8)$$

where τ_h is the heating time constant of the actuator to be determined from dimensionless modelling of the experimental results.

Once this phase transformation is completed the wire will start warming again until it reaches a maximum temperature (T_{\max}), given by

$$T_{\max} = T_a + \frac{VI}{hA}, \quad (9)$$

after a time period $(t_3 - t_2)$, given by

$$(t_3 - t_2) = 4\tau_{th} - t_1. \quad (10)$$

If the applied voltage (V) is switched off suddenly, the NITINOL actuator will begin to cool as heat is lost, a process that is accelerated by natural convection. After a period of time $(t_4 - t_3)$, given by

$$(t_4 - t_3) = \tau_{th} \ln \left[\frac{(T_{\max} - T_a)}{(T_T - T_a)} \right], \quad (11)$$

the actuator's temperature reaches the martensite transformation temperature T_T . At that temperature the NITINOL starts to transform from austenite to martensite as it loses its latent heat to the ambient. This transformation will take place over a period of time $(t_5 - t_4)$ given by:

$$(t_5 - t_4) = 4\tau_c \quad (12)$$

where τ_c is the cooling time constant of the actuator to be determined from dimensionless modelling of the experimental results.

Following the completion of this transformation process the actuator continues to cool exponentially from T_T to T_a over a time period $(t_6 - t_5)$ given by:

$$(t_6 - t_5) = 4\tau_{th} - (t_4 - t_3) \quad (13)$$

Equations (5) through (13) describe completely the thermal behavior of a NITINOL actuator when subjected to step voltage changes.

2. Equation of Motion.

The motion of the NITINOL actuator is caused by the generation and the recovery of forces resulting from its phase transformation. Figure 18c shows the history of these phase transformation forces, conforming to the temperature history outlined above. As indicated, forces resulting from the thermal expansion and contraction of the wire during its heating (from T_a to T_T) and cooling (from T_T to T_a) are neglected in comparison to the much larger phase transformation forces. Furthermore, it is assumed that the phase transformation forces are generated and recovered, during the phase change, exponentially in time.

With such simplifying assumptions, one can write the equations that govern the motion of the actuator and appendages attached to it as follows:

$$M_s \ddot{x} + (K_s + K_w)x = F \quad (14)$$

where

M_s is the equivalent moving mass of the actuator and its attached appendages

K_s is the stiffness of the return spring

K_w is the stiffness of the actuator given by⁽³²⁾

$$K_w = \frac{d^4 G}{8D^3 N} \text{ (for helical actuators) ,} \quad (15)$$

G is modulus of rigidity of NITINOL

D is the coil diameter of the actuator

N is the number of turns of the actuator

or

$$K_w = \frac{\pi d^2 E}{4L} \text{ (for straight wire actuators) ,} \quad (16)$$

E is Young's Modulus of elasticity of NITINOL

F is the force acting on the actuator system given by:

$$\begin{aligned}
 F &= 0 && \text{For } 0 \leq t \leq t_1 \quad (a) \\
 &= F_{\max}(1 - e^{-\frac{t}{\tau_h}}) && t_1 \leq t \leq t_2 \quad (b) \\
 &= F_{\max} && t_2 \leq t \leq t_4 \quad (c) \\
 &= F_{\max}[e^{-\frac{(t-t_4)}{\tau_c}}] && t_4 \leq t \leq t_5 \quad (d) \\
 &= 0 && t_5 \leq t \leq t_6 \quad (e),
 \end{aligned} \tag{17}$$

where

$$F_{\max} = (K_s + K_w)X_{\max}, \tag{18}$$

with X_{\max} as the maximum deflection of actuator to be determined from dimensionless modelling of the experimental results.

The displacement history of a NITINOL actuator subjected to sudden voltage changes is obtained on integrating Equation (14). The result is shown in Figure 18d. It is seen that the actuator remains stationary until its temperature reaches the phase transformation temperature T_T . Then, it starts shrinking according to the second order differential Equation (14) under the influence of the gradually increasing phase transformation force F , of Equation (17b). A final steady state deflection X_{\max} is then attained and maintained as long as the applied voltage is maintained.

Once the applied voltage is switched off, the actuator will stay stationary at X_{\max} for a duration of $(t_4 - t_3)$ until its temperature cools to T_T . At that point, the phase recovery force will gradually bring the actuator back to its original position. This is then followed by a period $(t_6 - t_5)$ during which the actuator remains stationary as it continues to cool, once again achieving the temperature of the ambient.

It is, therefore, evident that the three processes of heating and cooling, phase transformation as well as actuator's motion are interacting closely to control the operation of the actuator. Furthermore, the developed model shows that the physical properties of the NITINOL (ρ, c_p, T_T, G , and E), the geometrical design parameters of the actuator

(d, D, L , or N), the cooling strategy (h) and the operating conditions (V, I, K_s , and M_s) each alone and all combined influence the dynamic performance of the actuator system.

In order to complete the development of the dynamic model of the NITINOL actuator, one must describe the three parameters τ_h, τ_c and ΔT_L in terms of the physical properties, geometrical parameters as well as the cooling and operating conditions. This process is achieved through dimensionless modelling of the experimental results.

B. Dimensionless Modeling of the NITINOL Actuator

In view of the developed model of the NITINOL actuator, one can easily see that there are 19 main parameters that influence its performance. These parameters are:

(i) Physical properties of actuator

| | | |
|----------------------------------|--------|-------------------------------|
| 1. density | ρ | kg/m^3 |
| 2. specific heat | c_p | $\text{J/kg } ^\circ\text{C}$ |
| 3. Latent heat of transformation | Q_L | J/kg |
| 4. Transformation Temperature | T_T | $^\circ\text{C}$ |
| 5. Young's Modulus of Elasticity | E | N/m^2 |

(ii) Geometrical design parameters of actuator

| | | |
|------------------|-----|------------|
| 6. Wire diameter | d | m |
| 7. Wire length | L | m |

(iii) Cooling strategy parameters

| | | |
|---|----------|--------------------------------------|
| 8. Convective heat transfer coefficient | h | $\text{W/m}^2\text{ }^\circ\text{C}$ |
| 9. Density of cooling medium | ρ_a | kg/m^3 |
| 10. Conductivity of cooling medium | k_a | $\text{W/m } ^\circ\text{C}$ |
| 11. Viscosity of cooling medium | μ_a | kg/ms |
| 12. Thermal expansion coefficient of cooling medium | β | $^\circ\text{C}^{-1}$ |

| | | |
|-------------------------------------|-------|------------------|
| 13. Specific heat of cooling medium | c_a | J/kg °C |
| 14. Gravitational acceleration | g | m/s ² |
| 15. Temperature of cooling medium | T_a | °C |

(iv) Operating conditions

| | | |
|---------------------------------|-------|-------|
| 16. Mass of elastic system | | |
| connected to actuator | M_s | kg |
| 17. Stiffness of elastic system | K_s | N/m |
| 18. Applied voltage to actuator | V | volts |
| 19. Applied current to actuator | I | Amp. |

Accordingly, one can write 15 independent dimensionless groups which are:

| | |
|--|---|
| 1. Nusselt number | $Nu = hd/k_a$ |
| 2. Grashoff number | $Gr = g\beta(T_T - T_a)d^3 / \left(\frac{\mu_a}{\rho_a}\right)^2$ |
| 3. Prandtl number | $Pr = c_a\mu_a/k_a$ |
| 4. Thermal expansion number | βT_a |
| 5. Density ratio | ρ_a/ρ |
| 6. Specific heat ratio | c_a/c_p |
| 7. Length to diam ratio | L/d |
| 8. Stiffness ratio $\left(\frac{K_s}{D_s}\right)$ | $= K_s L / \frac{\pi}{4} d^2 E$ for straight wire actuator |
| 9. Thermal dynamic time constant ratio | $\rho c_p d / \left(\frac{8\pi h}{\sqrt{K_s/M_s}}\right)$ |
| 10. Transformation to cooling medium temperature ratio | T_T/T_a |
| 11. Maximum wire to cooling medium temperature ratio | $\frac{VI}{hA}/T_a$ |
| 12. Stored to transformation thermal heat energy ration | $c_p(T_T - T_a)/Q_L$ |

- | | |
|--|----------------------------------|
| 13. Mass ratio | $\rho \frac{\pi}{4} L d^2 / M_s$ |
| 14. Elastic to transformation energy ratio | $E / \rho Q_L$ |
| 15. Dimensionless time | $2\pi \sqrt{g K_s / d M_s}$ |

These fifteen independent groups can be used to model the experimental results in a dimensionless form. This can be useful in extending the applicability of the model to actuators of other geometries operating under different operating conditions using the developed dimensionless similarity conditions.

C. Modeling of Experimental Results.

The developed 15 dimensionless groups are used to model τ_h , τ_c and X_{\max} by writing

$$\begin{aligned} \frac{\tau_h}{\left(\frac{2\pi}{\sqrt{\frac{K_s}{M_s}}} \right)} = & a_0 Nu^{a_1} Gr^{a_2} \left(\frac{L}{d} \right)^{a_3} \cdot \left(\frac{K_s}{K_w} \right)^{a_4} \cdot \left(\frac{\rho c_p d}{\frac{8\pi h}{\sqrt{K_s/M_s}}} \right)^{a_5} \\ & \cdot \left(\frac{\left(\frac{VI}{hA} \right)}{T_a} \right)^{a_6} \cdot \left(\frac{\frac{\pi}{4} \rho d^2 L}{M_s} \right)^{a_7} \cdot \left(2\pi \sqrt{\frac{g K_s}{d M_s}} \right)^{a_8} \end{aligned} \quad (19)$$

$$\begin{aligned} \frac{\tau_c}{\left(\frac{2\pi}{\sqrt{\frac{K_s}{M_s}}} \right)} = & b_0 Nu^{b_1} Gr^{b_2} \left(\frac{L}{d} \right)^{b_3} \cdot \left(\frac{K_s}{K_w} \right)^{b_4} \cdot \left(\frac{\rho c_p d}{\frac{8\pi h}{\sqrt{K_s/M_s}}} \right)^{b_5} \\ & \cdot \left(\frac{\left(\frac{VI}{hA} \right)}{T_a} \right)^{b_6} \cdot \left(\frac{\frac{\pi}{4} \rho d^2 L}{M_s} \right)^{b_7} \cdot \left(2\pi \sqrt{\frac{g K_s}{d M_s}} \right)^{b_8} \end{aligned} \quad (20)$$

and

$$\begin{aligned} \frac{X_{\max}}{L} = & c_0 Nu^{c_1} Gr^{c_2} \left(\frac{L}{d} \right)^{c_3} \cdot \left(\frac{K_s}{K_w} \right)^{c_4} \cdot \left(\frac{\rho c_p d}{\frac{8\pi h}{\sqrt{K_s/M_s}}} \right)^{c_5} \\ & \cdot \left(\frac{\left(\frac{VI}{hA} \right)}{T_a} \right)^{c_6} \cdot \left(\frac{\frac{\pi}{4} \rho d^2 L}{M_s} \right)^{c_7} \cdot \left(2\pi \sqrt{\frac{g K_s}{d M_s}} \right)^{c_8}, \end{aligned} \quad (21)$$

where the constants a_0 through a_8 , b_0 through b_8 , and c_0 through c_8 are to be determined from the test data using nonlinear multivariable regression analysis⁽³³⁾. In writing these

equations we included only the dimensionless groups that were pertinent to the experimental procedures. Other groups that were not varied during the testing protocols were excluded. Table 3 lists the computed values of the coefficients in Equations (19) through (21).

TABLE 3. MODELING COEFFICIENTS FOR τ_h , τ_c , AND X_{\max}

| Coefficient Subscript | a | b | c |
|--------------------------|-----------------------|------------------------|------------------------|
| 0 | 2.57×10^{26} | 1.746×10^{37} | 0.794×10^{-6} |
| 1 | -2.6020 | -2.48600 | 0.69910 |
| 2 | 0.4080 | 0.53300 | -0.40160 |
| 3 | -0.6945 | -1.13500 | 1.09490 |
| 4 | 0.0305 | 0.00372 | 0.02885 |
| 5 | -4.1190 | -7.06000 | 0.98220 |
| 6 | -1.0726 | 0.65840 | -0.47800 |
| 7 | -0.1196 | -1.25710 | -0.00373 |
| 8 | -3.7000 | -3.65300 | 2.64600 |

Figures 19-a, 19-b, and 19-c show a comparison between the experimental and the modelled dimensionless τ_h , τ_c and X_{\max} respectively. The figures indicate that the obtained dimensionless models simulate closely the experimental results. This is manifested clearly by the computed multiple correlation coefficients which are found to be 0.925, 0.868 and 0.910 for τ_h , τ_c and X_{\max} respectively.

The mathematical model of the actuator given by Equations (3) through (18) along with the dimensionless Equations (19), (20) and (21) can be used to describe the thermal and dynamic behavior of NITINOL actuators of different geometries, subjected to various operating conditions. These equations are utilized as a basis for designing active vibration control systems that are based on NITINOL actuators.

VI. DESIGN AND TESTING OF ACTIVE CONTROL SYSTEM USING NITINOL ACTUATOR

The developed experimental and theoretical characteristics of NITINOL actuators

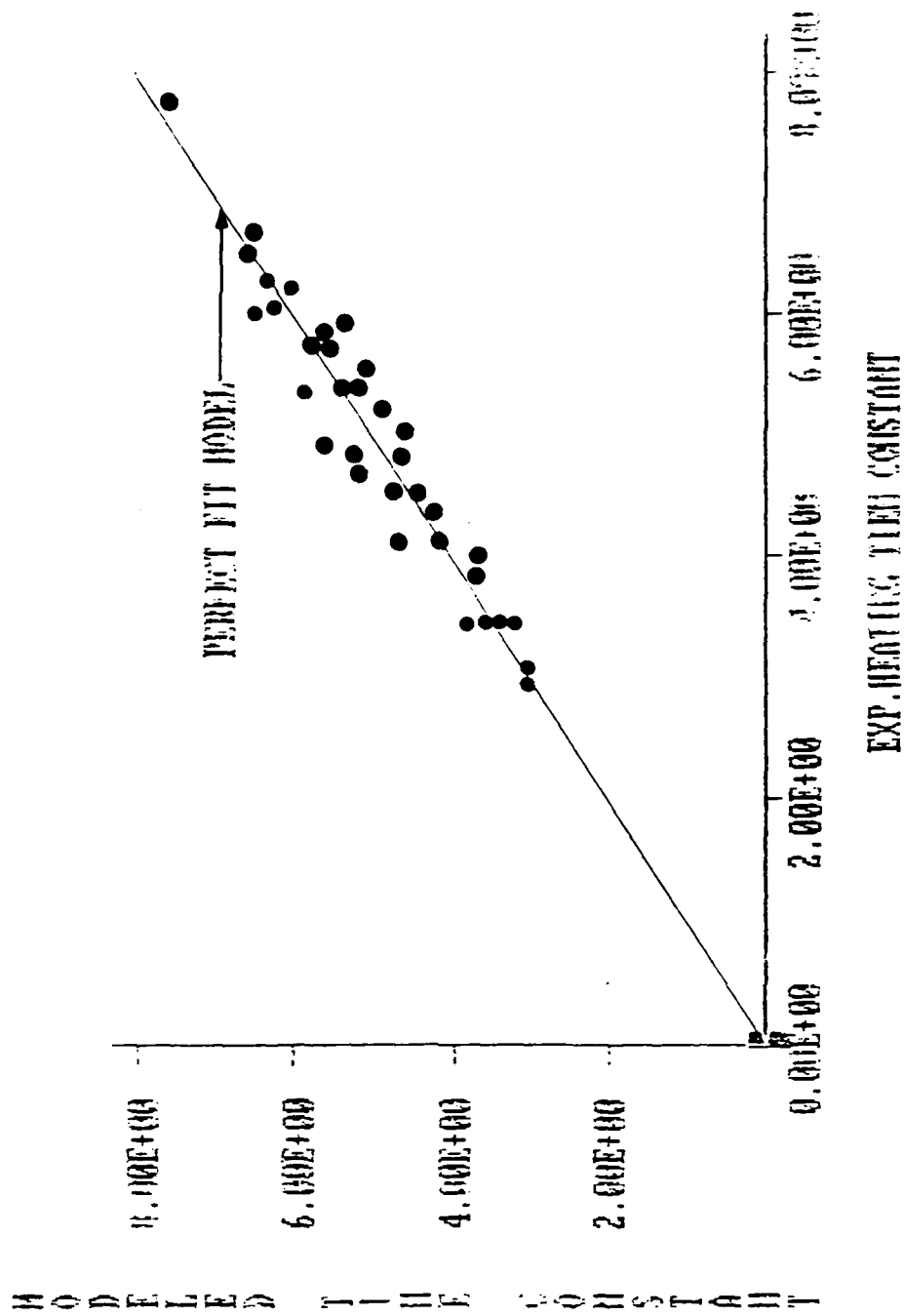


FIGURE 19-a. A COMPARISON BETWEEN
EXPERIMENTAL AND MODELED DIMENSIONLESS HEATING TIME CONSTANT:
FOR NITINOL ACTUATORS OF DIFFERENT GEOMETRIES
SUBJECTED TO DIVERSE VOLTAGE CHANGES.

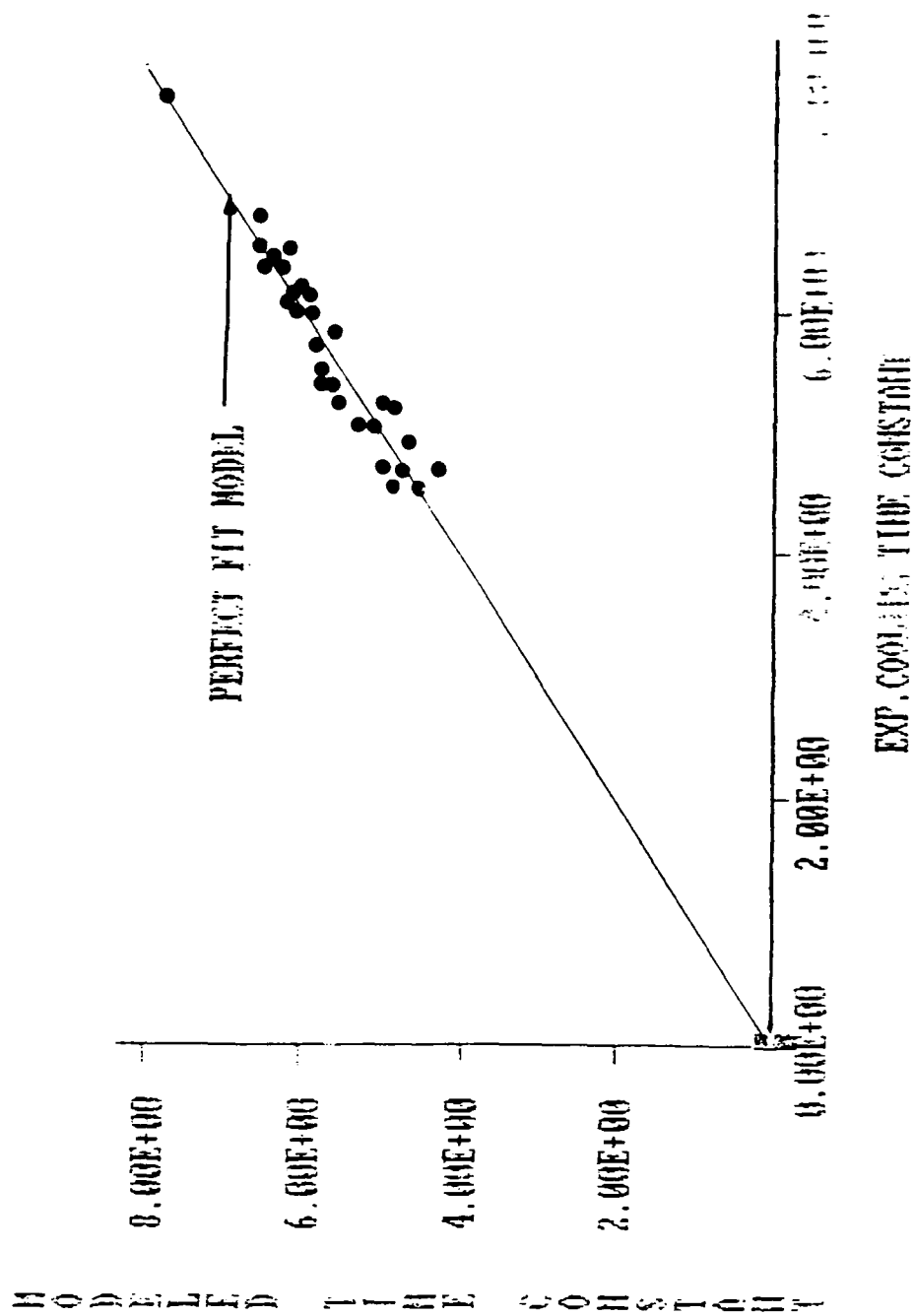


FIGURE 19-b. A COMPARISON BETWEEN
EXPERIMENTAL AND MODELED DIMENSIONLESS COOLING TIME CONSTANT;
FOR NITINOL ACTUATORS OF DIFFERENT GEOMETRIES
SUBJECTED TO DIVERSE VOLTAGE CHANGES.

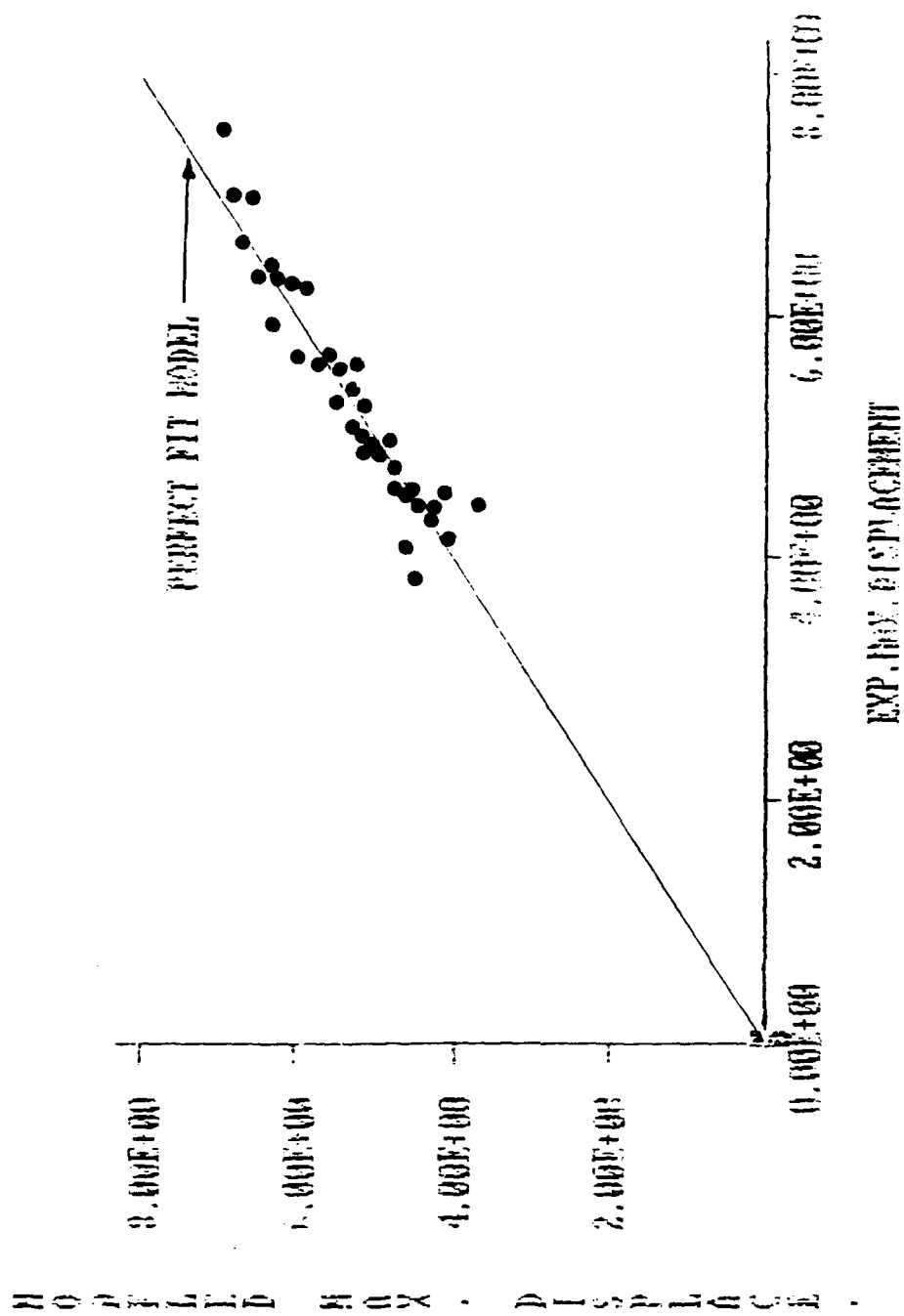


FIGURE 19-c. A COMPARISON BETWEEN
EXPERIMENTAL AND MODELED DIMENSIONLESS MAXIMUM DISPLACEMENT.
FOR NITINOL ACTUATORS OF DIFFERENT GEOMETRIES
SUBJECTED TO DIVERSE VOLTAGE CHANGES.

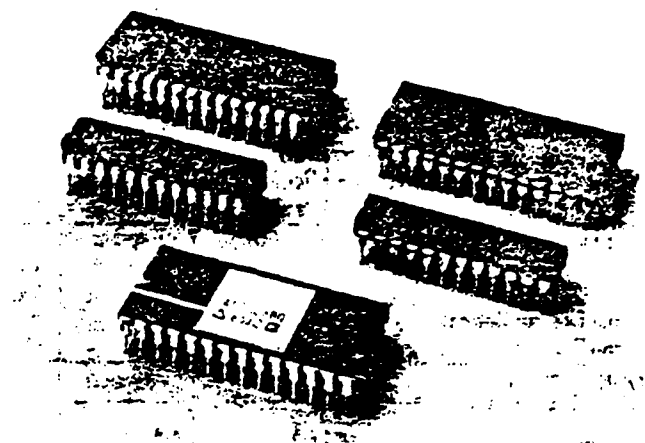


LC²MOS High Speed 4- & 8-Channel 8-Bit ADCs

AD7824/AD7828

FEATURES

- 4- or 8-Analog Input Channels
- Built-In Track/Hold Function
- 10kHz Signal Handling on Each Channel
- Fast Microprocessor Interface
- Single +5V Supply
- Low Power: 40mW
- Fast Conversion Rate, 2.5 μ s/Channel
- Tight Error Specification: 1/2LSB



GENERAL DESCRIPTION

The AD7824 and AD7828 are high-speed, multichannel, 8-bit ADCs with a choice of 4 (AD7824) or 8 (AD7828) multiplexed analog inputs. A half-flash conversion technique gives a fast conversion rate of 2.5 μ s per channel and the parts have a built-in track/hold function capable of digitizing full-scale signals of up to 10kHz (157mV/ μ s slew rate) on all channels. The AD7824 and AD7828 operate from a single +5V supply and have an analog input range of 0 to +5V, using an external +5V reference.

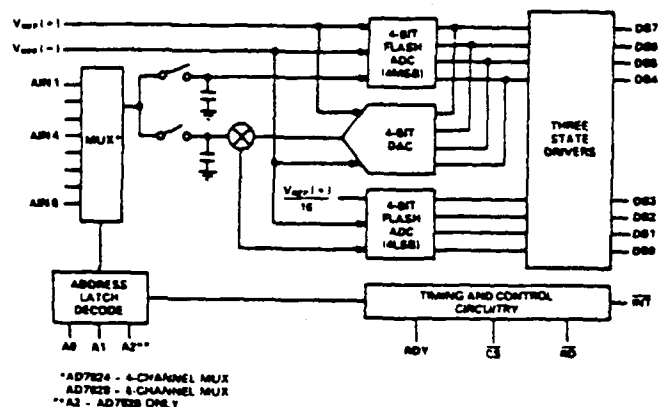
Microprocessor interfacing of the parts is simple, using standard Chip Select (\overline{CS}) and Read (\overline{RD}) signals to initiate the conversion and read the data from the three-state data outputs. The half-flash conversion technique means that there is no need to generate a clock signal for the ADC. The AD7824 and AD7828 can be interfaced easily to most popular microprocessors.

The AD7824 and AD7828 are fabricated in an advanced, all ion-implanted, Linear-Compatible CMOS process (LC²MOS) and have low power dissipation of 40mW (typ). The AD7824 is available in a 0.3" wide, 24-pin "skinny" DIP, while the AD7828 is packaged in a 0.6" wide, 28-pin DIP.

PRODUCT HIGHLIGHTS

- 4- or 8-channel input multiplexer gives cost-effective space-saving multichannel ADC system.
- Fast conversion rate of 2.5 μ s/channel features a per channel sampling frequency of 100kHz for the AD7824 or 50kHz for the AD7828.
- Built-in track-hold function allows handling of 4- or 8-channels up to 10kHz bandwidth (157mV/ μ s slew rate).
- Tight total unadjusted error spec and channel-to-channel matching eliminate the need for user trims.
- Single +5V supply simplifies system power requirements.
- Fast, easy-to-use digital interface allows connection to most popular microprocessors with minimal external components. No clock signal is required for the ADC.

AD7824/AD7828 FUNCTIONAL DIAGRAM



Information furnished by Analog Devices is believed to be accurate and reliable. However, no responsibility is assumed by Analog Devices for its use; nor for any infringements of patents or other rights of third parties which may result from its use. No license is granted by implication or otherwise under any patent or patent rights of Analog Devices.

Route 1 Industrial Park; P.O. Box 280; Norwood, Mass. 02062
Tel: 617/329-4700
West Coast
714/641-9391
Mid-West
312/653-5000
Texas
214/231-5094
TWX: 710/394-6577

FEATURES

Four 8-Bit DACs with Output Amplifiers
0.3" Wide, 20-Pin DIP
Microprocessor Compatible
TTL/CMOS Compatible
No User Trims
Single Supply Operation Possible

APPLICATIONS

Process Control
Automatic Test Equipment
Automatic Calibration of Large System Parameters
e.g., Gain/Offset

GENERAL DESCRIPTION

The AD7226 contains four 8-bit voltage-output digital-to-analog converters, with output buffer amplifiers and interface logic on a single monolithic chip. No external trims are required to achieve full specified performance for the part.

Separate on-chip latches are provided for each of the four D/A converters. Data is transferred into one of these data latches through a common 8-bit TTL/CMOS (5V) compatible input port. Control inputs A0 and A1 determine which DAC is loaded when \overline{WR} goes low. The control logic is speed-compatible with most 8-bit microprocessors.

Each D/A converter includes an output buffer amplifier capable of driving up to 5mA of output current. The amplifiers' offsets are laser-trimmed during manufacture, thereby eliminating any requirement for offset nulling.

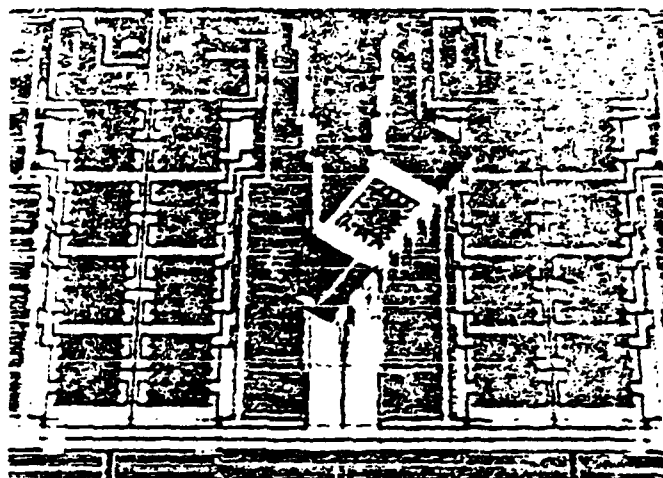
Specified performance is guaranteed for input reference voltages from -2V to +12.5V with dual supplies. The part is also specified for single supply operation at a reference of +10V.

The AD7226 is fabricated in an all ion-implanted high speed Linear Compatible CMOS (LC²MOS) process which has been specifically developed to allow high speed digital logic circuits and precision analog circuits to be integrated on the same chip.

PRODUCT HIGHLIGHTS

- 1. DAC-to-DAC Matching:**
Since all four DACs are fabricated on the same chip at the same time, precise matching and tracking between the DACs is inherent.
- 2. Single Supply Operation:**
The voltage mode configuration of the DACs allows the AD7226 to be operated from a single power supply rail.

Information furnished by Analog Devices is believed to be accurate and reliable. However, no responsibility is assumed by Analog Devices for its use; nor for any infringements of patents or other rights of third parties which may result from its use. No license is granted by implication or otherwise under any patent or patent rights of Analog Devices.



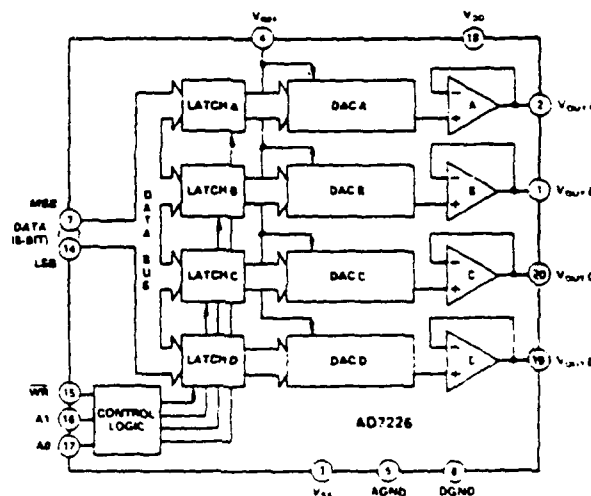
3. Microprocessor Compatibility:

The AD7226 has a common 8-bit data bus with individual DAC latches, providing a versatile control architecture for simple interface to microprocessors. All latch enable signals are level triggered.

4. Small Size:

Combining four DACs and four op-amps plus interface logic into a small, 0.3" wide, 20-pin DIP allows a dramatic reduction in board space requirements and offers increased reliability in systems using multiple converters. Its pinout is aimed at optimizing board layout with all the analog inputs and outputs at one end of the package and all the digital inputs at the other.

AD7226 FUNCTIONAL BLOCK DIAGRAM



Route 1 Industrial Park; P.O. Box 280; Norwood, Mass. 0206:
Tel: 617/329-4700 TWX: 710/394-657

West Coast
714/641-9391

Mid-West
312/653-5000

Texas
214/231-509

SINGLE SUPPLY SPECIFICATIONS

($V_{DD} = +15V \pm 5\%$; $V_{SS} = AGND = DGND = 0V$; $V_{REF} = +10V$
unless otherwise stated). All specifications T_{MIN} to T_{MAX} unless otherwise noted.

| PARAMETER | AD7226K.B, T ¹ | UNITS | CONDITIONS/COMMENTS |
|--|---------------------------|-------------------|---|
| STATIC PERFORMANCE | | | |
| Resolution | 8 | Bits | |
| Total Unadjusted Error ² | ± 2 | LSB max | Guaranteed Monotonic |
| Differential Nonlinearity ³ | ± 1 | LSB max | |
| REFERENCE INPUT | | | |
| Input Resistance | 2 | k Ω min | Occurs when each DAC loaded with all 0's. |
| Input Capacitance ⁴ | 65 | pF min | Occurs when each DAC loaded with all 1's. |
| | 300 | pF max | |
| DIGITAL INPUTS | | | |
| Input High Voltage, V_{INH} | 2.4 | V min | |
| Input Low Voltage, V_{INL} | 0.8 | V max | $V_{IN} = 0V$ or V_{DD} |
| Input Leakage Current | ± 1 | μA max | |
| Input Capacitance | 8 | pF max | |
| Input Coding | Binary | | |
| DYNAMIC PERFORMANCE | | | |
| Voltage Output Slew Rate ⁵ | 2 | V/ μs min | |
| Voltage Output Settling Time ⁵ | 5 | μs max | Settling Time to $\pm 1/2$ LSB |
| Positive Full Scale Change | 20 | μs max | Settling Time to $\pm 1/2$ LSB |
| Negative Full Scale Change | 50 | nV secs typ | |
| Digital Crosstalk ³ | 2 | k Ω min | $V_{OUT} = +10V$ |
| Minimum Load Resistance | | | |
| POWER SUPPLIES | | | |
| V_{DD} Range | 14.25 to 15.75 | V_{MIN}/V_{MAX} | For Specified Performance |
| I_{DD} | 13 | mA max | Outputs Unloaded; $V_{IN} = V_{INL}$ or V_{INH} |
| SWITCHING CHARACTERISTICS⁵ | | | |
| Address to Write Setup Time, t_{AS} | 0 | ns min | |
| @ 25°C | 0 | ns min | |
| T_{MIN} to T_{MAX} | | | |
| Address to Write Hold Time, t_{AH} | 10 | ns min | |
| @ 25°C | 10 | ns min | |
| T_{MIN} to T_{MAX} | | | |
| Data Valid to Write Setup Time, t_{DS} | 90 | ns min | |
| @ 25°C | 100 | ns min | |
| T_{MIN} to T_{MAX} | | | |
| Data Valid to Write Hold Time, t_{DH} | 10 | ns min | |
| @ 25°C | 10 | ns min | |
| T_{MIN} to T_{MAX} | | | |
| Write Pulse Width, t_{WP} | 150 | ns min | |
| @ 25°C | 200 | ns min | |
| T_{MIN} to T_{MAX} | | | |

VEEDER-ROOT INDUCTIVE PROXIMITY SWITCH

INSTALLATION INSTRUCTIONS 576013-190
for all:

5 - 24 VDC, 2 Wire, N.C. Proportional (NAMUR)
Output models

having 9-digit part numbers with the following
specific designations

6 X X X X 6 - 3 X X

Where "X" can be any
number 0-9 except where
otherwise specified

5,6

This switch is suggested for use with the
following Veeder-Root amplifiers:
669010-100, 669010-101, and 669010-102.

A. NOMINAL ELECTRICAL CHARACTERISTICS

| Electrical Characteristics | |
|--|----------------|
| Operating Voltage Limits with Load Resistance RL of 1K Ω | 5-15VDC |
| with Load Resistance RL of 2K Ω | 12-24VDC |
| Current Consumption Target Present | ≤ 1 mA |
| Current Consumption Target Absent | ≥ 4 mA |
| Max. Current Consumption | 10 mA |
| Ambient Temperature | |
| Operating Range | -25°C to +75°C |

For full product specifications, please consult the catalog.

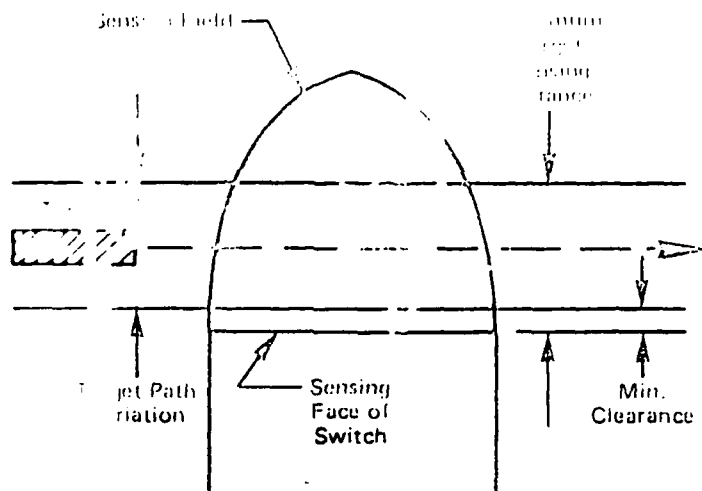
B. LOCATION SELECTION. Veeder-Root inductive proximity switches detect all metal targets approaching the sensing face laterally (slide-by mode), axially (head-on mode), or in any other direction. Veeder-Root does not recommend the use of the axial mode (head-on) when the application might expose the switch to damage by being struck by the target should some control device not operate properly.

WARNING: IN INSTALLATION AND USE OF THIS PRODUCT, COMPLY WITH THE NATIONAL ELECTRICAL CODE; FEDERAL, STATE AND LOCAL CODES; AND ANY OTHER APPLICABLE SAFETY CODES. IN ADDITION, TURN OFF POWER AND TAKE OTHER NECESSARY PRECAUTIONS DURING INSTALLATION TO PREVENT PERSONAL INJURY, PROPERTY LOSS AND EQUIPMENT DAMAGE. IF INSTALLATION IS TO BE IN A VOLATILE, COMBUSTIBLE OR EXPLOSIVE ATMOSPHERE, THIS PRODUCT MUST BE HOUSED IN AN APPROPRIATE ENCLOSURE AS REQUIRED FOR USE IN SUCH ATMOSPHERE BY NATIONAL ELECTRICAL CODE AND ANY LOCAL APPLICABLE STANDARDS.

1. Select locations which allow easy installation and inspection. Avoid locations where approaching targets are subject to direct contact with switch. Avoid locations where excessive accumulations of chips, dust or dirt exist.
2. Avoid locations where the switch is located in water or where it is subject to jets of liquid or continuous liquid splashes.
3. Minimum spacings as described in the catalog must be maintained between two or more proximity switches and when metallic object, other than the target, exists in the area surrounding the detecting field.

C. INSTALLING THE PROXIMITY SWITCH. After considering the factors described in Paragraph B, select a mounting site for the switch. Position the switch so the target moves laterally past the sensing face of the switch.

The lateral movement of the target past the sensing face is called the Target Path. The nature of the various mechanical linkages, guides and conveyors that typically



move targets past the switch are such that variations due to mechanical play and other factors create a variable Target Path. Since the sensing distance on some of these switches is very short, they must be precisely adjusted. Follow the procedure here to determine the actual mounting relationship between the switch and target.

1. Position the switch so the target moves laterally past the sensing face of the switch.
2. Temporarily connect the switch to a suitable control amplifier or to test circuit (See Figure 1).
3. To see that the switch and indicator are functioning, bring a metal object, such as a screwdriver blade, into contact with the switch sensing face and see that the output indicator changes state, or reads less than 1 mA.
4. Determine the actual target path variation by examining those items which physically constrain the target as it moves past the switch location.
5. Place the actual target in the position where it is to operate the switch. Place the switch in its approximate mounting position but far enough away from the target so the switch does not operate.
6. Move the target away from the switch to the outer extremity of the actual target path as determined in step 4.
7. Slowly move the switch toward the target until the switch operates. Measure the distance from the sensing face to the target. This is the actual sensing distance.
8. Move the switch toward the target until the distance from the sensing face to the target is 80% of the actual sensing distance as determined in step 7. This is the usable sensing distance for the actual target and allows for variations in line voltage and temperature.
9. Move the target toward the switch so that the target is positioned at the inner extremity of the target path as determined in step 4. If the target touches the sensing face, the target path variation must be reduced or a switch with a greater sensing distance must be selected.
10. If the target does not touch the sensing face of the switch, keep the target at the innermost extremity of the target path, and move the switch toward the target 1/2 of the remaining distance. This centralizes the target path within the usable sensing distance.
11. Secure the switch to the mounting surface.
12. Disconnect all power to the switch and remove the temporarily connected indicator. Connect desired load per Paragraph D.

are used to guide the design of an active vibration control system which uses a NITINOL actuator to suppress the vibration of a flexible cantilever beam system.

A. The Flexible Beam System.

(i) **Physical system.** Figure 20 shows a schematic drawing of the flexible cantilever beam used in this study. The beam is 2.5 cm wide, 0.075 cm thick and 25 cm long. It is made of polymethyl methacrylate which has a Young's Modulus of Elasticity of 3500 Mpa and density of 1.2 gm/cm³.

A simple 3 element model is used to describe the dynamic characteristics of the flexible beam. The first element is 5 cm long which is as long as the used NITINOL wire actuator (A). The second element is taken to be 2.5 cm long such that node 2 lies exactly at the same location as the position sensor (B). The third element represents the remaining part of the beam.

In spite of the simplicity of this model, the procedure used in developing it and integrating it with the remaining part of the control system is general, and can be extended to other more complex systems.

(ii) Mathematical model of beam-actuator element.

1. Stiffness Matrix. Let us consider the beam-actuator element of length L_i extending between nodes i and j as shown in Figure 21. Let us also denote that the external forces and moments acting on nodes i and j are V_i and M_i and V_j and M_j respectively. These are related to the linear and angular deformations of the element y_i and θ_i and y_j and θ_j , at nodes i and j respectively, by the finite element constitutive equations which can be written in the matrix form⁽³⁴⁾

$$\begin{bmatrix} V_i \\ M_i + M_N \\ -V_j \\ -M_j - M_N \end{bmatrix} = \frac{E_i I_i}{L_i^3} \begin{bmatrix} 12 & 6L_i & -12 & 6L_i \\ 6L_i & 4L_i & -6L_i & 2L_i \\ -12 & -6L_i & 12 & -6L_i \\ 6L_i & 2L_i & -6L_i & 4L_i \end{bmatrix} \begin{bmatrix} y_i \\ \theta_i \\ y_j \\ \theta_j \end{bmatrix}, \quad (22)$$

where

$$\begin{aligned} E_i I_i &= \text{flexural rigidity of the beam-actuator system} \\ &= E_b I_b + E_a I_a, \end{aligned} \quad (23)$$

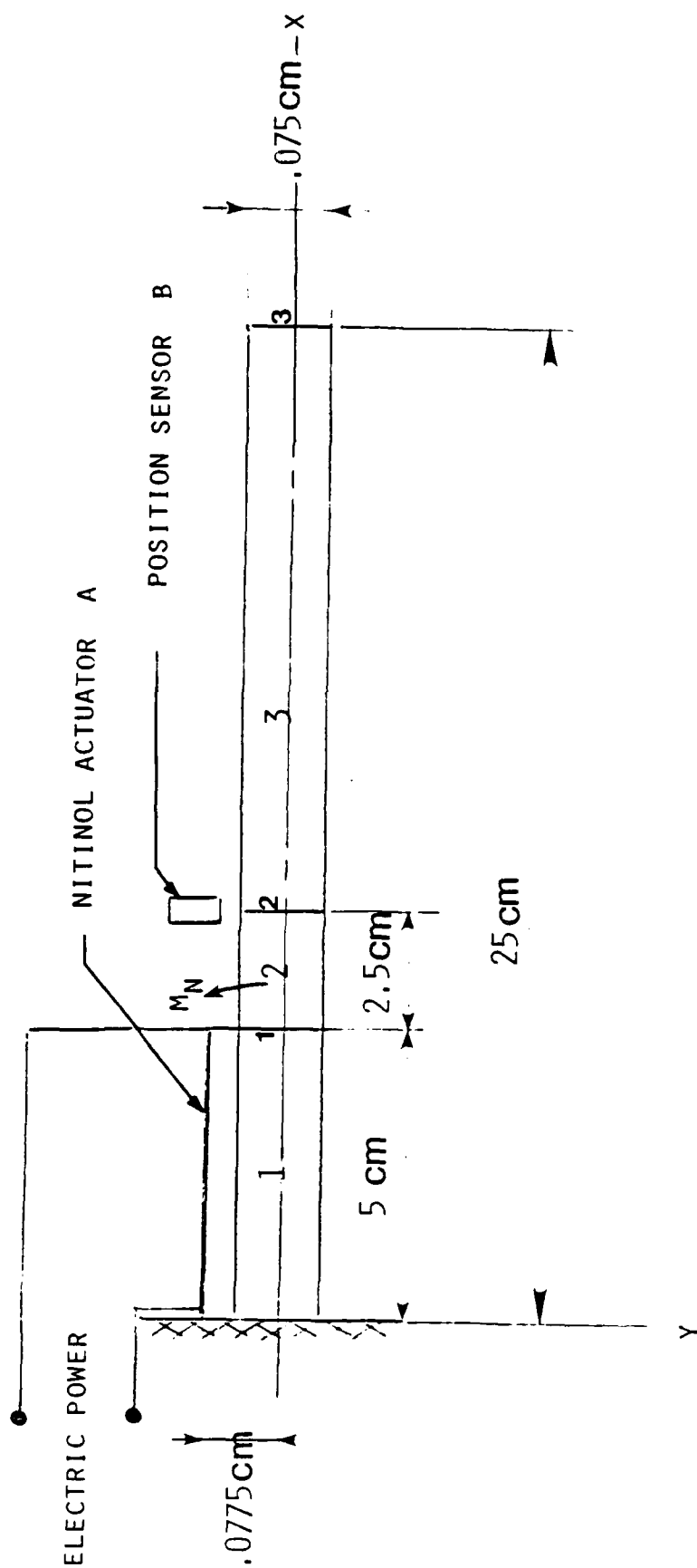


FIGURE 20. SCHEMATIC DRAWING OF THE FLEXIBLE CANTILEVER BEAM.

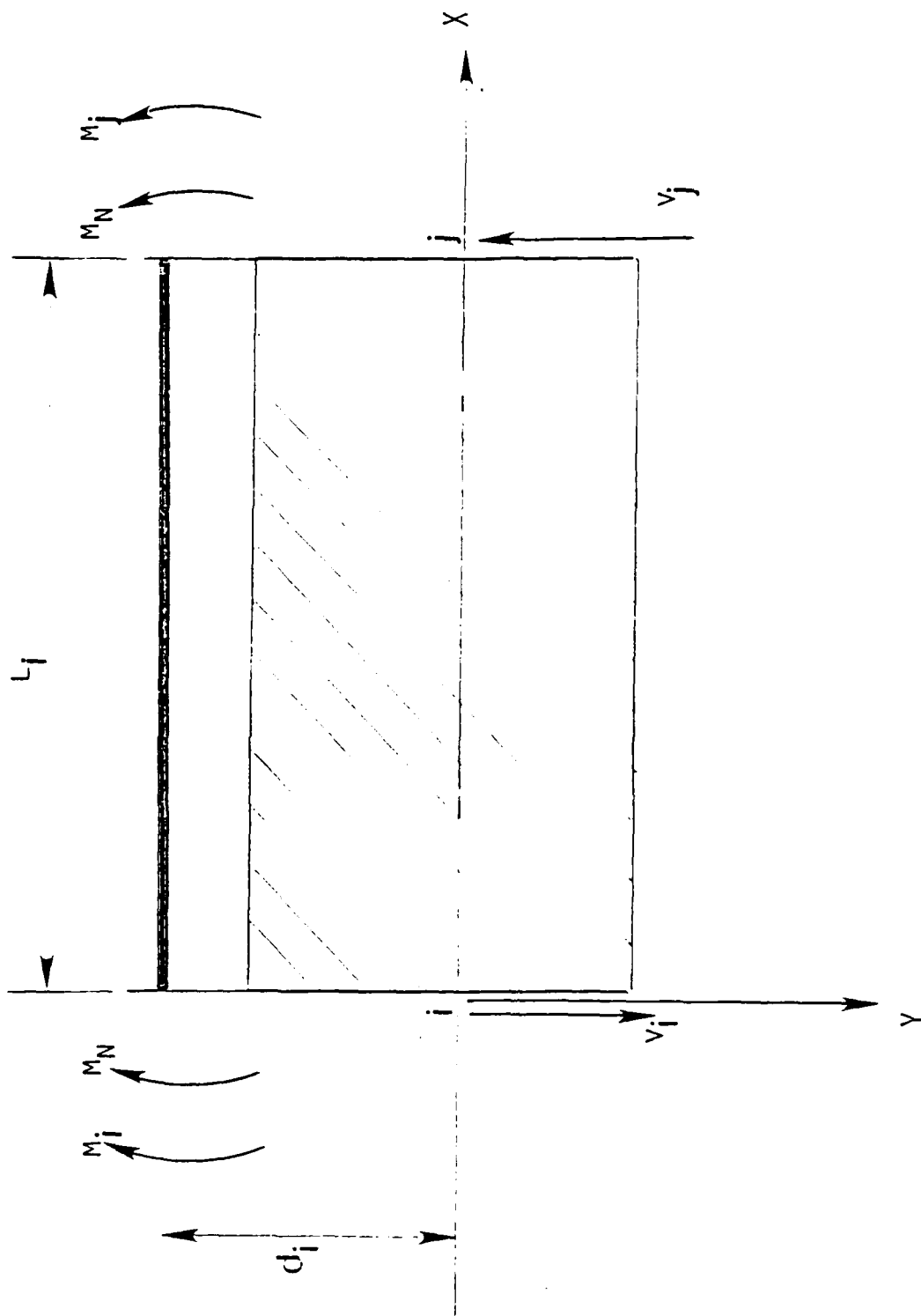


FIGURE 21. SCHEMATIC DRAWING OF BEAM-NITINOL ACTUATOR ELEMENT.

where

$E_{a,b}$ is Young's Modulus of the actuator and beam respectively

$I_{a,b}$ is the area of inertia of actuator and beam respectively,

and

M_N is the control moment developed by the NITINOL actuator. It can be written as a product of an actuator force and the wire diameter:

$$M_N = F_{\text{actuator}} \cdot d_w \quad (24)$$

Introducing a shorthand notation, Equation (23) can be written as

$$F_i = K_i \delta_i, \quad (25)$$

where

F_i is the resultant forces and moments vector acting on the beam element i , N

K_i is the stiffness matrix of the beam - actuator element i , N/m

and

δ_i is the deflection vector of the nodes bounding the beam element, m.

Equation (25) applies to any element of the beam, whether it has a NITINOL actuator attached to it or not. In the latter case, M_N is set to zero and flextural rigidity $E_i I_i$ is set equal to that of the flexible beam element under consideration.

The force-displacement characteristics of the individual elements of the beam-actuator system, given for element i by Equation (25), are combined to determine the overall stiffness of the beam system. The equilibrium conditions of the overall structure will be expressed as the external forces and moment acting on the nodes of the overall system = \sum forces and moments acting on the elements at these nodes; or:

$$F = \sum_{i=1}^{N+1} F_i = \sum_{i=1}^{N+1} K_i \delta_i = K \delta \quad (26)$$

where K is the overall stiffness matrix of the system ($2n \times 2n$). Bathe and Wilson⁽³⁵⁾, Yang⁽³⁶⁾ and Fenner⁽³⁴⁾, for example, show how to generate the overall matrix, K from

the stiffness matrices K_i of the individual elements. For the beam-actuator system under consideration, the overall stiffness matrix K is given in Table 4 when a 16 mils (0.04 cm) actuator is used.

2. Mass matrix. The inertial properties of the composite actuator-beam system are determined using the lumped mass method where the mass and rotational inertia of each element is distributed among the nodes bounding the element⁽³⁷⁾. The diagonal mass matrix M ($2n * 2n$) for the actuator-beam system, shown in Figure 21, is written as

$$M = \begin{bmatrix} m_1 & 0 & \cdot & \cdot & \cdot & \cdot & \cdot & \cdot & \cdot & \cdot & \cdot & \cdot & \cdot & \cdot & \cdot & 0 \\ 0 & J_1 & 0 & \cdot & \cdot & \cdot & \cdot & \cdot & \cdot & \cdot & \cdot & \cdot & \cdot & \cdot & \cdot & \cdot \\ 0 & 0 & m_2 & 0 & \cdot & \cdot & \cdot & \cdot & \cdot & \cdot & \cdot & \cdot & \cdot & \cdot & \cdot & \cdot \\ \cdot & \cdot & 0 & J_2 & 0 & \cdot & \cdot & \cdot & \cdot & \cdot & \cdot & \cdot & \cdot & \cdot & \cdot & \cdot \\ \cdot & \cdot & \cdot & \cdot & \cdot & \cdot & \cdot & \cdot & \cdot & \cdot & \cdot & \cdot & \cdot & \cdot & \cdot & \cdot \\ \cdot & \cdot & \cdot & \cdot & \cdot & 0 & m_i & 0 & \cdot & \cdot & \cdot & \cdot & \cdot & \cdot & \cdot & \cdot \\ \cdot & \cdot & \cdot & \cdot & \cdot & \cdot & 0 & J_i & 0 & \cdot & \cdot & \cdot & \cdot & \cdot & \cdot & \cdot \\ \cdot & \cdot & \cdot & \cdot & \cdot & \cdot & \cdot & 0 & m_{i+1} & 0 & \cdot & \cdot & \cdot & \cdot & \cdot & \cdot \\ \cdot & \cdot & \cdot & \cdot & \cdot & \cdot & \cdot & \cdot & 0 & J_{i+1} & 0 & \cdot & \cdot & \cdot & \cdot & \cdot \\ \cdot & \cdot & \cdot & \cdot & \cdot & \cdot & \cdot & \cdot & \cdot & \cdot & 0 & m_N & 0 & \cdot & \cdot & \cdot \\ \cdot & \cdot & \cdot & \cdot & \cdot & \cdot & \cdot & \cdot & \cdot & \cdot & \cdot & 0 & J_N & 0 & \cdot & \cdot \\ \cdot & \cdot & \cdot & \cdot & \cdot & \cdot & \cdot & \cdot & \cdot & \cdot & \cdot & \cdot & 0 & m_{N+1} & 0 & \cdot \\ \cdot & \cdot & \cdot & \cdot & \cdot & \cdot & \cdot & \cdot & \cdot & \cdot & \cdot & \cdot & \cdot & 0 & J_{N+1} & \cdot \end{bmatrix}, \quad (27)$$

where $m_1 = [(w_b + \gamma_1 w_a) * L_1]/2$

$$J_1 = [(w_b + \gamma_1 w_a) * L_1^3]/2$$

$$m_i = [(w_b + \gamma_{i-1} w_a) * L_{i-1} + (w_b + \gamma_i w_a) * L_i]/2$$

$$J_i = [(w_b + \gamma_{i-1} w_a) * L_{i-1}^3 + (w_b + \gamma_i w_a) * L_i^3]/12$$

$$m_{N+1} = [(w_b + \gamma_N w_a) * L_N]/2$$

$$J_{N+1} = [(w_b + \gamma_N w_a) * L_N^3]/12$$

$w_{a,b}$ = actuator and beam mass per unit length respectively, kg/m.

γ_i = 1 if an actuator is attached to beam element i . 0 if not.

The stiffness and mass matrices K and M , are used in the dynamic equations of motion of the actuator-beam system. The free vibration solutions of these equations then define the natural frequencies and normal modes for the cantilevered beam system.

The mass matrix, normal modes of vibration and the modal shape matrix for the beam model under consideration is given in Table 4.

3. Dynamic model. The equations of motion of the actuator-beam system can be written as

$$M\ddot{\delta} + K\delta = F, \quad (28)$$

a highly coupled system of ordinary differential equations. Using the modal shape matrix obtained from the free vibration analysis these equations can be transformed into a system of uncoupled equations, expressed in the modal coordinates of the system⁽³⁷⁾

The relationship between the physical displacement coordinates, δ , and the modal coordinates, U , is

$$\delta = \phi U \quad (29)$$

where ϕ is the weighted modal shape matrix formed from the eigenvectors of the flexible system. The equations of motion in the transformed modal space are written

$$\ddot{U} + \sigma U = f, \quad (30)$$

where σ is a diagonal matrix of the eigenvalues of the system and f is the modal force matrix given in terms of the physical control forces, F , by

$$f = \phi^T F. \quad (31)$$

Therefore, monitoring the displacement of the flexible system and generating the appropriate control forces through a proper control law one can determine the modal forces f from Equation (31), the modal displacements from Equation (30) and the physical displacements from Equation (29). Accordingly, the effectiveness of the controller in suppressing the physical oscillations can be determined.

B. Modeling of the Control System

TABLE 4. THE DYNAMIC CHARACTERISTICS
OF THE TESTED FLEXIBLE BEAM SYSTEM

Stiffness Matrix

$$\begin{bmatrix} 2266 & 19 & -2014 & 25.6 & 0 & 0 \\ 19 & .65 & -25.6 & .22 & 0 & 0 \\ -2014 & 25.6 & 2020 & -25.1 & -5.87 & .52 \\ 25.6 & .22 & -25.1 & .5 & -.52 & 0.031 \\ 0 & 0 & -5.87 & -.52 & 5.87 & -.52 \\ 0 & 0 & .52 & .031 & -.52 & 0.06 \end{bmatrix}$$

Mass Matrix

$$\begin{bmatrix} 9.31E-4 & 0 & 0 & 0 & 0 & 0 \\ 0 & 1.51E-7 & 0 & 0 & 0 & 0 \\ 0 & 0 & 2.48E-3 & 0 & 0 & 0 \\ 0 & 0 & 0 & 5.74E-6 & 0 & 0 \\ 0 & 0 & 0 & 0 & 2.17E-3 & 0 \\ 0 & 0 & 0 & 0 & 0 & 5.72E-6 \end{bmatrix}$$

Normal Modes (cps)

2.27 11.8 23.17 34.23 205.05 387.75 Hz

Modal Shape Matrix

1.13E+00 - 4.83E+00 6.77E+00 1.14E+01 2.45E+01 1.64E+01
4.28E+01 - 1.63E+02 2.01E+02 1.71E+02 - 1.54E+03 2.05E+03
2.45E+00 - 9.30E+00 1.16E+01 1.01E+01 - 5.31E+00 - 6.77E+00
6.06E+01 - 1.83E+02 1.65E+02 - 3.26E+02 4.72E+01 3.08E+01
2.01E+01 - 2.05E+00 - 7.06E+00 1.32E+00 1.84E-03 1.84E-03
1.21E+02 3.12E+02 2.49E+02 - 2.71E+01 - 1.39E-01 - 7.62E-02

(i) **Layout of the control system.** Figures 22-a and 22-b show a layout of an active vibration control system in which the physical position of the beam is monitored by a noncontacting sensor. The sensor signal is compared, in the computer, with a desired equilibrium position. The error signal is processed and sent to the controller via a D/A converter to power the NITINOL actuator to provide the control action necessary to damp out the vibration of the beam.

Using the mathematical models of the NITINOL actuator, developed in Section V, and the beam, developed in Section VI, one can study the effect of the control law on the dynamic performance of the system.

The effectiveness of the controller is determined by comparing the performance of the beam with and without the controller, subjected to step input disturbance. The disturbance is generated by deflecting the tip of the beam a known distance (0.228 in) and releasing it setting up a free vibration in the absence of a controller or a controlled forced vibration when the controller is activated. The free vibration of the beam serves as a datum, for measuring the effectiveness of the controller. Figures 23-a and 23-b show the experimental and theoretical behavior of the freely vibrating beam, respectively.

(ii) **Control with one NITINOL actuator.** If one NITINOL actuator is placed parallel to the beam, and mounted between node 1 and the foundation of the beam, then the control algorithm can be as shown in Figure 24. In this algorithm the control action is generally ON-OFF where the actuator is switched on when the beam displacement is positive. In this way the actuator can generate a moment that would counteract the beam deflection from \dot{y}_j (taken as 0) as shown in Figure 25-a. When the beam deflection becomes negative the actuator is switched also off as it can not provide any resistance to the beam motion.

Theoretical performance of the beam under the action of one NITINOL actuator is shown in Figures 26-a, 26-b and 26-c for dead band levels of 0.0025, 0.005, and 0.0075 in respectively. The figures indicate clearly that the NITINOL actuator has damped out effectively the positive amplitudes of vibration of the beam. It has, however, increased the amplitudes of negative displacement of the beam. For example, it reduced the maximum positive amplitudes by 18.9 % but also increased the maximum negative amplitude by 60.0

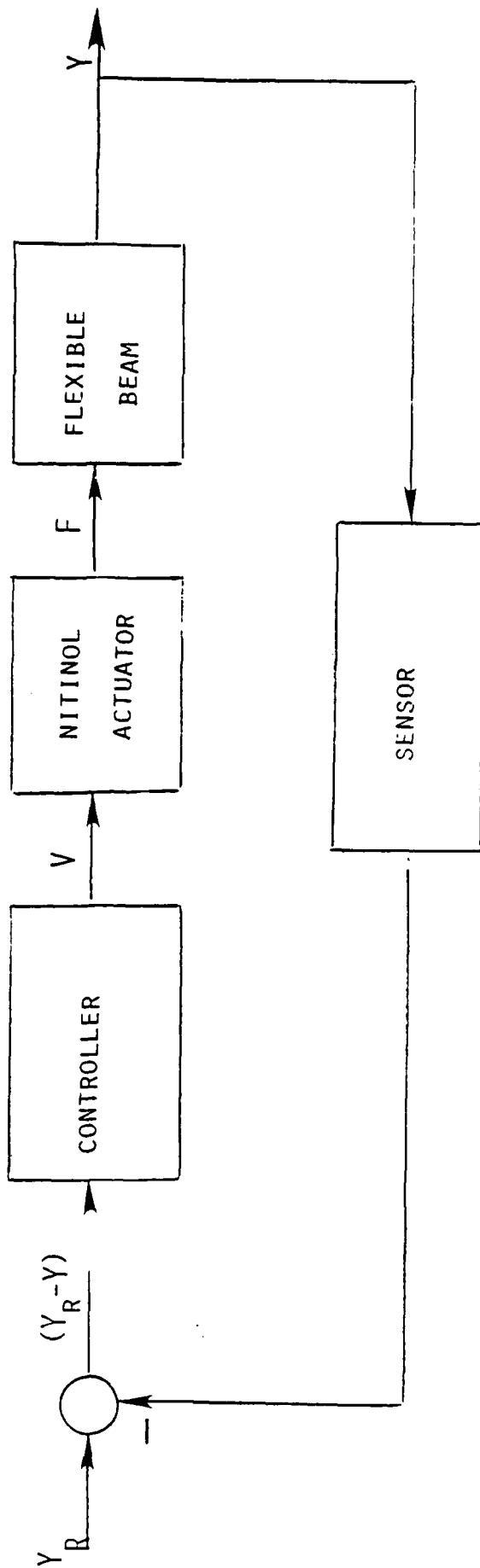


FIGURE 22-a. LAYOUT OF AN ACTIVE VIBRATION CONTROL SYSTEM
USING NITINOL ACTUATOR.

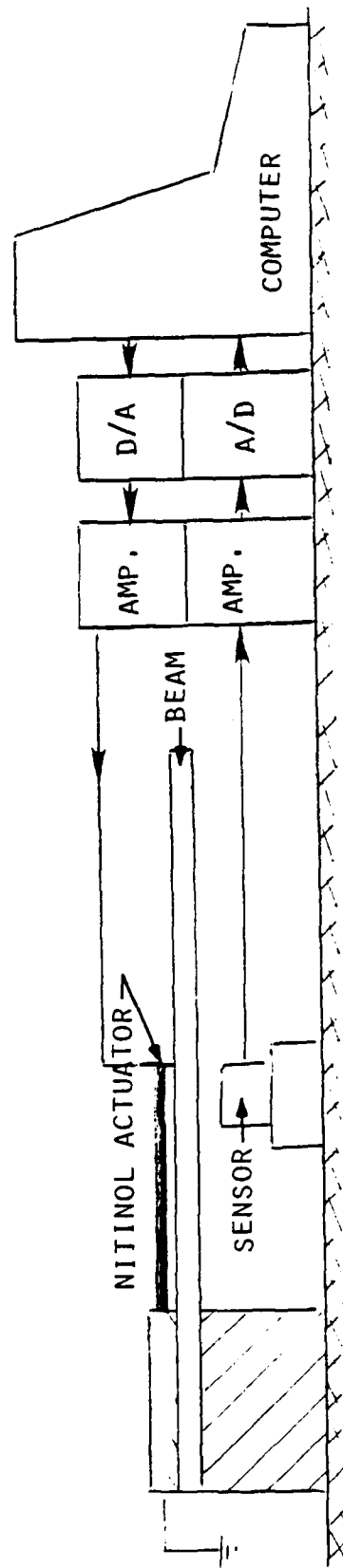


FIGURE 22-b. SCHEMATIC DRAWING OF
A COMPUTER-CONTROLLED ACTIVE CONTROL SYSTEM.

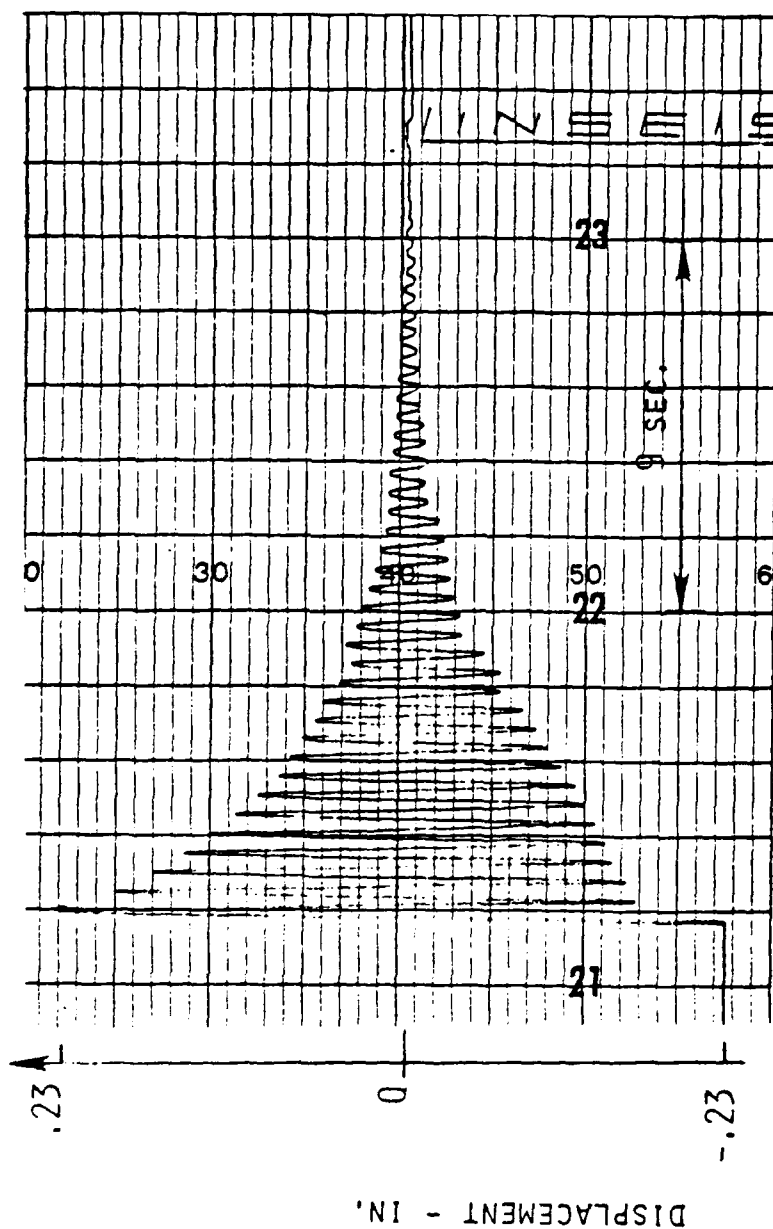


FIGURE 23-a. TIME HISTORY OF THE EXPERIMENTAL AMPLITUDE OF TRANSVERSE VIBRATION OF THE CANTILEVER BEAM UNDER FREE VIBRATION CONDITIONS (DAMPING RATIO = 0.02).

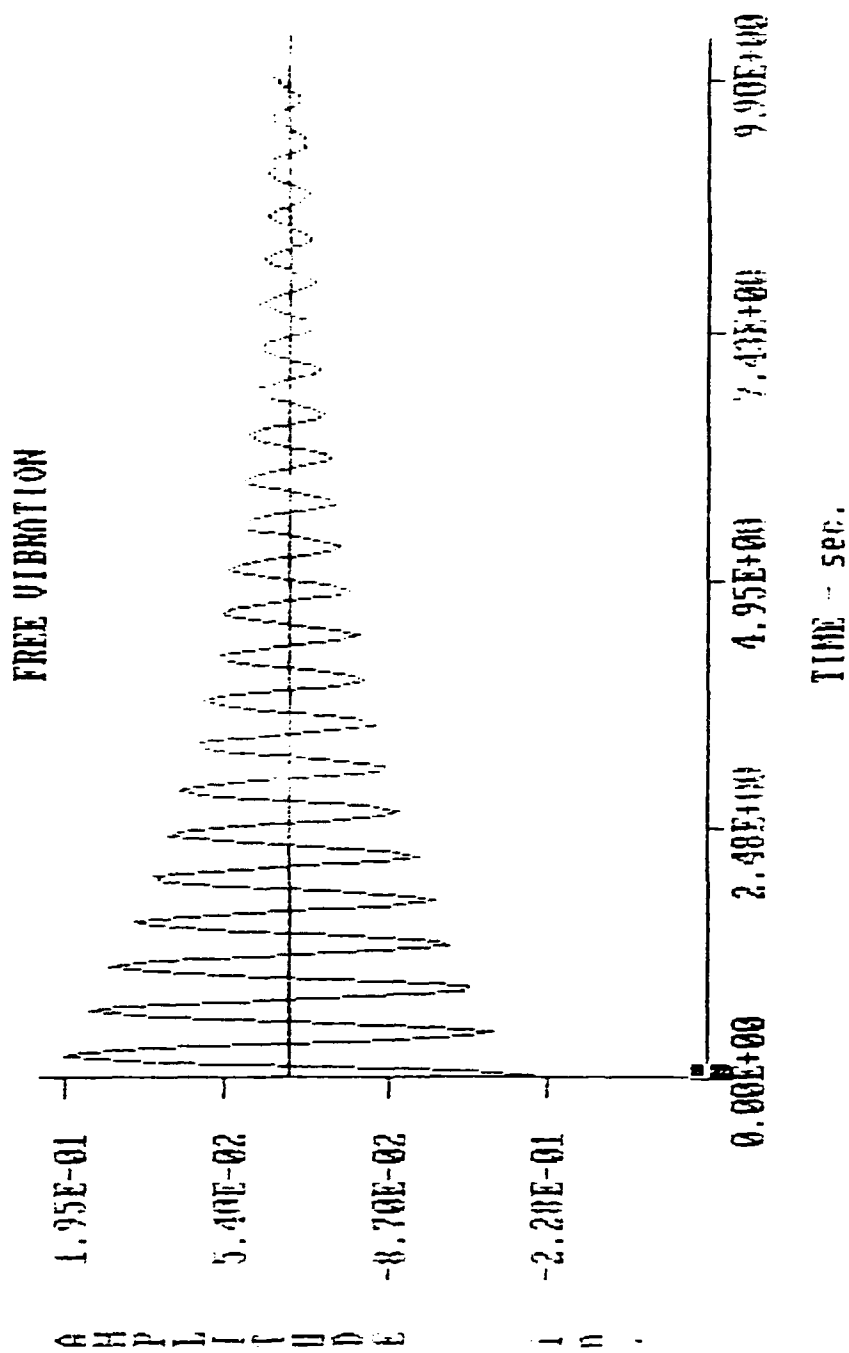


FIGURE 23-b. TIME HISTORY OF THE THEORETICAL AMPLITUDE
OF TRANSVERSE VIBRATION OF THE CANTILEVER BEAM
UNDER FREE VIBRATION CONDITIONS (DAMPING RATIO = 0.02).

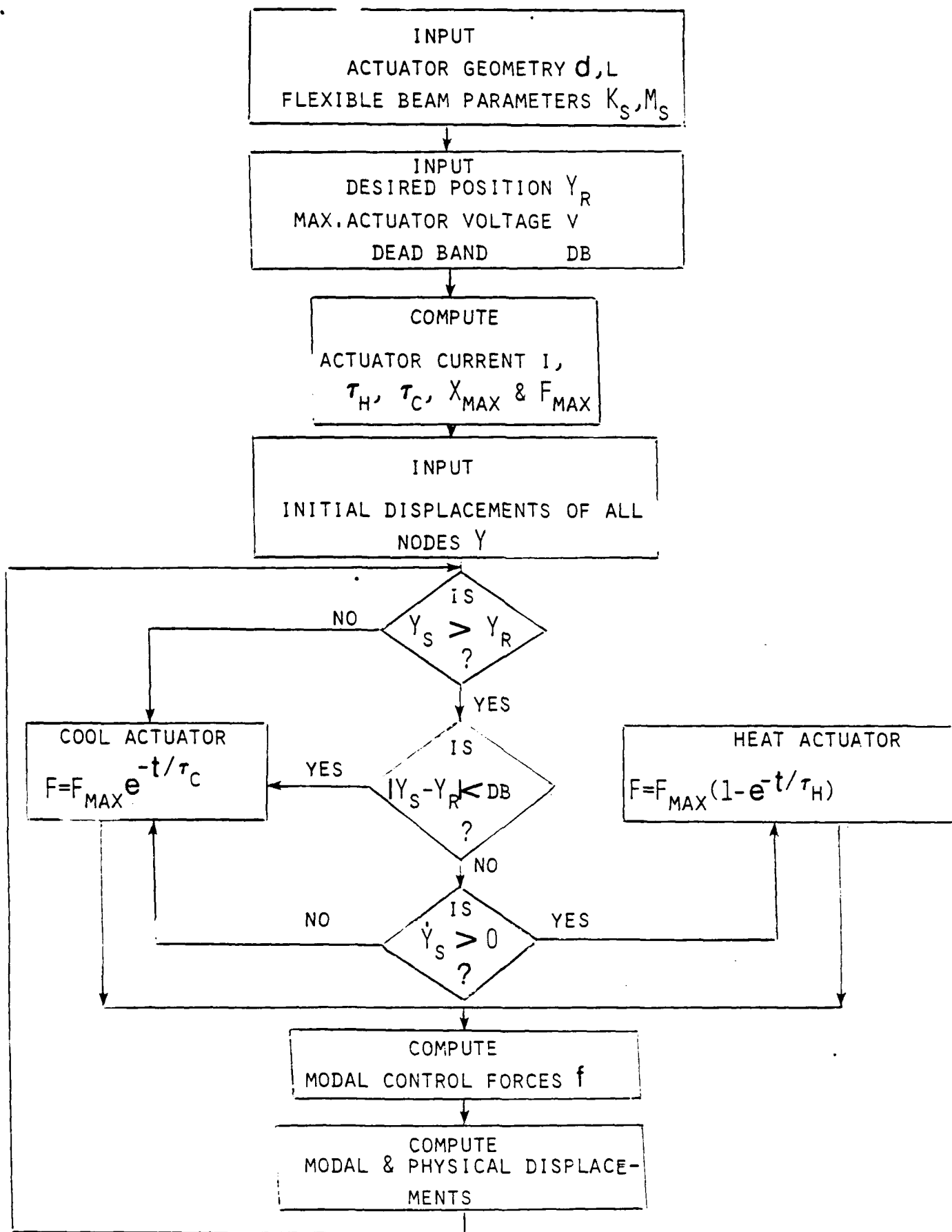


FIGURE 24. FLOW CHART OF THE CONTROL SYSTEM ANALYSIS ALGORITHM

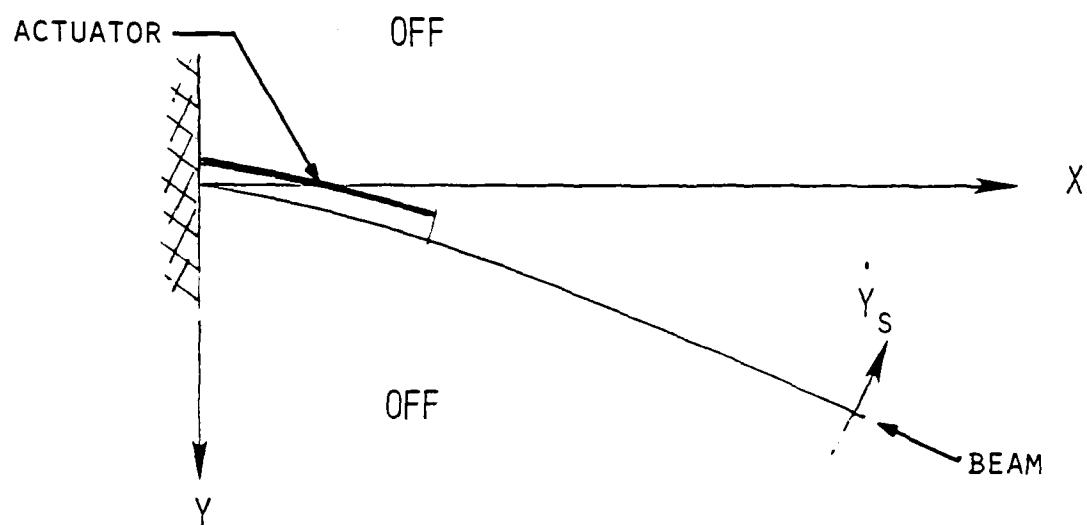
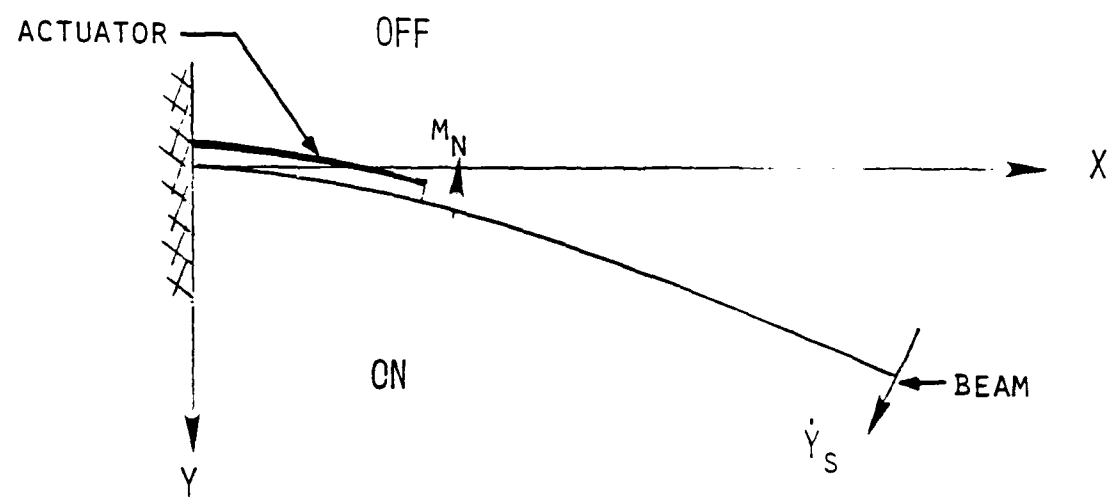


FIGURE 25. ENERGIZATION STRATEGIES OF NITINOL ACTUATOR.

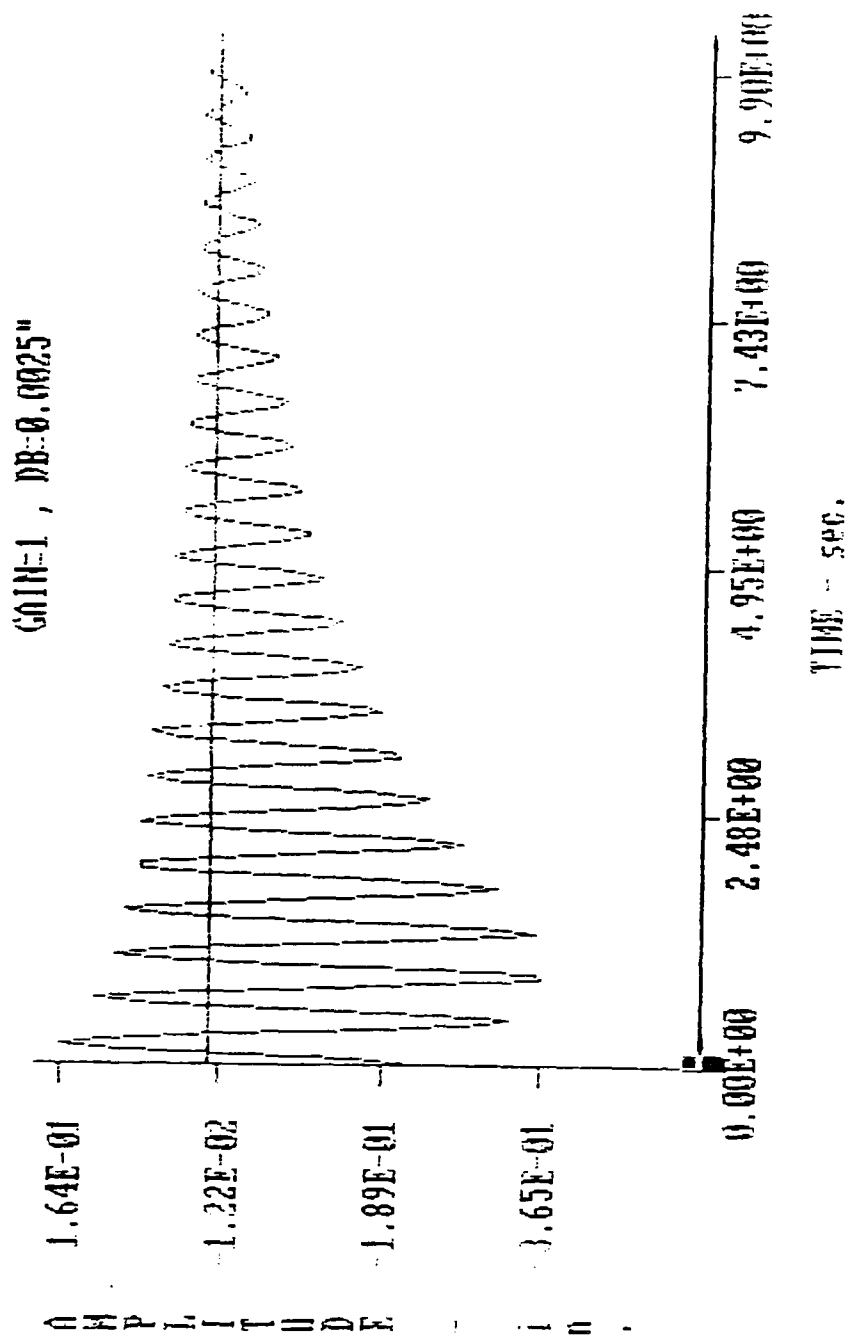


FIGURE 26-a. TIME HISTORY OF THEORETICAL AMPLITUDE OF VIBRATION OF THE BEAM WHEN CONTROLLED WITH ONE NITINOL ACTUATOR WITH A DEAD BAND OF 0.0025 in.

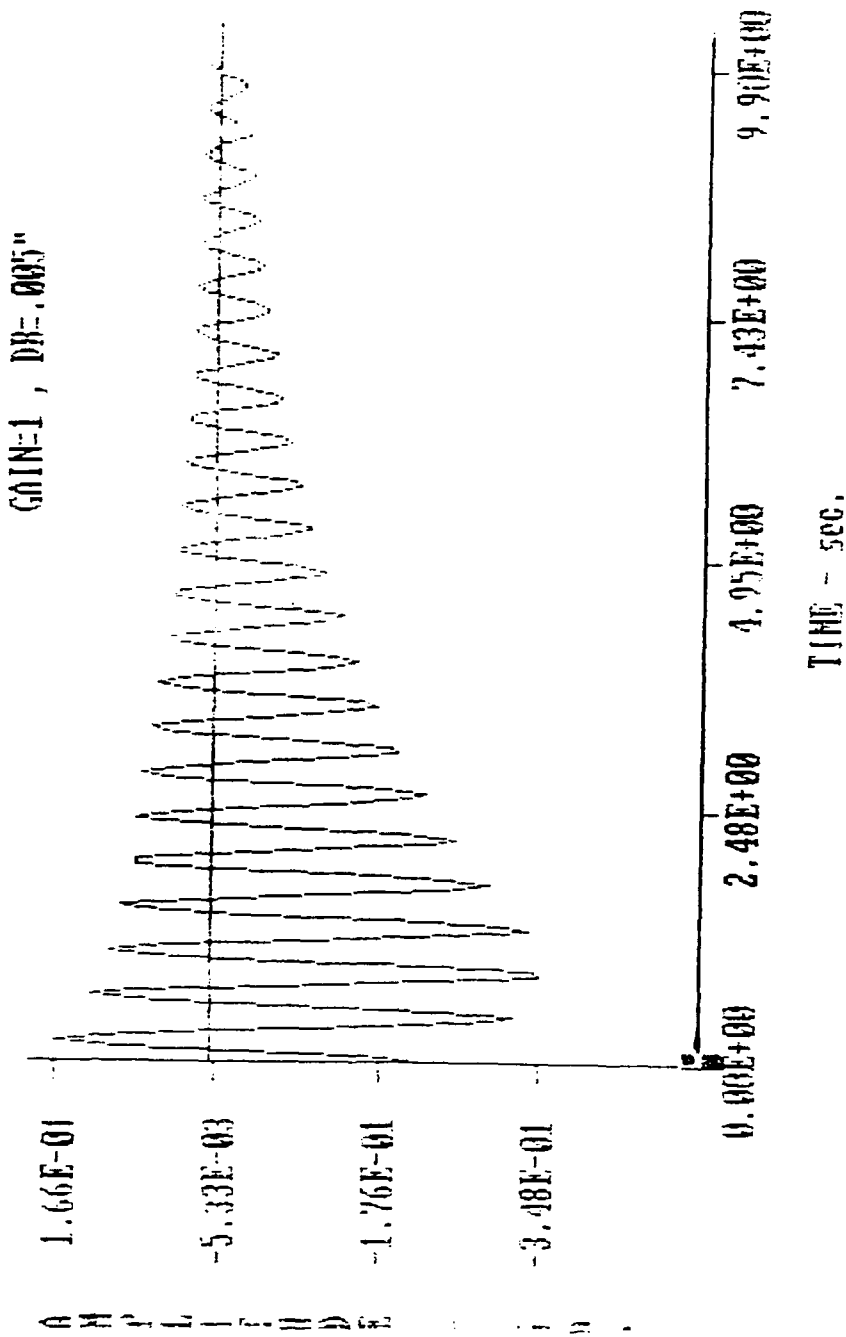


FIGURE 26-b. TIME HISTORY OF THEORETICAL AMPLITUDE OF VIBRATION OF THE BEAM WHEN CONTROLLED WITH ONE NITINOL ACTUATOR WITH A LEAD BAND OF 0.005 in.

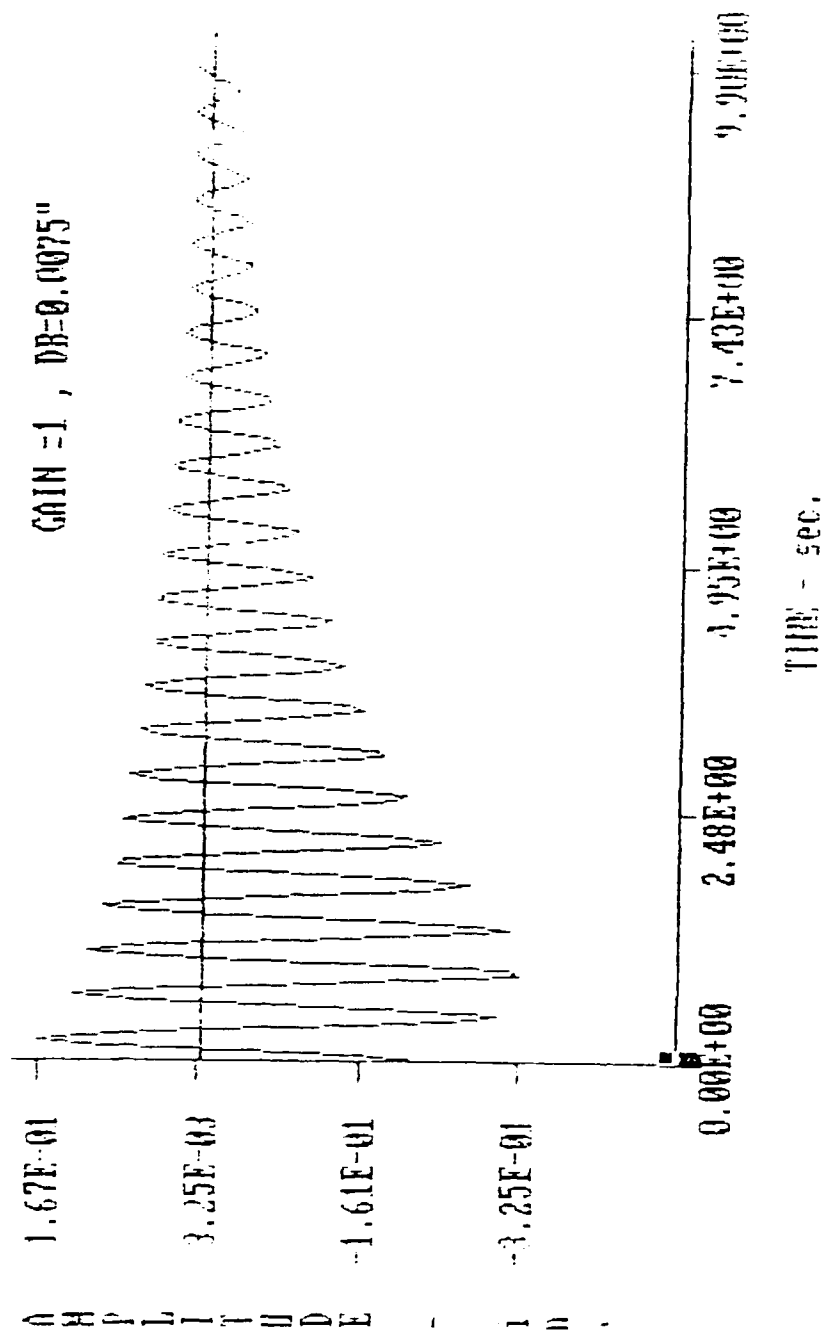


FIGURE 26-c. TIME HISTORY OF THEORETICAL AMPLITUDE
OF VIBRATION OF THE BEAM WHEN CONTROLLED WITH
ONE NITINOL ACTUATOR WITH A DEAD BAND OF 0.0075 in.

%, when the dead band is 0.0025". This unfavorable characteristic is attributed to the fact that the energization of the NITINOL actuator is maintained whether the beam velocity \dot{y}_j is positive or negative. Of course, when the NITINOL produces a moment which acts against the beam velocity effective damping is produced. But, when the two have the same sense then the NITINOL moment assists the beam motion rather than suppresses it.

This undesirable behavior can be improved in two ways. The first is to increase the dead band of the controller, a strategy illustrated in Figures 26-a through 26-c. But, a more pronounced improvement can be achieved by deenergizing the actuator when the beam velocity becomes negative, as shown in Figure 25-b. This would result in the performance characteristics shown in Figures 27-a and 27-b for dead bands of 0.005 and 0 in respectively.

A comparison between Figures 27-a and 26-b shows that the degree of overshoot, for negative displacement has been reduced by 12.4 % . However, the performance of the control system is still judged inadequate and a desirable vibration control function has not yet been achieved.

(iii) **Control with two NITINOL actuators.** In order to achieve better performance of the active control system, two actuators are used, each connected to opposite sides of the beam, as shown in Figure 28. The performance of the system is shown in Figures 29-a, 29-b, and 29-c for values of the dead band of 0.005, 0.001 and 0.0005 in respectively. Significant improvement is achieved both over the single wire controller and the uncontrolled case, shown, in Figure 23-b.

This theoretically predicted performance of the controller will next be checked against the experimental behavior of a prototype of the system.

C. The Physical Control System

(i) **Electronic circuits.** The actual active vibration control system relied in its operation on three basic electronic circuits.

1. Input/output circuit. This circuit provides an interface between the sensor and actuator of the active control system and the 6510 micro-computer. Figure 30 shows a schematic drawing of the circuit to indicate its basic components. The circuit utilizes an 8-bit A/D converter model AD7824 from Analog devices to provide up to 4 analog

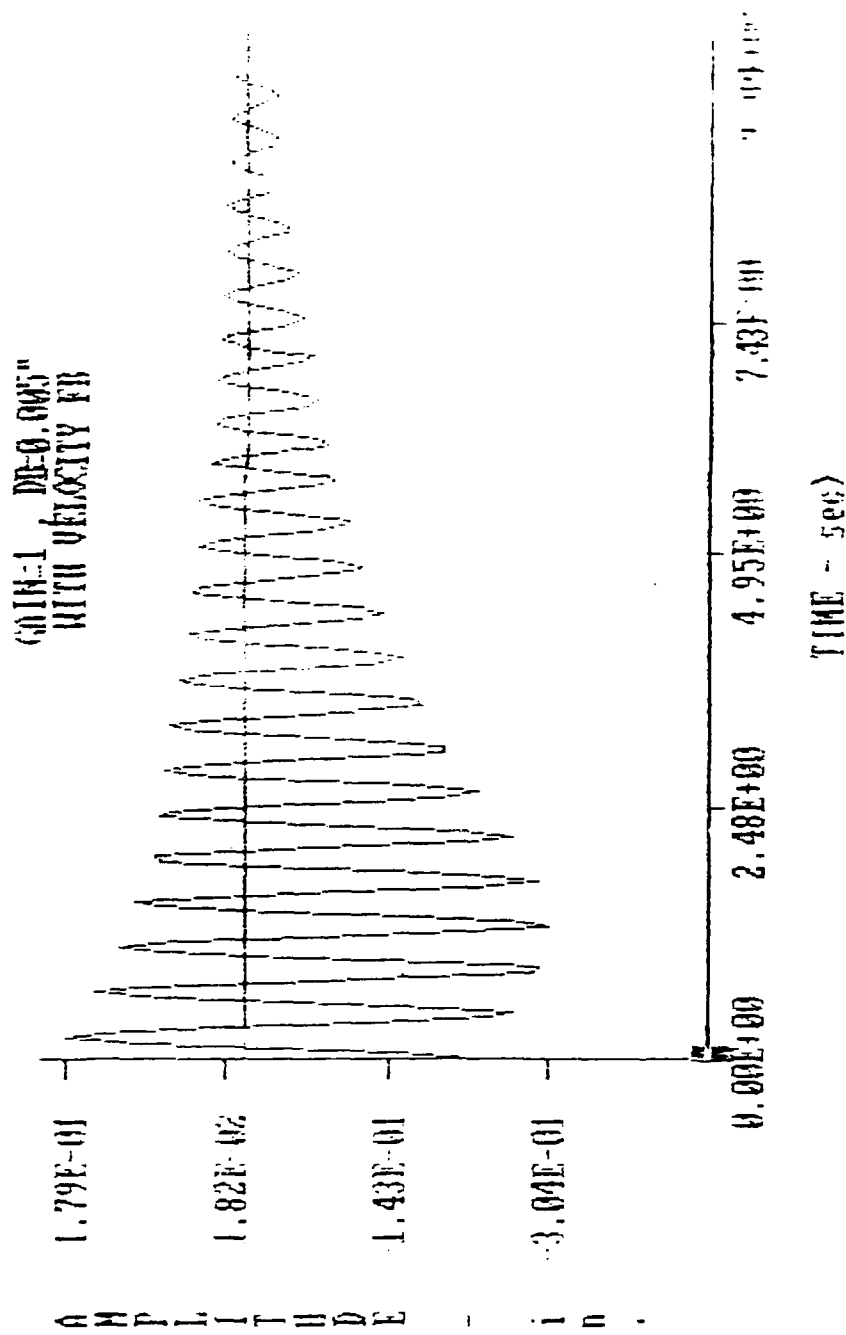


FIGURE 27-a. TIME HISTORY OF THEORETICAL AMPLITUDE OF VIBRATION OF THE BEAM WHEN CONTROLLED WITH ONE NITINOL ACTUATOR WITH A DEAD BAND OF 0.005 in AND A VELOCITY FEEDBACK LOGIC.

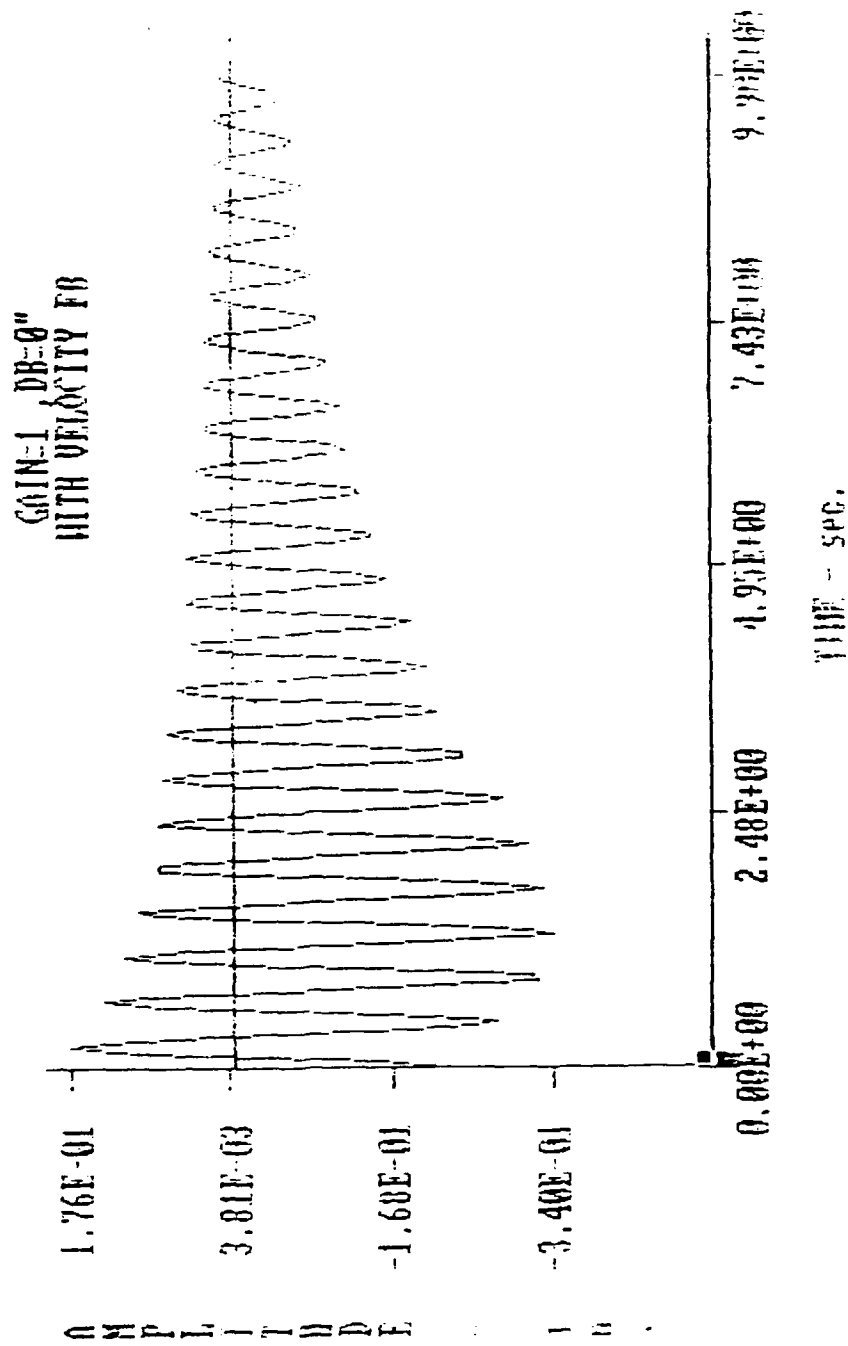


FIGURE 27-b. TIME HISTORY OF THEORETICAL AMPLITUDE
OF VIBRATION OF THE BEAM WHEN CONTROLLED WITH
ONE NITINOL ACTUATOR WITH A DEAD BAND OF 0 in
AND A VELOCITY FEEDBACK LOGIC.

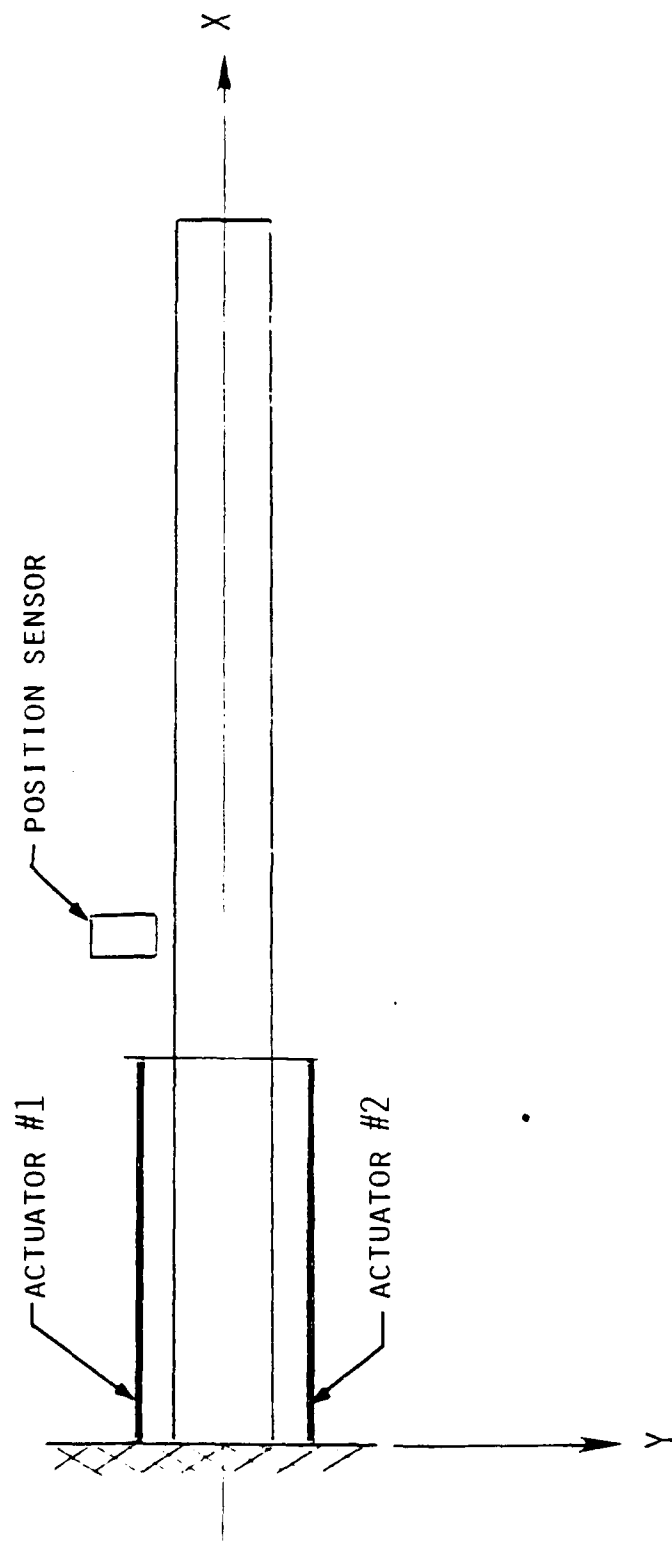


FIGURE 28. ACTIVE CONTROLLER WITH TWO NITINOL ACTUATORS.

GAIN=1, 2-WIRES, DB=0.005"
WITH VELOCITY FB

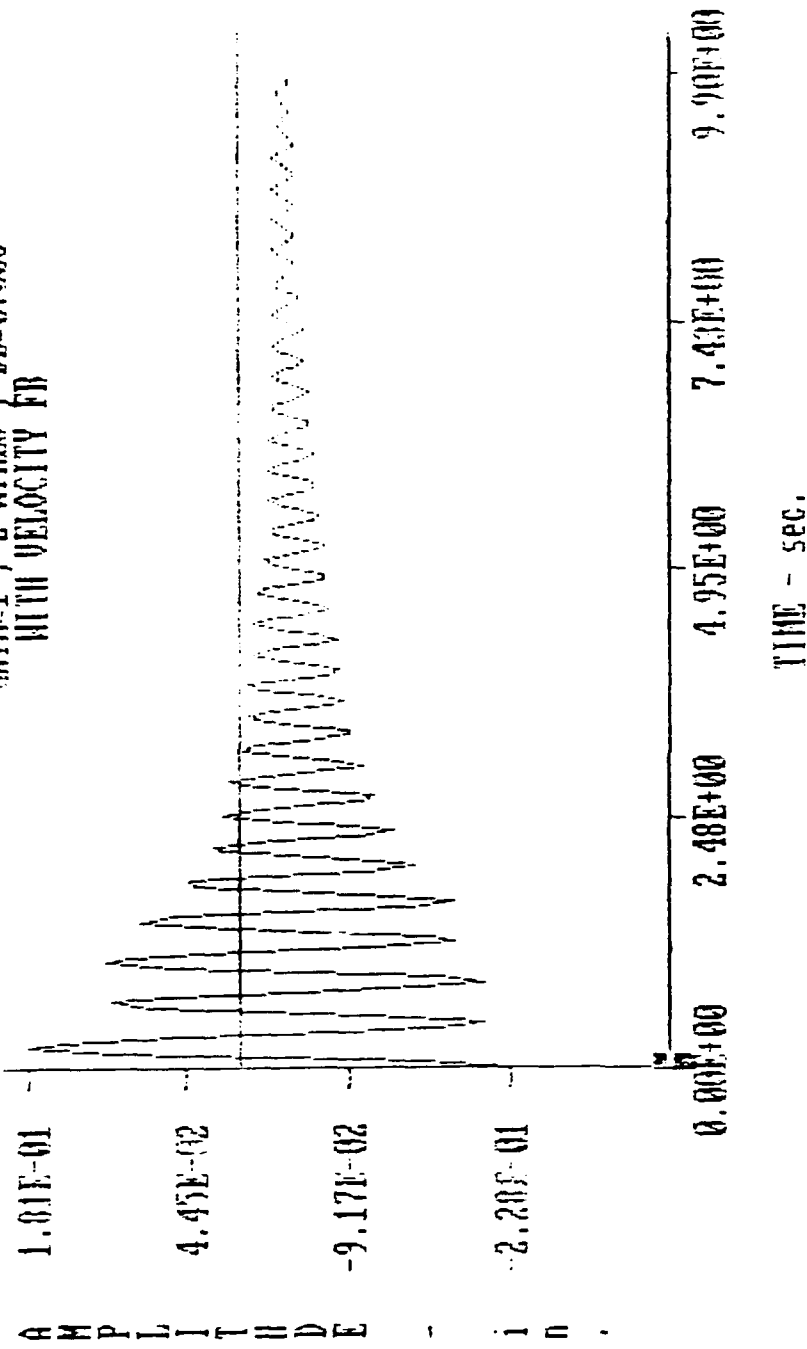


FIGURE 29-a. TIME HISTORY OF THEORETICAL AMPLITUDE OF TRANSVERSE VIBRATION OF THE BEAM WHEN CONTROLLED WITH TWO NITINOL ACTUATORS WITH DEAD BAND OF 0.005 in AND VELOCITY FEEDBACK LOGIC.

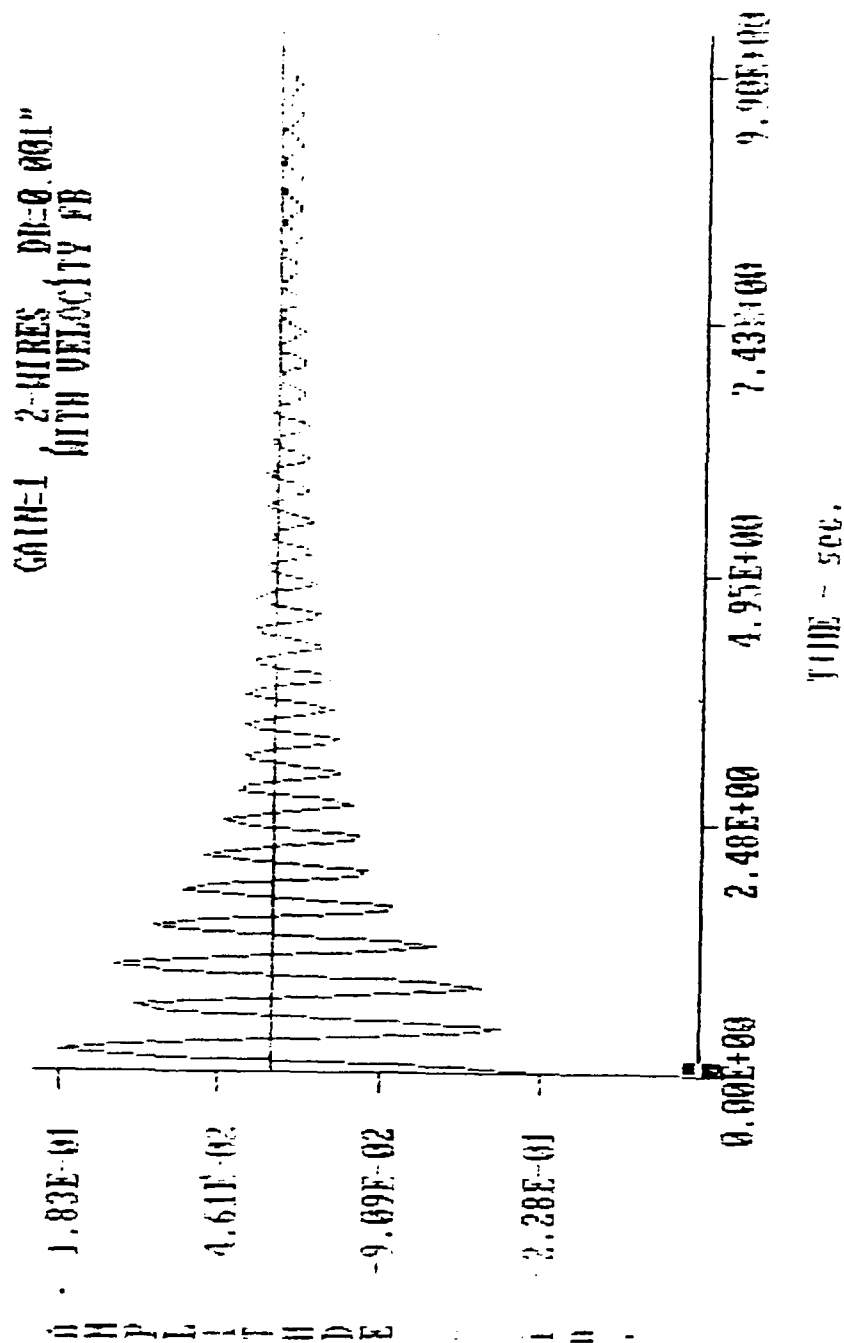


FIGURE 29-b. TIME HISTORY OF THEORETICAL AMPLITUDE
OF TRANSVERSE VIBRATION OF THE BEAM WHEN CONTROLLED WITH
TWO NITINOL ACTUATORS WITH DEAD BAND OF 0.001 in
AND VELOCITY FEEDBACK LOGIC.

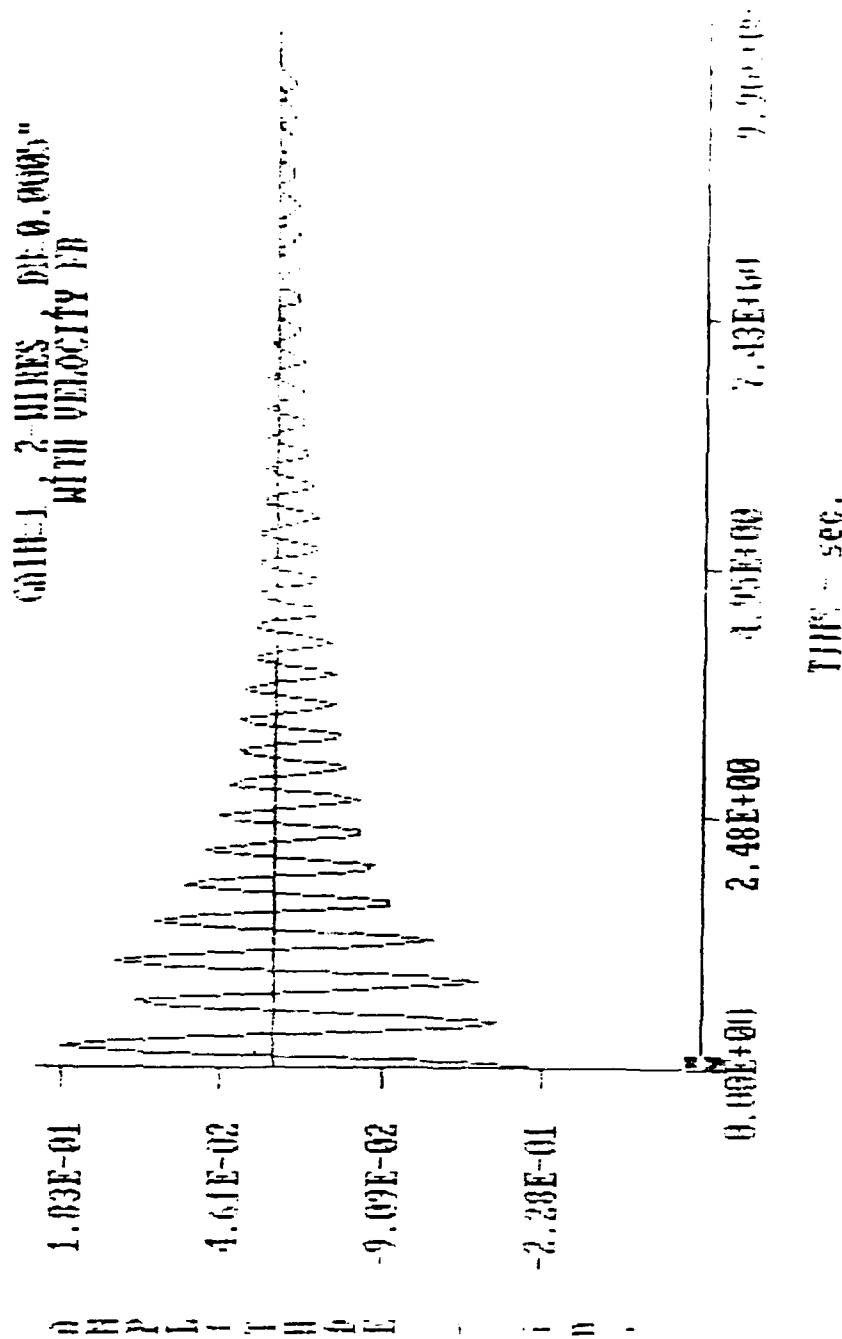


FIGURE 29-c. TIME HISTORY OF THEORETICAL AMPLITUDE
OF TRANSVERSE VIBRATION OF THE BEAM WHEN CONTROLLED WITH
TWO NITINOL ACTUATORS WITH DEAD BAND OF 0.0005 in
AND VELOCITY FEEDBACK LOGIC.

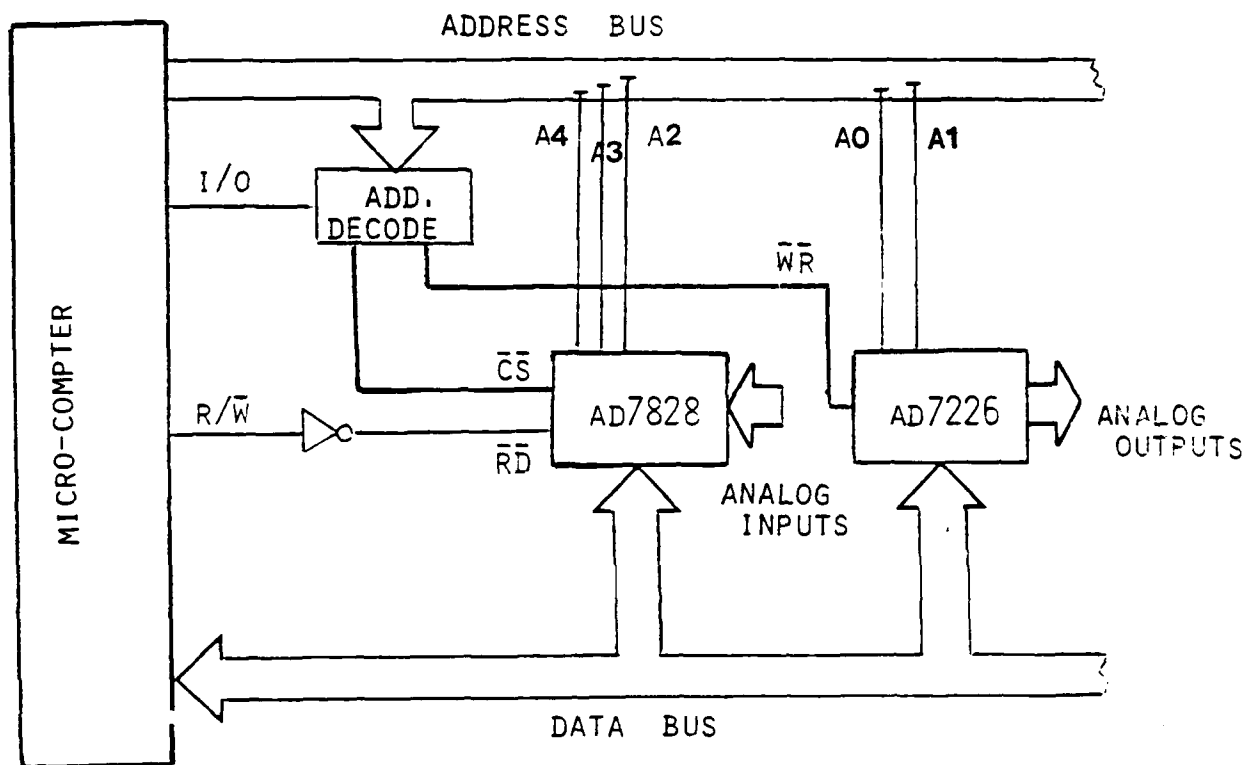


FIGURE 30. SCHEMATIC DRAWING OF THE INPUT/OUTPUT CIRCUIT.

input channels. The converter has a conversion rate of $2.5 \mu\text{s}$ per channel using half-flash conversion technique. It operates from a 5 V supply and has an analog input range of 0 to 5 V. Detailed specifications of the A/D converter is given in the Appendix.

The circuit also incorporates an 8-bit D/A converter model AD7226 which is capable of sending 4 output signals that are buffered by a CMOS amplifier. The D/A can develop +10 V signals across a $2 \text{ k}\Omega$ resistor. It has separate on-chip latches to which data is transferred through a common 8-bit TTL/CMOS (5V) compatible input port. The D/A converter has address to write hold time of 10 ns. Detailed specifications of the D/A converter are given in the Appendix.

An address decode chip 74L138 is used to control the operation of the A/D and D/A chips.

2. Actuator Control Circuit. The energization and deenergization of the NITINOL actuator are controlled by the control circuit shown in Figure 31. In this circuit, the output from the D/A is biased by a trim potentiometer and amplified by 741 operational amplifier. The output of the amplifier is used to trigger an NPN power transistor (2N3055). The transistor provides, through its collector/emitter amplification, the current necessary to power the NITINOL actuator from an external power supply.

3. Sensor Circuit. An inductive proximity sensor Model 576013-190 from Veeder-Root is used to monitor the vibration of the cantilever beam. The sensor is of the non contacting type and therefore provides information about the beam displacement without influencing its dynamic behavior.

The sensor output is amplified by an operational amplifier after controlling its bias level and then sampled by the A/D converter as shown in Figure 32.

Details of the specifications of the sensor are given in the Appendix.

(ii) Performance of controller. The performance of the controller is determined experimentally under different conditions to demonstrate the effectiveness of the NITINOL actuator in damping out the vibration of the experimental beam.

The effect of using one or two actuators on the performance of the controller is investigated for different maximum actuator voltages and controller dead bands. Furthermore,

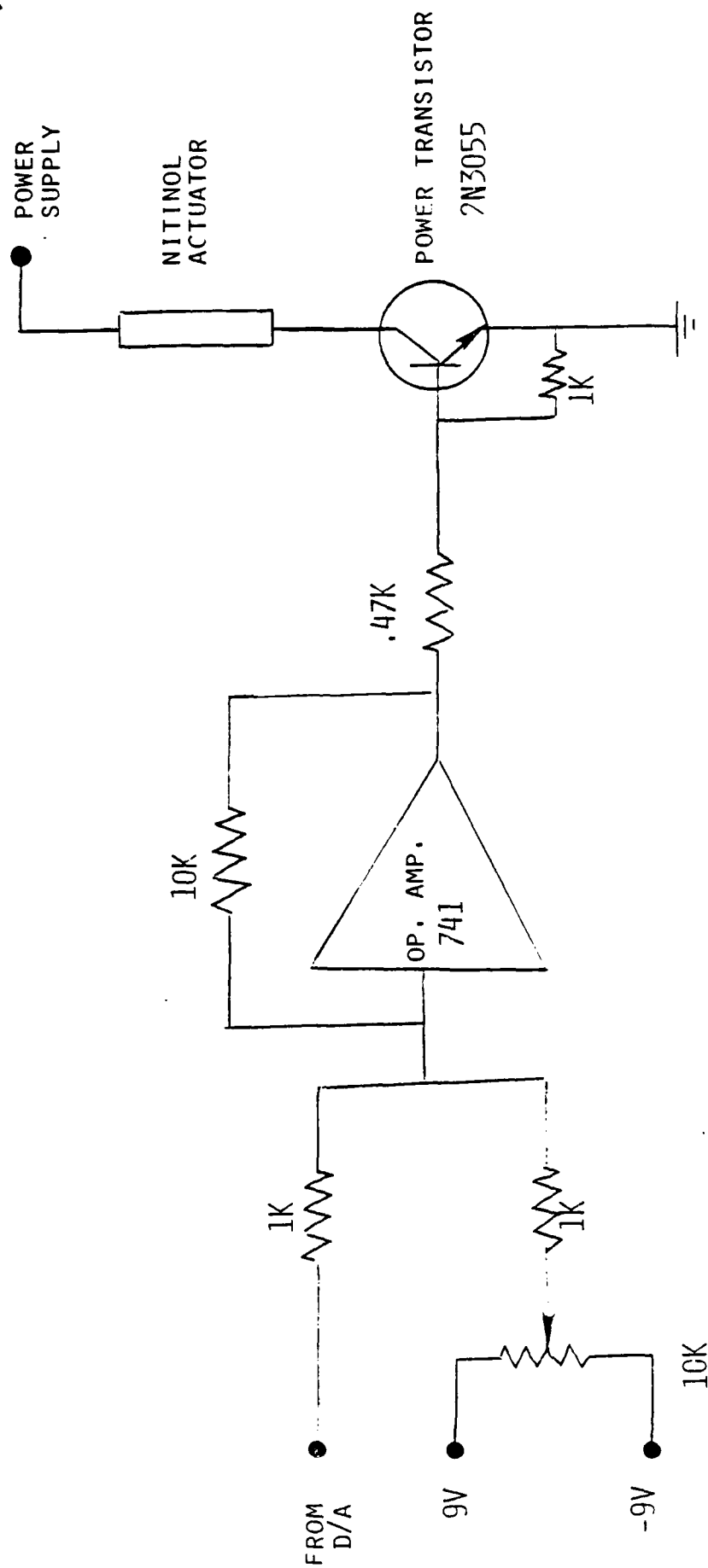


FIGURE 31. ACTUATOR CONTROL CIRCUIT.

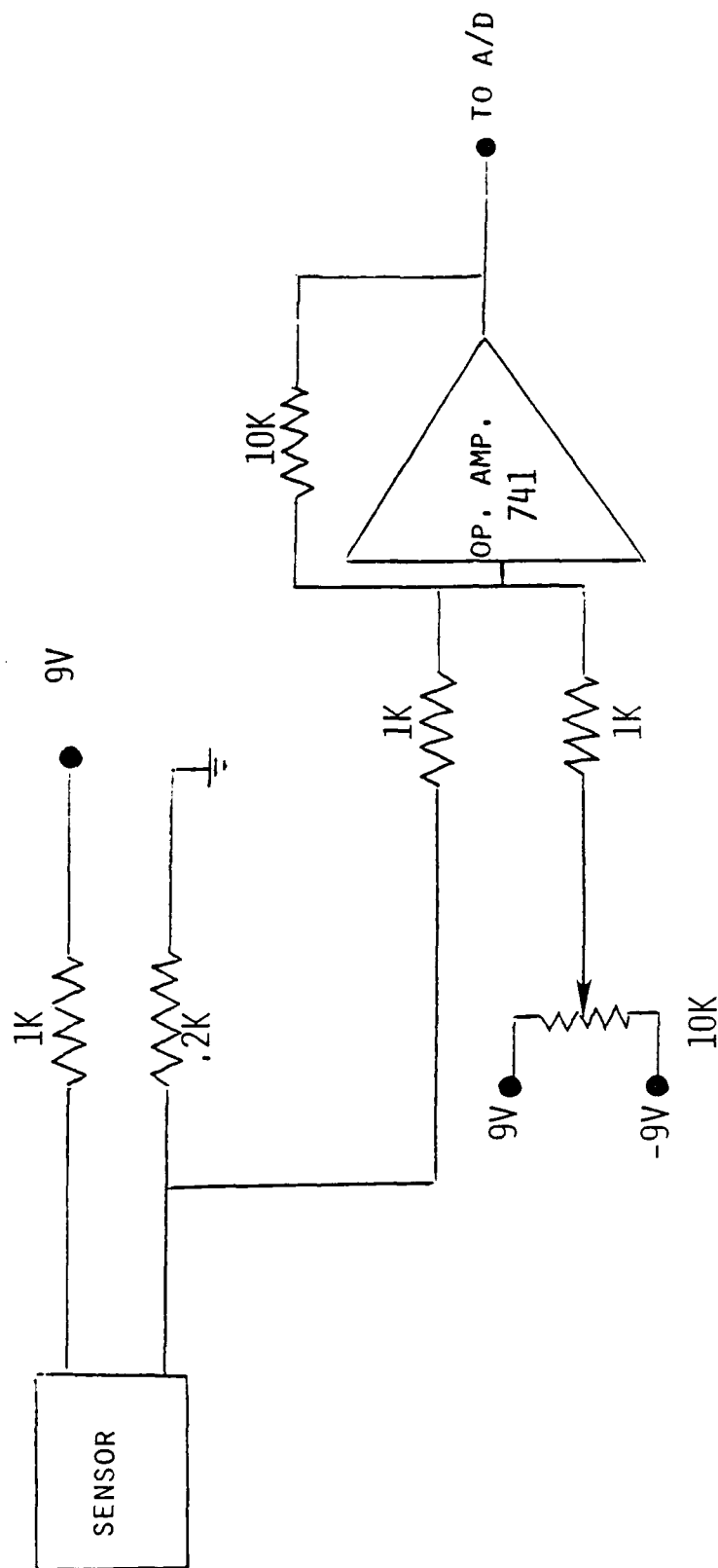


FIGURE 32. SCHEMATIC DRAWING OF SENSOR CIRCUIT.

the effectiveness of the controller is checked for changes in the natural frequency of the flexible beam, achieved by the addition of a weight at different locations along the beam.

1. Performance with Single-Wire Actuator Figures 33-a and 33-b show the time response of the cantilever beam without and with the active controller respectively. The actuator is energized by 0.4 V and 1 A with a dead band of 0.0025 in. The close agreement between the measured performance of Figures 33-a and 33-b and the theoretical predictions shown in Figures 23-b and 26-a is evident. Notice particularly the previously mentioned features of a single wire controller which are effective in damping the oscillation in the positive direction only, with increased overshoot in the negative direction.

Increasing the applied voltage from 0.4 V to 0.6 and 0.8 V results in improved damped characteristics of the controller as shown in Figures 34-a and 34-b respectively. But, this is at the expense of bending the beam too far from its original position. The controller is seen however, to take some time to bring it back to that position as it relies only on natural cooling to achieve such a task.

2. Performance with Two-Wire Actuator

a. Original beam. Figures 35-a, 35-b and 35-c show the time response of the original cantilever beam without the controller operating at 0.6 A and 1 A respectively. The dead band of the controller is taken, in the two later cases, as zero. It is evident that the controller is extremely effective in damping out the vibration, when it is powered by 0.6 A. Based on Figures 35-a and 35-b one sees that the controller has reduced the time needed to damp out the vibration from 13.6 s to 6 s. Increasing the power input to the actuators from 0.6 A to 1 A resulted in further reduction in the time needed to come to the original position. But, once the beam is close to that position the energization and deenergization of the actuators is seen to excite the beam rather than damp out its vibration.

Introducing dead band in the controller is found to be extremely effective in utilizing the fast damping characteristics resulting from increased input power to the actuator without exciting the beam when it reaches its desired destination. This is manifested in Figures 36-a and 36-b when the actuators are powered by 1 A but with dead bands of 0.0008" and 0.0016" respectively. It can be seen that the self-excited vibration problem

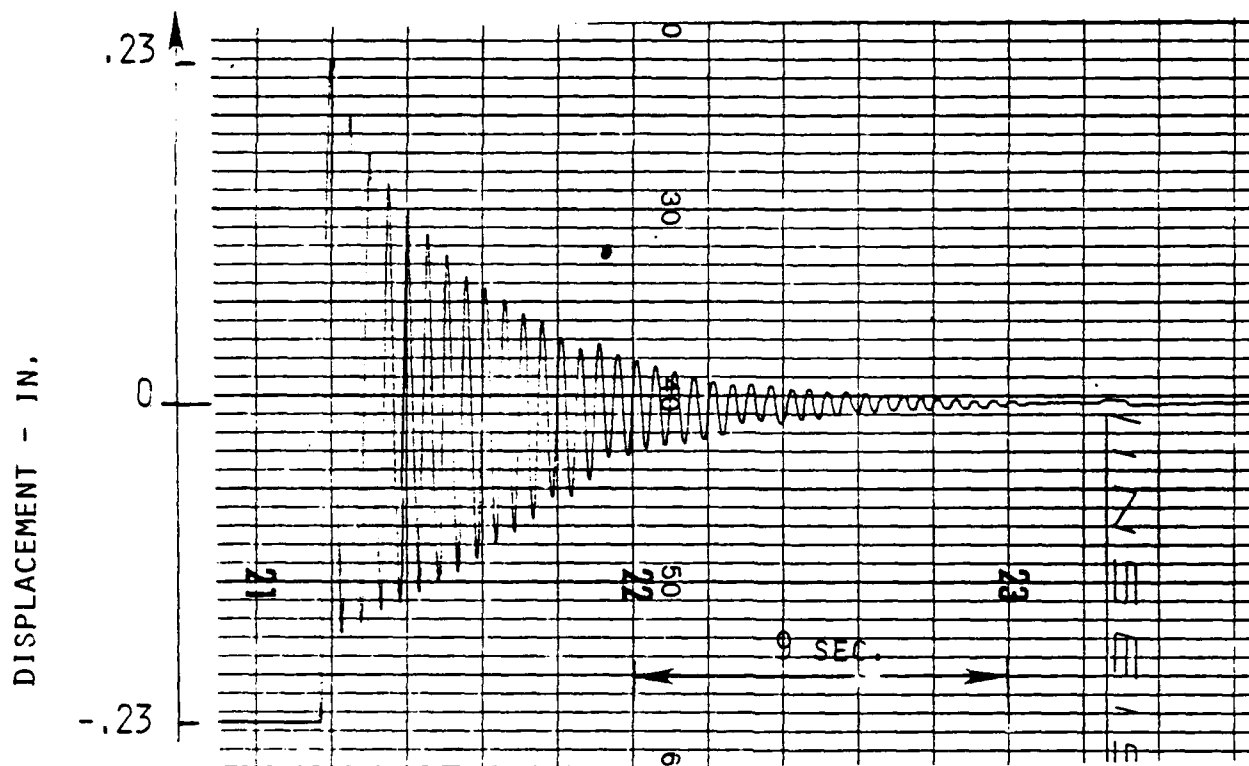


FIGURE 33-a. TIME HISTORY OF THE EXPERIMENTAL AMPLITUDE OF VIBRATION OF THE BEAM, WITH ONE ACTUATOR, UNDER FREE VIBRATION CONDITIONS.

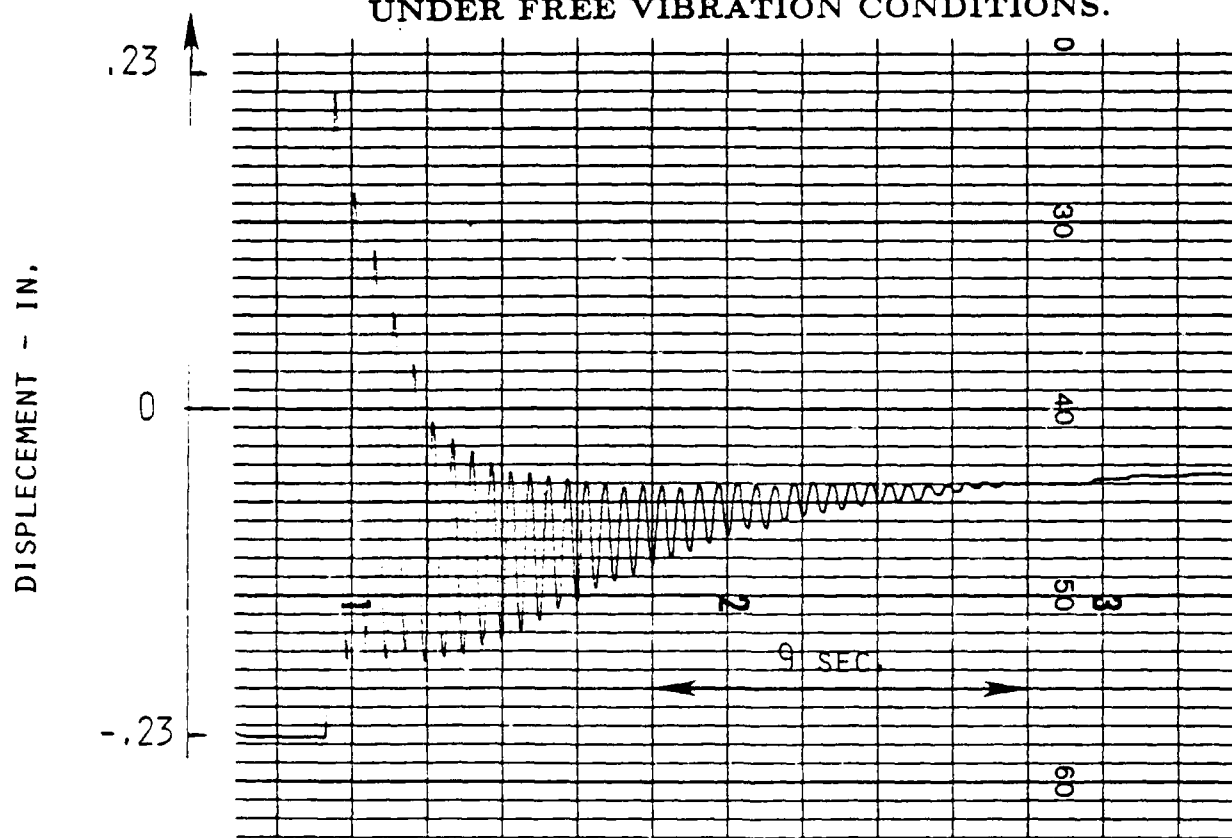


FIGURE 33-b. TIME HISTORY OF THE EXPERIMENTAL AMPLITUDE OF VIBRATION OF THE BEAM WHEN CONTROLLED WITH ONE ACTUATOR (ACTUATOR VOLTAGE = 0.4 V AND DEAD BAND = 0.0025 in).

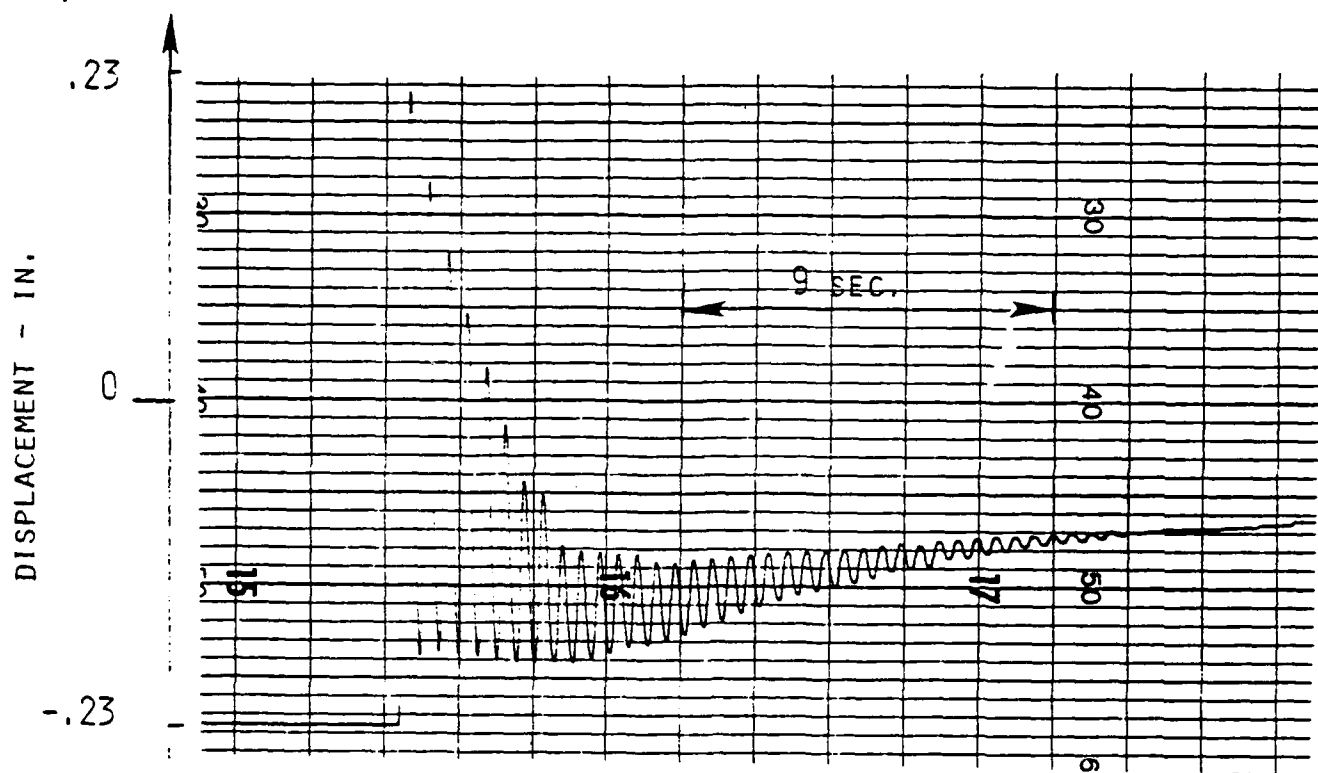


FIGURE 34-a. TIME HISTORY OF THE EXPERIMENTAL AMPLITUDE OF VIBRATION OF THE BEAM WHEN CONTROLLED WITH ONE ACTUATOR (ACTUATOR VOLTAGE = 0.6 V AND DEAD BAND = 0.0025 in).

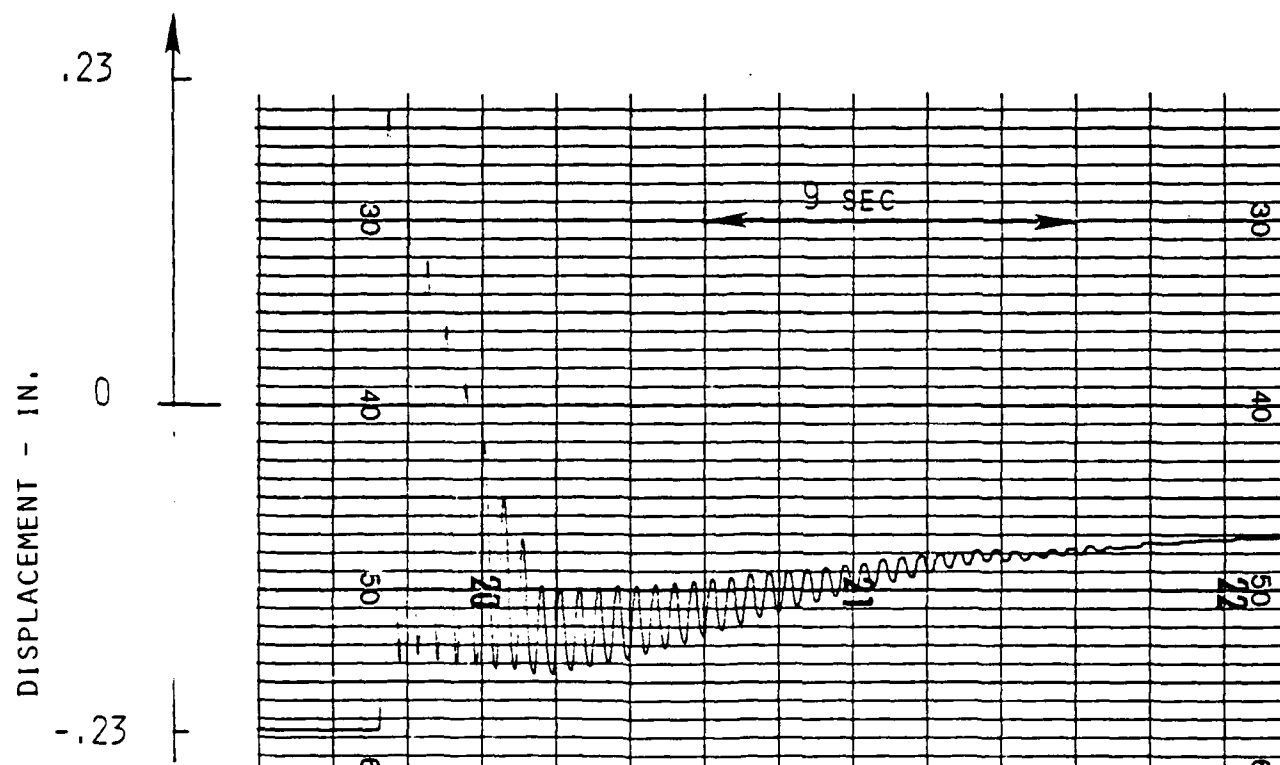


FIGURE 34-b. TIME HISTORY OF THE EXPERIMENTAL AMPLITUDE OF VIBRATION OF THE BEAM WHEN CONTROLLED WITH ONE ACTUATOR (ACTUATOR VOLTAGE = 0.8 V AND DEAD BAND = 0.0025 in).

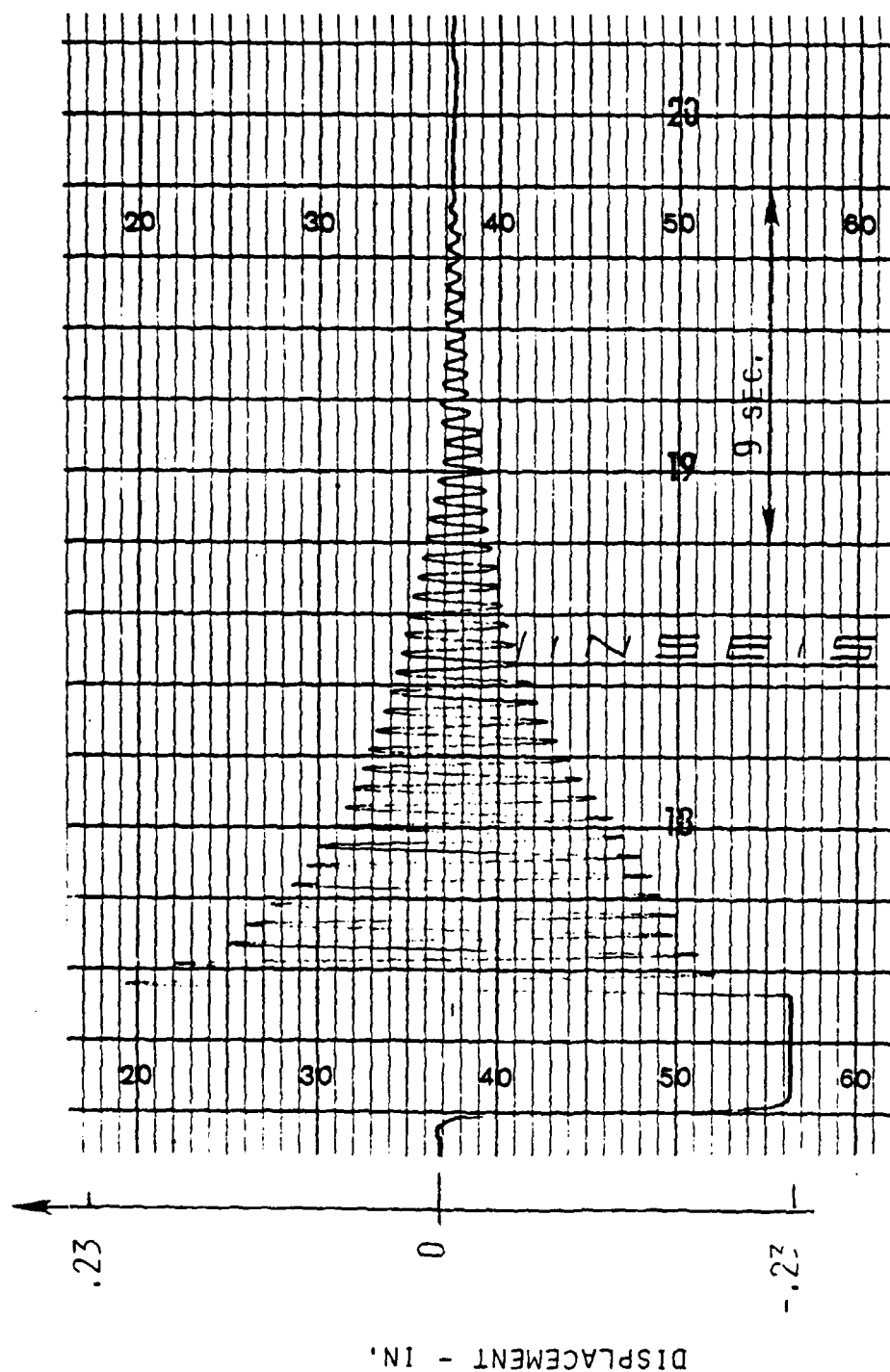


FIGURE 35-a. TIME HISTORY OF THE EXPERIMENTAL AMPLITUDE
OF VIBRATION OF THE BEAM, WITH TWO ACTUATORS,
UNDER FREE VIBRATION CONDITIONS.

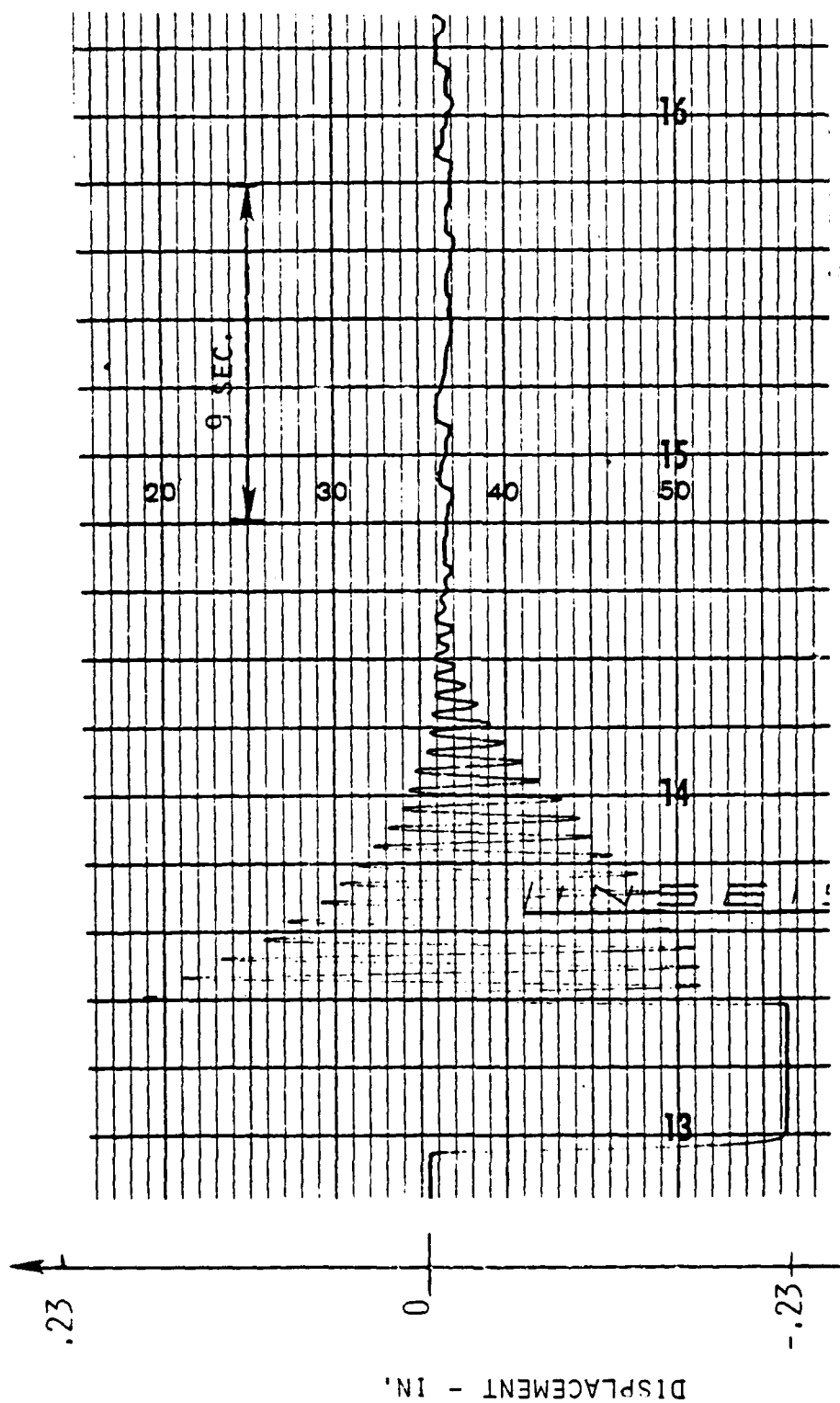


FIGURE 35-b. TIME HISTORY OF THE EXPERIMENTAL AMPLITUDE
OF VIBRATION OF THE BEAM WHEN CONTROLLED WITH
TWO ACTUATORS (ACTUATOR CURRENT = 0.6 A AND DEAD BAND = 0 in).

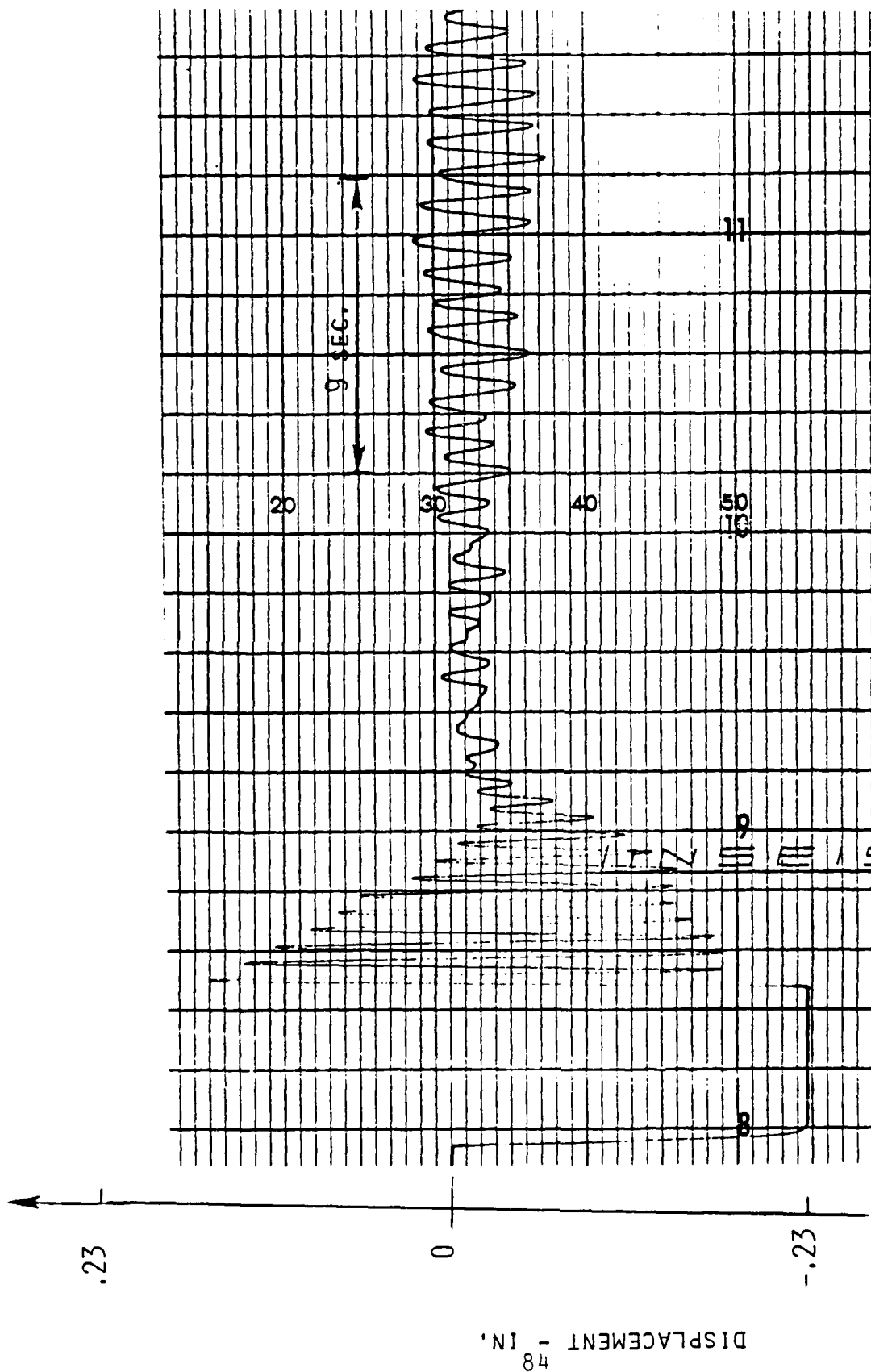


FIGURE 35-c. TIME HISTORY OF THE EXPERIMENTAL AMPLITUDE
OF VIBRATION OF THE BEAM WHEN CONTROLLED WITH
TWO ACTUATORS (ACTUATOR CURRENT = 1 A AND DEAD BAND = 0 in).

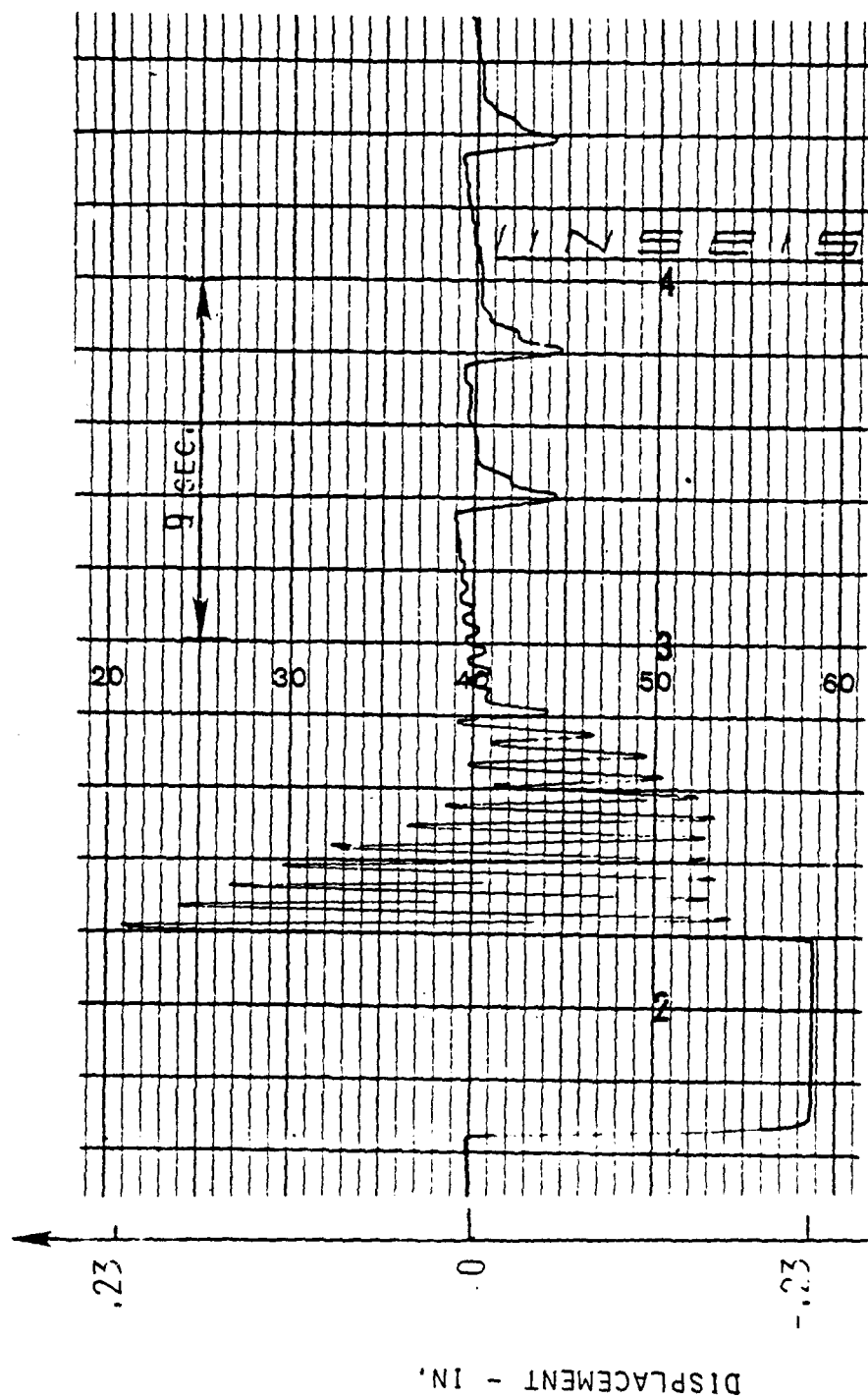


FIGURE 36-a. TIME HISTORY OF THE EXPERIMENTAL AMPLITUDE OF VIBRATION OF THE BEAM WHEN CONTROLLED WITH TWO ACTUATORS (ACTUATOR CURRENT = 1 A AND DEAD BAND = 0.0008 in.)

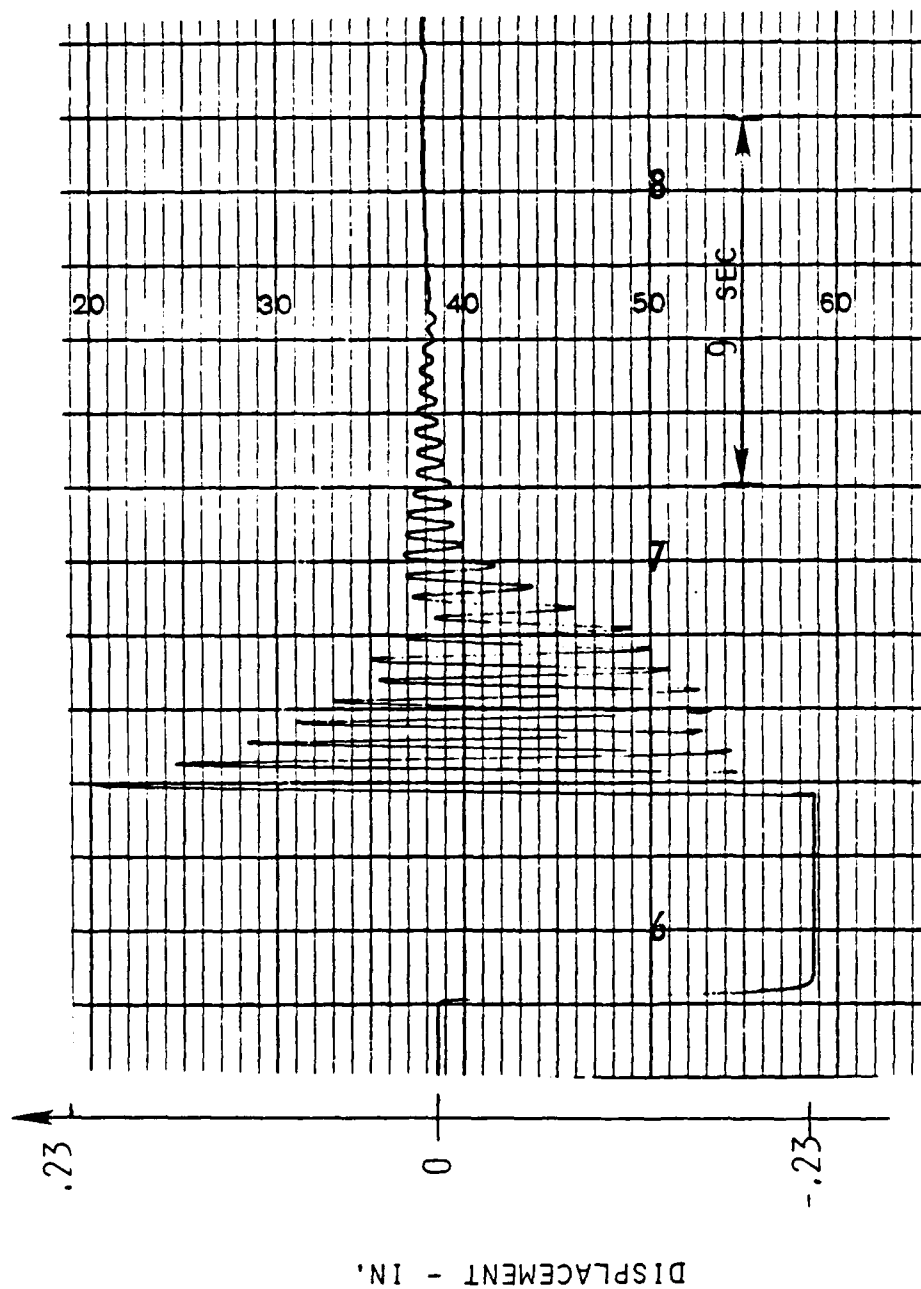


FIGURE 36-b. TIME HISTORY OF THE EXPERIMENTAL AMPLITUDE OF VIBRATION OF THE BEAM WHEN CONTROLLED WITH TWO ACTUATORS (ACTUATOR CURRENT = 1 A AND DEAD BAND = 0.0016 in)

displayed in Figure 35-c is reduced in Figure 36-a and eliminated in Figure 36-b.

b. Beam with added weight. Figures 37-a and 37-b show the time response of the beam without and with the active controller respectively when a weight of 12.45 gm is glued to the beam at 12.5 cm from its fixed end. Figure 34-a indicates that the natural frequency of the beam dropped from 2.25 Hz to 2 Hz. With the controller parameters maintained as those for the original beam, i.e. 1 A and dead band of 0.0016", it can be seen that this controller is still effective in suppressing the vibration of the beam with the added weight. Placing the 12.45 gm weight at a distance of 20 cm from the fixed end of the beam resulted in reducing its natural frequency to about 1 Hz as can be seen from the time response of the uncontrolled beam shown in Figure 38-a. When the same control law is applied to this beam the resulting response is shown in Figure 38-b. Significant vibration reduction is still evident.

The developed controller is judged to be effective and also insensitive to large changes in the parameters of the flexible system. Accordingly, it is a robust controller.

VII. CONCLUSIONS

This report presented a detailed experimental and theoretical study which aims at demonstrating the feasibility of utilizing NITINOL actuators in suppressing the vibrations of simple flexible systems.

The dynamic characteristics of NITINOL actuators have been measured over a wide range of design parameters and operating conditions. Mathematical modelling of the dynamic characteristics of the actuators have been developed and guided by the obtained experimental results.

The dynamic model of the actuator is combined with that of the flexible system to form the bases necessary for designing a NITINOL-based active control system to suppress the vibration of the flexible system.

Detailed design of the control circuits used in the implementation of the controller is presented. Presented also are the results of testing a prototype of the controller under a wide variety of control strategies.

The presented theoretical and experimental procedures are general in nature and

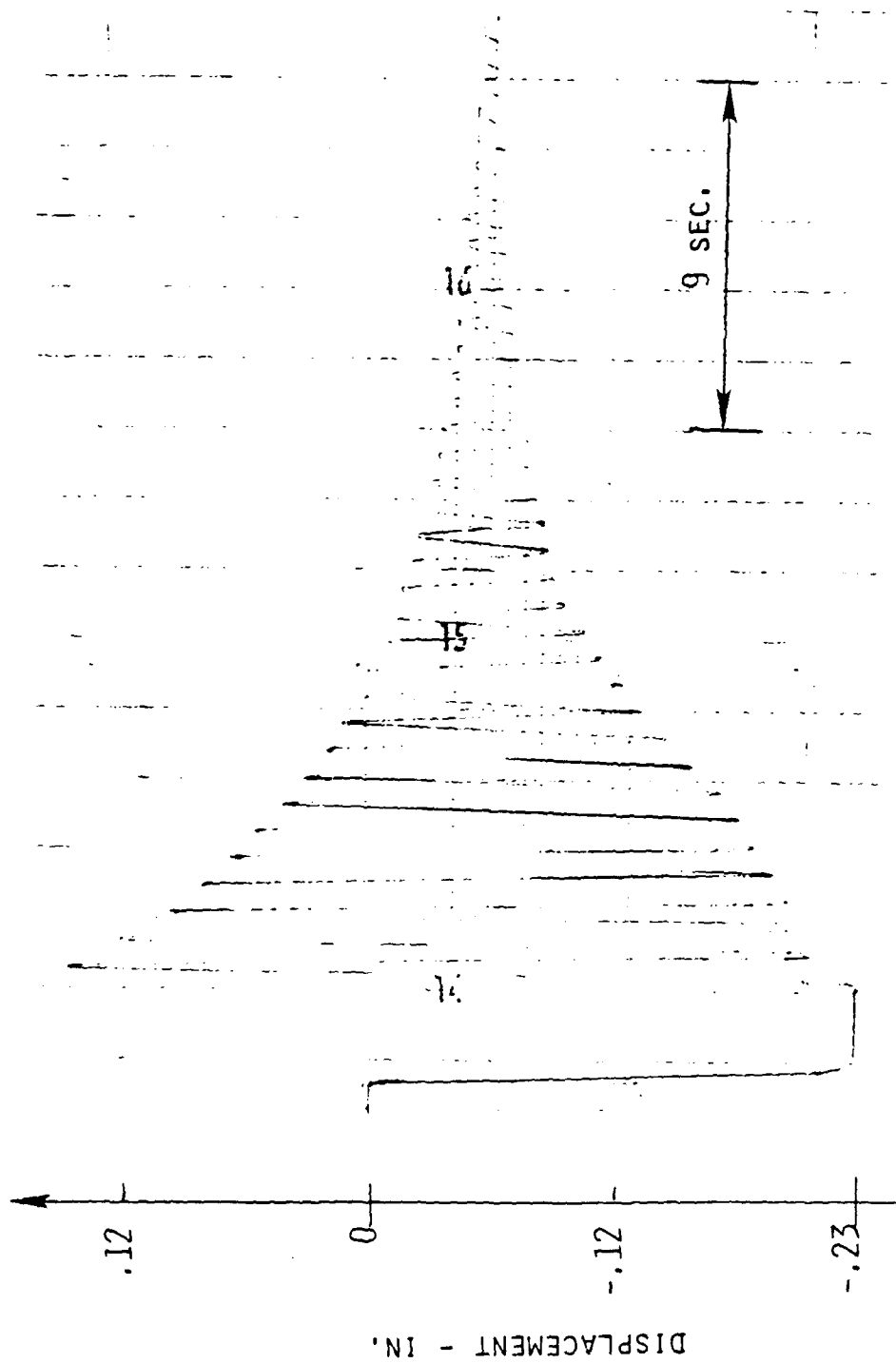


FIGURE 37-a. TIME HISTORY OF THE EXPERIMENTAL AMPLITUDE
OF VIBRATION OF THE BEAM WITH 12.45 gm PLACED AT
12.5 cm FROM FIXED END, USING TWO ACTUATORS,
UNDER FREE VIBRATION CONDITIONS.

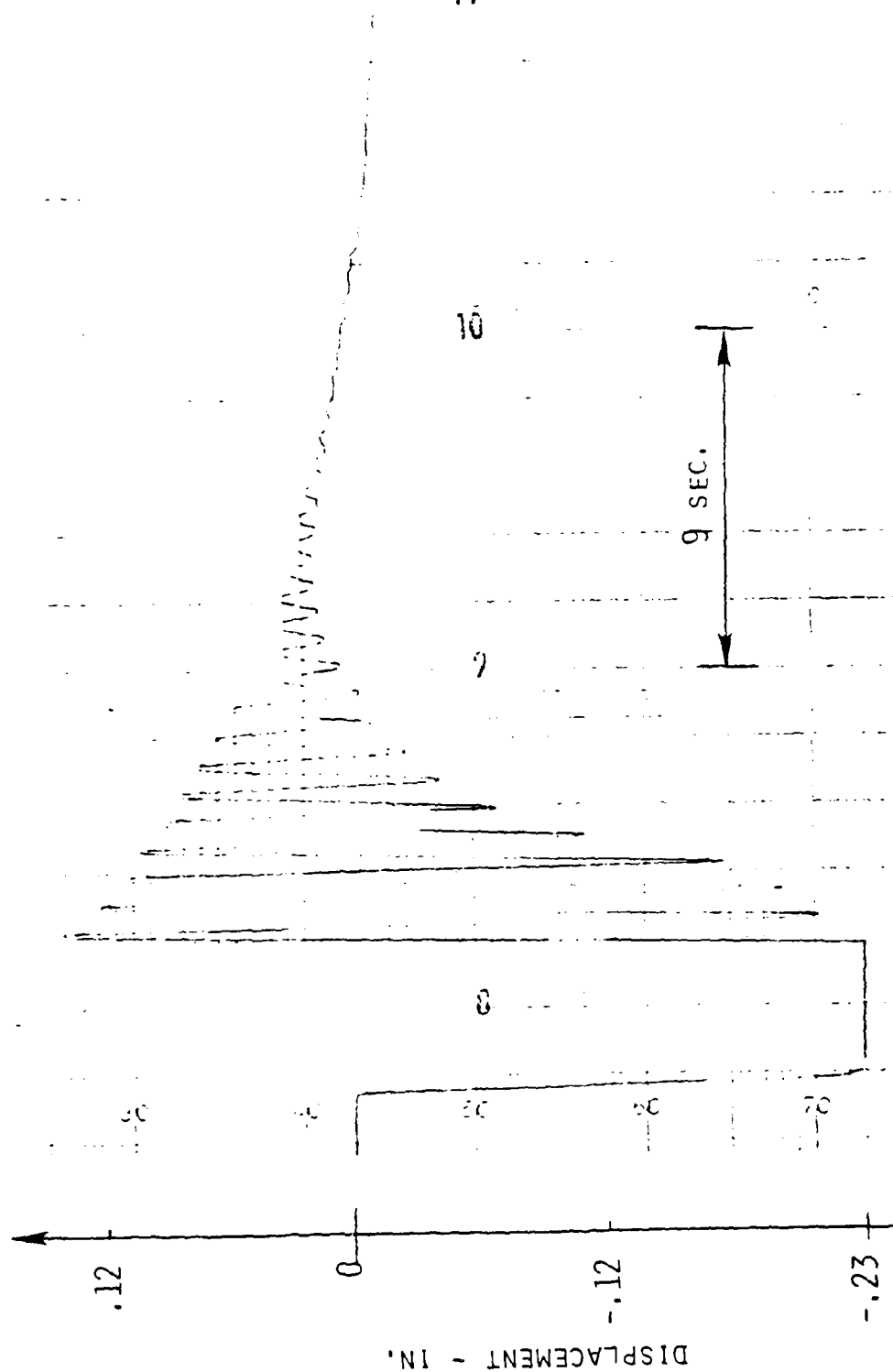


FIGURE 37-b. TIME HISTORY OF THE EXPERIMENTAL AMPLITUDE
OF VIBRATION OF THE BEAM WITH 12.45 gm PLACED AT
12.5 cm FROM FIXED END WHEN CONTROLLED WITH TWO ACTUATORS
(ACTUATOR CURRENT = 1 A AND DEAD BAND = 0.0016 in).

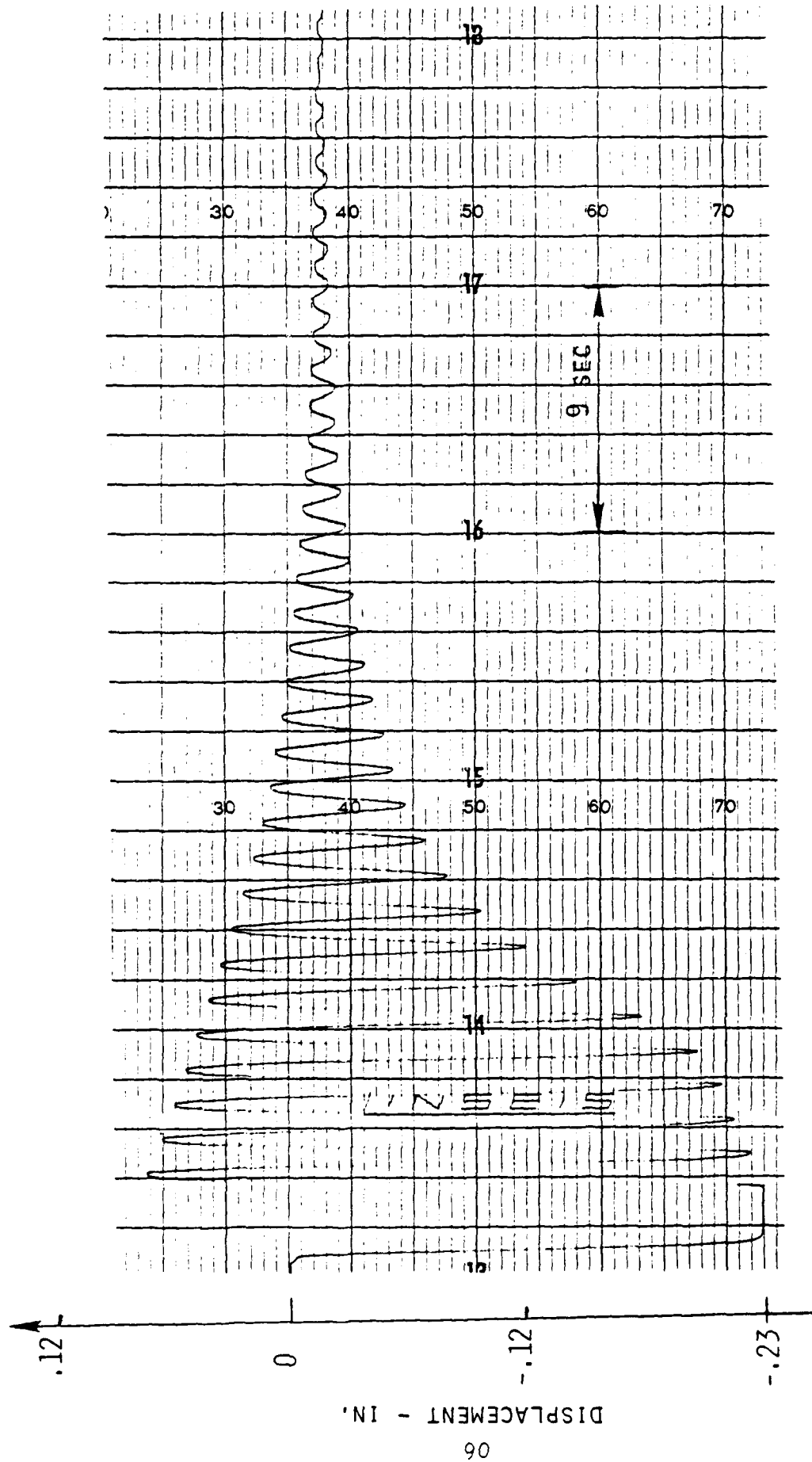


FIGURE 38-a. TIME HISTORY OF THE EXPERIMENTAL AMPLITUDE
OF VIBRATION OF THE BEAM WITH 12.45 gm PLACED AT
20 cm FROM FIXED END, USING TWO ACTUATORS
UNDER FREE VIBRATION CONDITIONS.

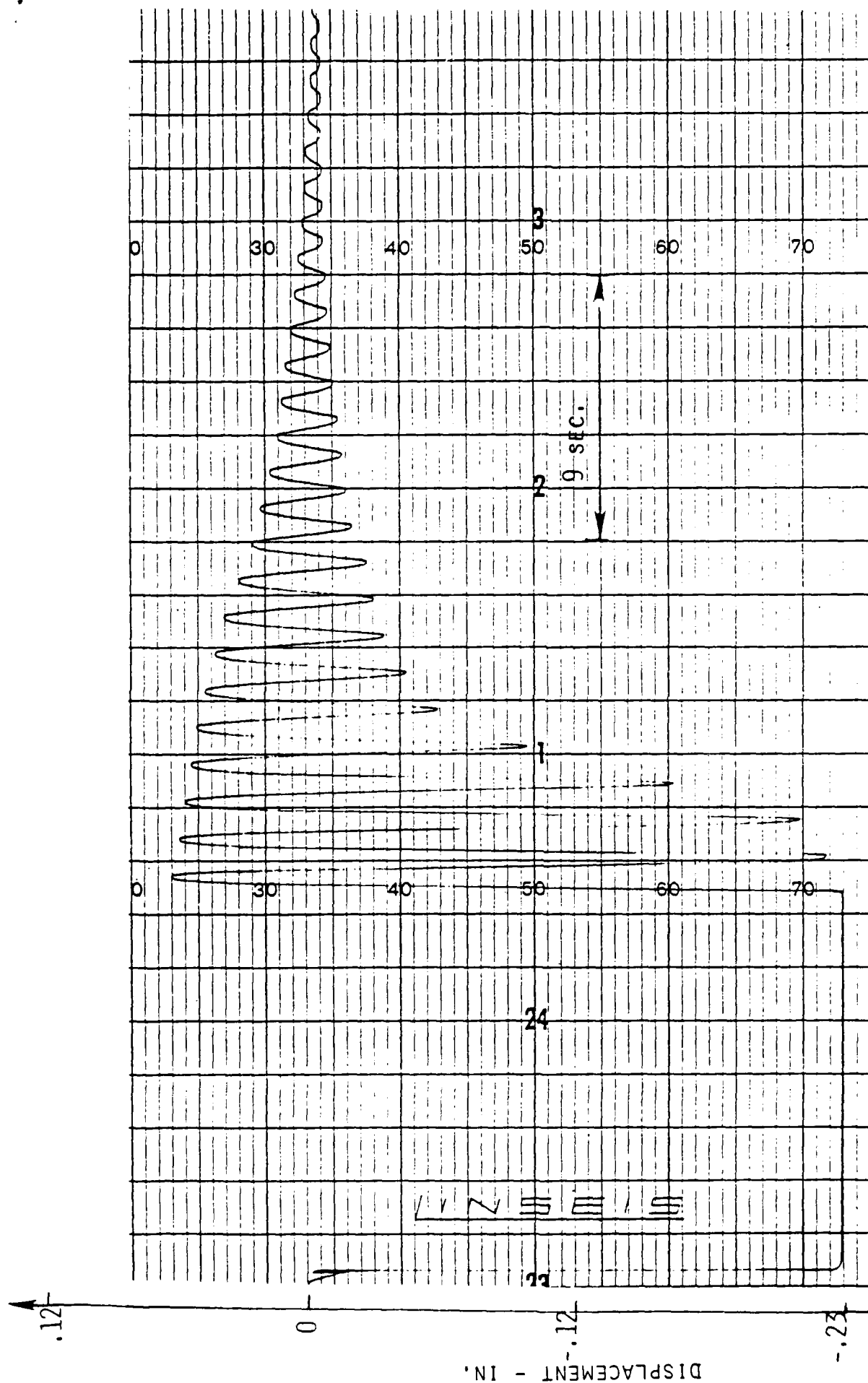


FIGURE 38-b. TIME HISTORY OF THE EXPERIMENTAL AMPLITUDE
OF VIBRATION OF THE BEAM WITH 12.45 gm PLACED AT
20 cm FROM FIXED END WHEN CONTROLLED WITH TWO ACTUATORS
(ACTUATOR CURRENT = 1 A AND DEAD BAND = 0.0016 in).

can be equally extended to more complex flexible systems. Furthermore, the presented results demonstrate clearly the feasibility and the potential of using NITINOL actuator in controlling the vibrations of flexible structures.

VIII. REFERENCES

1. Amos, A.K. , *Structural Control Research at AFOSR*, Air Force Office of Scientific Research, Bolling AFB, Washington, D.C. 20332.
2. Beards, C.F., *The Damping of Structural Vibration by Controlled Interfacial Slip in Joints*, Trans. ASME, Journal of Vibration, Acoustics, Stress and Reliability in Design, **105**, 369-373 (1983).
3. Jezequel, L., *Structural Damping by Slip in Joints*, Trans. ASME, Journal of Vibration, Acoustics, Stress and Reliability in Design, **105**, 497-504 (1983).
4. Gaul, L., *Wave Transmission and Energy Dissipation at Structural and Machine Joints*, Trans. ASME, Journal of Vibration, Acoustics, Stress and Reliability in Design, **105**, 489-496 (1978).
5. Snowdon, J.C., *Vibration and Shock in Damped Mechanical Systems*, J. Wiley & Sons, Inc., New York, 1968.
6. Balas, M.J., *Active Control of Flexible Structure*, Journal of Optimization Theory and Applications, **25**, 415-436 (1978).
7. Balas, M.J., *Feedback Control of Flexible System*, IEEE Trans. on Automatic Control, **AC23**, 673-679 (1978).
8. Balas, M.J., *Direct Velocity Feedback Control of Large Space Structures*, Journal of Guidance and Control, **2**, 252-253 (1979).
9. Luzzato, E. and M. Jean, *Mechanical Analysis of Active Vibration Damping Continuous Structures*, Journal of Sound and Vibrations, **86**, 455-473 (1983).
10. Luzzato, E., *Active Protection of Domains of a Vibrating Structure by Using Optimal Control Theory: A Model Determination*, Journal of Sound and Vibrations, **91**, 161-180 (1983).
11. Meirovitch, L. and H. Oz, *Modal-Space Control of Distributed Gyroscopic Systems*, Journal of Guidance and Control, **3**, 523-528 (1980).

12. Os, H., L. Meirovitch and C.R. Johnson, Jr. , *Some Problems Associated with Digital Control of Dynamical Systems*, Journal of Guidance and Control, 3, 523-538 (1980).
13. Meirovitch, L. and H. Baruh, *Optimal Control of Damped Flexible Gyroscopic Systems*, Journal of Guidance and Control, 4, 157-163 (1981).
14. Baz, A., S. Poh and P. Studer, *Modified Independent Modal Space Control Method for Active Control of Flexible Systems*, Proc. of 6th Conference on Dynamics and Control of Large Structures. VPI and State University, June 29 - July 1, 1987, Blacksburg, Virginia.
15. Baz, A. and S. Poh, *A Comparison Between IMSC, PI and MIMSC Methods for Controlling the Vibration of Flexible Systems*, to appear in Journal of Sound and Vibration, (1987).
16. Strunce, T., et al, *An Investigation of Enabling Technologies for Large Precision Space Systems*, Charles Stark Draper Laboratory, CSDL-R1499, Vol. III, Nov. 1981.
17. Aubrun, J. and M. Ratner, *Structural Control for a Circular Plate*, Journal of Guidance and Control, 7, 535-545 (1984).
18. Schaecter, D. and D. Eldred, *Experimental Demonstration of the Control of Flexible Structures*, Journal of Guidance and Control, 7, 527-534 (1984).
19. Cannon, R. and D. Rosenthal, *Experiments in Control of Flexible Structures with Non-Collocated Sensors and Actuators*, Journal of Guidance and Control, 7, 546-553 (1983).
20. Horner, G. *Active Damping of a Flexible Beam*, Proceedings of Symposium on Structural Dynamics and Control of Large Space Structures, NASA Langley Research Center, Pub. #N83-22256, 1-8 (1982).
21. Baz, A., *Experimental Control of Vibrations by Piezo-electric Biomorphs*, U.S. Army Research Office, Contract # 23185-EG-11 (1985).
22. Baz, A., S. Poh and P. Studer, *Optimum Vibration Control of Flexible Beams by Piezo-electric Actuators*, Proc. of the 6th Conference on Dynamics and Control of Large Structures, VPI and State University, June 29 - July 1, 1987, Blacksburg, Virginia.
23. Paz, A. and S. Poh, *Effect of Bonding on the Performance of a Piezo Actuator-based*

- Active Control System*, to appear in *Journal of Sound and Vibration* , (1987).
24. Bailey, T. and James E. Hubbard, Jr., *Distributed Piezo-electric Polymer Active Vibration Control of a Cantilever Beam*, *Journal of Guidance and Control*, 8, 5, 605-611, (1985).
 25. Forward, R.L., *Electronic Damping of Orthogonal Bending Modes in a Cylindrical Mast-Experiment*, *Journal of Spacecraft*, 18, 1, 11-17, (1981).
 26. Nakano, Y., *Hitachis Robot Hand*, *Robotics Age*, 6, 18-20 (1984).
 27. Schetky, L., *Shape Memory Effect Alloys for Robotic Devices*, *Robotics Ages*, 6, 13-17 (1984).
 28. Schetky, L., *Nitinol Devices*, Memory Metals, Inc., Stanford, CT (1985).
 29. Perkins, A. (ed.), *Shape Memory Effects in Alloys*, Plenum Press, NY, 1975.
 30. Wang, F., Innovative Technology International Inc., Beltsville, MD (1985).
 31. Benson, R., R. Flot and C. Sandberg, *The Use of Shape Memory Effect Alloys as an Engineering Material*, *Proc. of the 15th National SAMPE Tech. Conference*, Oct. 4-6, 1983, 403-414.
 32. Shigley, J. and L. Mitchell, *Mechanical Engineering Design*, 4th edition, McGraw-Hill Book Co., New York, NY, 1983.
 33. Kuester, J. and J. Mize, *Optimization Techniques with Fortran*, McGraw-Hill Book Co., New York, NY 1973.
 34. Fenner, R.T., *Finite Element Methods for Engineers*, McMillan Press Ltd., London, 1975.
 35. Bathe, K.J. and E.L. Wilson, *Numerical Methods in Finite Element Analysis*, Prentice-Hall Inc., Englewood Cliffs, NJ, 1976.
 36. Yang, T.Y., *Finite Element Structural Analysis*, Prentice-Hall Inc., Englewood Cliffs, NJ, 1986.
 37. Paz, M., *Structural Dynamics: Theory and Computation*. 2nd edition. Van Nostrand Reinhold Co. , New York, 1985.